UNIVERSITY OF TROMSØ UIT

FACULTY OF SCIENCE AND TECHNOLOGY
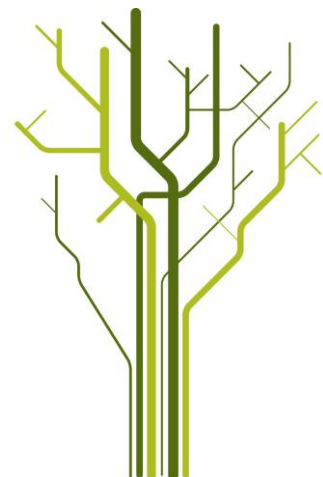DEPARTMENT OF GEOLOGY

Petrography, geochemistry and genesis of the Skiftesmyr Cu-Zn VMS-deposit, Grong, Norway

Kristoffer Jøtne Walsh

GEO-3900 Master's Thesis in Geology

November 2013

GEO-3900

Master's Thesis in Geology

PETROGRAPHY, GEOCHEMISTRY AND GENESIS OF THE SKIFTESMYR CU-ZN VMS-DEPOSIT, GRONG, NORWAY

Kristoffer Jøtne Walsh

Department of Geology, UiT – The Arctic University of Norway,
November, 2013

Acknowledgements

Abstract

The Skiftesmyr Cu-Zn VMS-deposit is located in the Grong municipality of Northern Trøndelag, Norway. The mineralization has been known since at least 1903, when mention of small workings in the area were first published, and has later been the subject of several exploration projects by different companies, of which MetPro AS is the latest. The Skiftesmyr deposit is a part of the Gjersvik Nappe, which is a part of the Köli Nappe Complex, which in turn is a part of the Upper Allochthon of the Scandinavian Caledonides, and is likely of Mid-Ordovician age. Petrographic and geochemical studies were carried out on samples from trenches cutting across the mineralized horizons. Geochemical analyses performed on the igneous rocks suggest that the deposit formed in a back-arc environment in relation to a relatively mature (compared to e.g. the Skorovas and Gjersvik deposits) island arc. In terms of lithological associations Skiftesmyr can be classified as bimodal-mafic and/or mafic-dominated, depending on the interpretation of the available geochemical data, and has several traits in common with both the Noranda deposits, Quebec, and the deposits of the Troodos Massif, Cyprus. The dominant ore minerals are chalcopyrite and sphalerite, with only minor amounts of Cu-enriched sulphides associated with supergene enrichment processes present.

Table of contents:

1. Introduction

1.1. Context of the study:

Although there have been fluctuations, the last few years have seen a substantial increase in the price of base and precious metals, an evolution which in turn has spurred global renewed interest in mining and exploration, both from a financial and academic perspective. The price of copper has since 2004 more than tripled, and during the summer of 2011, when the value of copper hit its peak, the price was set at ~10,000 USD per ton. As of the fall of 2013, the price has lowered rather substantially compared to this somewhat anomalous peak, and has now stabilized at 7200 USD per ton. A similar evolution can be seen with the price of Zn, where the price has more than doubled in the last 10 years, as well as for gold and silver, which have seen a steady rise over the same period of time. For the latter two, the last year, or rather the spring of 2013, has been marked by a substantial reduction in price, though the prices for Au and Ag respectively have tripled and doubled during the last decade, and so still remain strong (kitco.com; lme.com).

As previously mentioned, this has provided the mining industry with new-found incentives to increase the scope of their exploration activities, and has opened up new areas for exploration, as well as given cause to look upon older discoveries with new eyes. The Skiftesmyr deposit is once such discovery, as written records of workings on the property extend back as far as 1903 (Bernard, 1997), and several mining companies have in the following decades added much new information, a topic which will be expanded upon in section 1.4. of this paper. The Skiftesmyr deposit, together with several smaller nearby deposits, have, if worked in conjunction, been considered a financially viable operation for some time. The low metal prices in the 1980s and 1990s would however have resulted in small profit margins, in addition to larger opportunities in the vicinity, such as the deposits at Skorovas, Gjersvik and Joma which were likely prioritized (Bernard, 1997; Lindeman, 1992).

With the comparatively recent increase in base and precious metal prices and extensive knowledge of the Grong mining district in mind, Metal Prospecting AS, MetPro for short, was incorporated in 2007, with a total of 10 project areas and claims covering a total area of 96.7

km^2, among these the Skiftesmyr and Godejord deposits in Grong, and shortly thereafter started work on the properties (metproas.no).

1.2. Purpose of the study

The purpose of this study is to take a closer look at the Skiftesmyr Cu-Zn deposit in terms of petrology, mineralogy, geochemistry and economic geology, with the primary intent of determining the genesis of the deposit. Literature, in this case primarily reports by exploration companies who have worked in the area, propose several different theories on the genesis of the deposit. These range from Skiftesmyr being a Kuroko-type VMSD (Buer & Heim, 1991), primarily due to the presence of felsic volcanics, to a more classic Cyprus-type VMSD mode of formation, as a result of the surrounding rocks being mostly mafic. Other reports mention the presence of turbidite structures in the surrounding sediments (Heim, 1993b), which might indicate that the Skiftesmyr deposit might be an Ordovician analogue to the modern Escanaba system. However, the marshy nature of the terrain makes the identification and mapping of such features to a larger extent very difficult. All of the deposit types mentioned above are VMS-type deposits, volcanogenic massive sulphides, shortened to VMSD for the sake of convenience.

Determining the genesis of the deposit will be done by comparing mineralogical and petrographical findings from the study of thin sections to findings from other deposits from literature, and by using the geochemical data gathered from the same rocks. The rather disparate findings and field observations that have been made over the course of the work done in the Skiftesmyr area and in the Grong mining field will also be compared to my own observations. The work will be done utilizing petrology, mineralogy and geochemistry, though the focus will be on economic geology. As a result I will also look at potential economic uses for wall rocks and accessory minerals, in an effort to prepare for future processing technology and as a way to potentially reduce the size of the tailings from the mining operation. Similar to other countries and regions around the world, the Norwegian government requires that a deposit is made equal to the cost of a total environmental rehabilitation of the mine area before mining can commence. As a result, alternative uses for minerals otherwise deposited as tailings, or any effort to reduce the amount of tailings present at the mine site, will reduce costs, and help appease environmental concerns. Potential

depositional controls for precious metals, such as gold and silver, will also be examined using both the geochemical data available and observations from thin sections.

As a part of the mineralogical investigations in thin section a closer look will also be taken at grain sizes and the uniformity of said grain sizes, which will be of importance with regards to milling the ore, and alteration types that are present in the deposit. As the samples were collected from trenches, surface weathering and subsequent gossan formation, supergene enrichment and acid mine drainage will also be elaborated upon, as well as the importance of these features to exploration efforts.

1.3. The Skiftesmyr deposit

The Skiftesmyr deposit is located in the Grong municipality of Northern Trøndelag, about 15 km east of the Grong town center, about 150 km northeast of Trondheim (see Fig. 1). The area is commonly referred to as the Grong mining district in literature, as it is home to several historic mine sites and small scale workings. In the period between 1918 and 1975 the area was closed to mining companies by law, as the Norwegian government deemed it to be of great financial importance to the country (Haugen, 1982; Mørk, 1977). The immediate area surrounding Skiftesmyr, "myr" being the Norwegian term for marsh, is also home to several other similar deposits, such as Godejord and Finnbu, though these are outside the scope of this project. When the Norwegian government in 2013 announced a revised strategy to stimulate the future growth of the mining industry in Norway, Skiftesmyr was listed as a deposit of national importance (Regjeringens Mineralstrategi, 2013).

The current tonnage of the Skiftesmyr deposit is inferred to be approximately 2.75 Mt at a cut-off of 1% Cu-equivalents (based on 1992 metal prices), with an average grade of 1.23 % Cu, 1.86% Zn, 0.35 ppm Au and 11 ppm Ag (Lindeman, 1992b). The Pb content is negligible with respect to value. The orebody consists of massive Cu-Zn pyritic ore, arranged in thin layers and continuous lenses that vary in thickness between 2-20 m. The average thickness of the orebody is 4-6 m. The deposit and the surrounding area dips steeply (70°-80°) to the north, slightly towards the west/northwest on the eastern flank of the orebody, but the direction varies somewhat due to the polyphase folding the area has been subject to (Langley, 1973; Bernard, 1997; Haugen, 1982; Mørk, 1977). Langley (1973) describes three separate phases

of folding. The massive ore contains numerous fragments of country rock in the contact with the host rock, mostly in the upper part of the orebody. These have been proposed to be remnants of fold hinges, floating within the strongly sheared orebody (Reinsbakken, 1993).
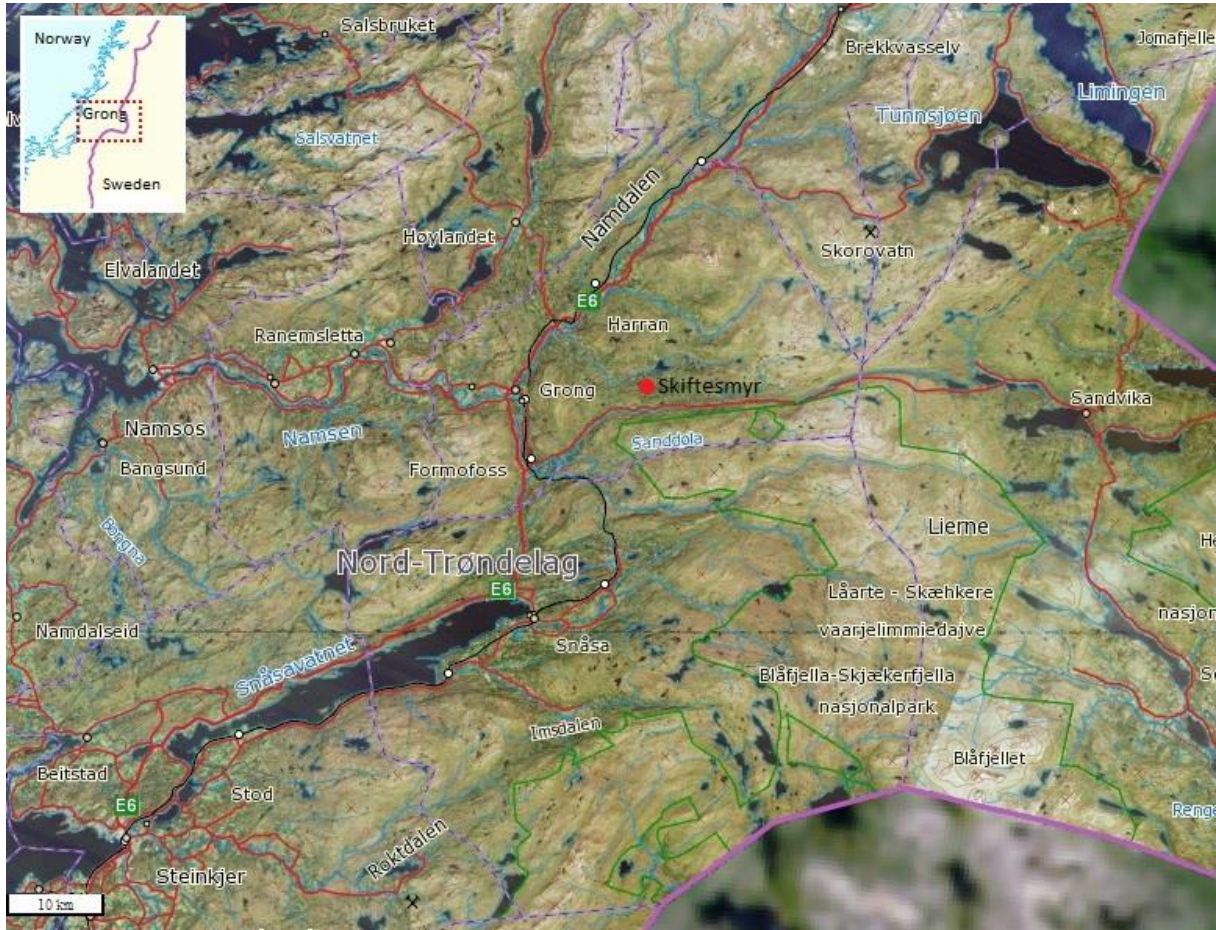
Figure 1: *Map of the study area and its location relative to the nearby town of Grong. Map modified from NGU's mapping service. The location of the Skiftesmyr deposit is indicated by the red dot.*

The layers and lenses of massive sulphides are surrounded by quartz-sericite, albite and chlorite rich schistose country rocks, most of which contain some disseminated sulphides (Bernard, 1997; Haugen, 1982; NGU Ore Database, Skiftesmyr).

1.4. Previous work

The first written reports on the Skiftesmyr deposit dates back to 1903, referencing the existence of small workings (Flood & Reinsbakken, 1997; Haugen, 1982; Mørk, 1977), followed by trenching efforts in 1910-1912, thereby confirming the existence of the deposit

(NGU Ore Deposit Database). Several other deposits in the area, such as Joma, Gjersvik and Skorovas were also discovered around this time, which lead to the Norwegian government adding a law giving it exclusive rights for mining in the area, primarily due to area's importance as a sulphur producer. This law was in effect between 1918 and 1975 (Haugen, 1982), and lead to a cessation of all new exploration and mining activities in the area, with the exception of the Skorovas mine. The first detailed geological study to be performed in the area was the mapping done by state geologist Steinar Foslie in 1920-30, and is considered to be surprisingly accurate and detailed considering the poor quality of the existing topographical maps and the remoteness and inaccessibility of the area at the time (Heim, 1993; Bernard, 1997; Flood & Reinsbakken, 1997).

Following this, very little work was done before the start of the first Grong Program (1971-1973), a collaboration between NGU (the Norwegian Geological Survey) and Grong Gruber AS, when the area was the focus of ground and airborne geophysical investigations, such as TURAM, EM, magnetic total field, SP (self/spontaneous potential) and VLF (very low-frequency). A diamond drilling program was started in 1973 by Grong Gruber AS, and lasted until 1979. In 1990 the diamond drilling was resumed, this time by Norsulfid AS, a Norwegian subsidiary of Finnish mining company Outokumpu OY, and continued until 1992. During this time, flotation tests of the ore from Skiftesmyr were also performed. Upon completion of the diamond drilling program in 1992, a total of 70 drill holes had been made, after which followed extensive assessment of exploration data, ore reserve calculations and evaluations of mining methods. These assessments were reevaluated in 1996 by Canadian company Braddick Resources Ltd., who had been contracted to do a prefeasibility study by Norwegian company Geologistke Tjenester AS. Due to the low metal prices at the time, they concluded not to start mining (Bernard, 1997; Flood & Reinsbakken, 1997).

Following incorporation in 2007, MetPro obtained the exploration permit for Skiftesmyr and Godejord in 2010, and continued airborne geophysical investigations, diamond drilling and trenching efforts, in addition to compiling exploration data from earlier efforts in the area, working towards getting the existing data up to NI 43-101 standards (metproas.no).

1.5. Geology of the Skiftesmyr area

1.5.1. Regional geology

The Scandinavian Caledonides are a fold and thrust belt created as a result of the collision between the Laurentian and Baltic cratons subsequent to the closing of the Iapetus Ocean during the Late Cambrian to Early Silurian periods. The Norwegian Caledonides are composed of four nappe complexes: the Lower, Middle, Upper and Uppermost Allochthons. The Lower and Middle Allochthons are interpreted as remnants of the Baltic margin, the Upper Allochthon represents oceanic crust from the Iapetus Ocean and the Uppermost Allochthon is thought to be composed of relict rocks from the Laurentian craton (Stephens, 1988).

The base metal bearing stratiform pyritic ores of the Scandinavian Caledonides are located within a 1500 km long belt of metamorphosed rocks that stretches from Rogaland in southwestern Norway to North Troms in northern Norway, most of which are Ordovician (Halls et al., 1977), and formed as a result of submarine igneous activity during the closing of the Iapetus Ocean (see Fig. 2).

Though stratigraphy and the metamorphic grade of the host rocks vary significantly from area to area, it is clear that the ores lie at a comparable structural level throughout the Caledonian allochthon of the Scandinavian Peninsula (Halls et al., 1977). "The Ordovician host rocks comprise a varied assemblage of supracrustal volcanic and sedimentary rocks with closely associated plutonic masses of ultrabasic, basic and acid composition", and though the ore bearing rocks "have a close genetic relationship with the volcanic rocks with which they are associated" this relationship "has been masked by the effects of metamorphic recrystallization and polyphase deformation, which affected both ores and host rocks during the process of allochthonous tectonic emplacement" (Halls et al., 1977). In the Skiftesmyr area, the ores are interpreted to have been formed in association with an ensimatic island-arc complex (Stephens et al., 1985; Halls et al., 1977).
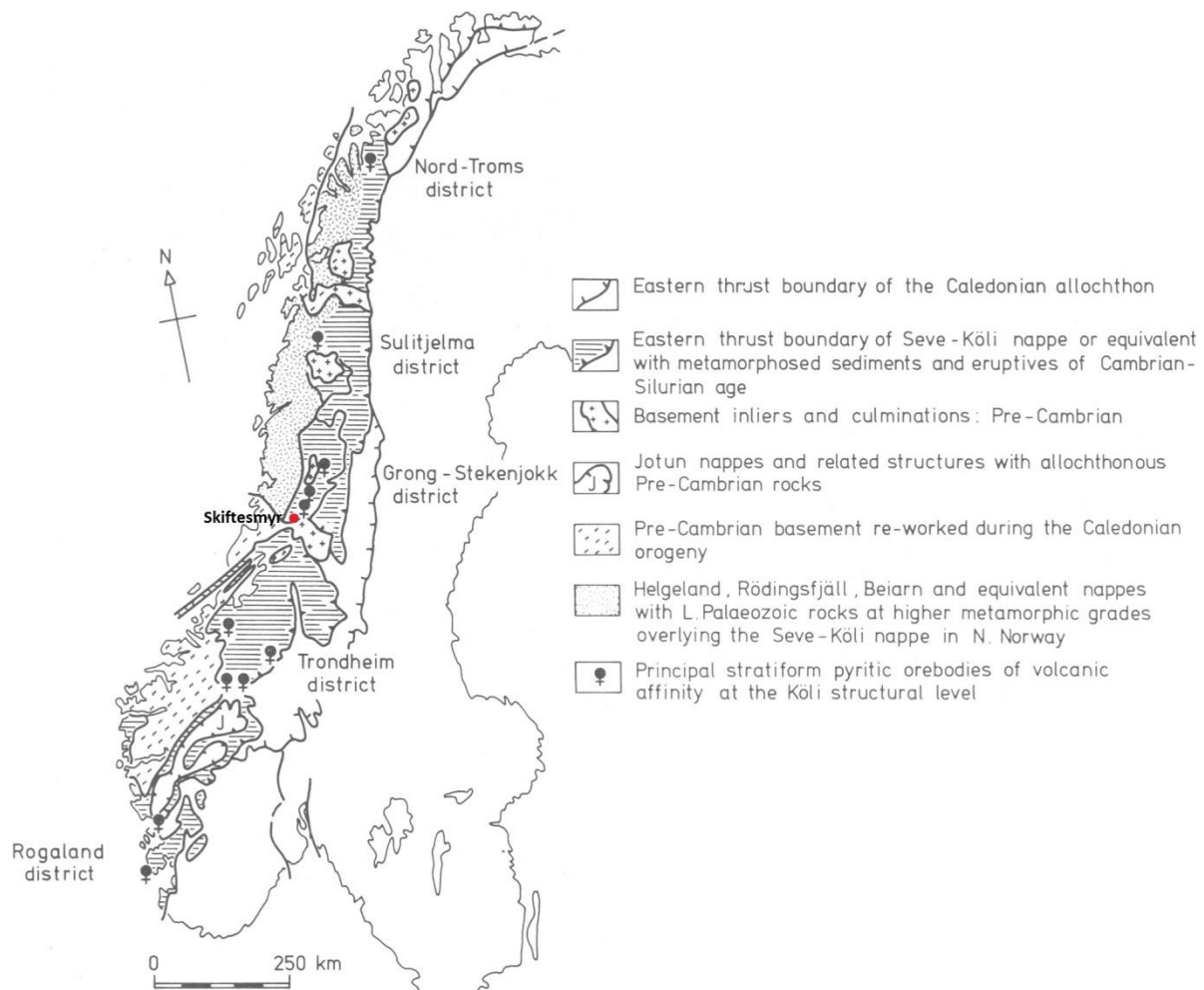
Figure 2: *Synoptic geological map of the Scandinavian Caledonides showing main districts of stratiform volcanogenic ores at the Köli structural level. Skiftesmyr is highlighted in red. (Modified from Halls et al., 1977)*

The Skiftesmyr deposit lies within the Gjersvik Nappe, which in turn is a part of the Köli structural level of the Seve-Köli Nappe complex. The Köli Nappes constitute the upper part of the Seve-Köli Nappe complex, which represent the Upper Allochthon of the Central Scandinavian Caledonides (Halls et al., 1977; Stephens et al., 1985). The Köli Nappes, containing early Paleozoic metamorphosed sediments, volcanites and intrusives, have been subdivided into three major units, referred to as the Lower, Middle and Upper Köli (Stephens et al., 1985). Each of the subdivisions of the Köli Nappes contains one or more thrust nappes, and in the Grong area the Gjersvik Nappe represents Middle Köli. The Gjersvik Nappe is bordered to the south by the Grong-Olden Culmination (GOC), which is composed of mid-Proterozoic (1650-1550 Ma) (Heim, 1993) gneisses and represents the border between the

Köli Nappes of the Upper Allochthon and the Lower and Middle Allochthons. On a regional scale the GOC gneisses are covered by the Särv and Seve Nappes of the Middle Allochthon. In Grong the border between the Gjersvik Nappe and the GOC is defined by the Sandøla Valley and the rocks of the Leipikvatnet Nappe exposed along the bottom of the valley, though in some areas along this stretch the Middle Allochthons are not present (Heim, 1993). The Leipikvatnet Nappe contains mafic volcanites, limestone, graphitic phyllites and cherts, and has been interpreted as a part of a pre-arc succession (see Fig. 3) (Stephens et al., 1985).

1.5.2. Rocks, structures and tectonostratigraphy of the Gjersvik Nappe

The youngest rocks of the Gjersvik Nappe are intrusive rocks of granodioritic to trondhjemitic composition. Two separate intrusions, the Møklevass Intrusion and the Ramsjø Intrusion, border the Skiftesmyr deposit to the north, both covering large areas (see Fig. 3). They are often subjected to retrograde alteration and resulting saussuritization, giving the rock a green colour. Towards the contact with the surrounding volcanites there is a chilled margin with subsequent grain size reduction, and xenoliths up to 1 m in size from the surrounding rocks are evident, which leaves little doubt that these rocks intruded into the surrounding volcanogenic greenstone. Veins and stocks of pink granodiorite are found in the periphery of the deposit, cutting both the intrusions and the greenstone, making them the youngest rocks in the area. These are thought to represent residual melt from the larger intrusions (Heim, 1993). The greenstones in the Skiftesmyr area can be divided into those of magmatic and volcanic and those of pyroclastic and volcano-sedimentary origin, where some of the former are interpreted as tectonic fragments containing partial ophiolite sequences. The narrow corridor that divides the Møklevass and Ramsjø Intrusions is dominated by dark and amphibolitic greenstone, and the lack of pillow lava structures indicate that these greenstones originated as sills or massive lava flows (Heim, 1993). The gabbro with disseminated sulphides further north has been proposed to be the deepest part of a continuous sequence, followed by the aforementioned amphibolitic greenstone, and further south towards the Skiftesmyr deposit, large areas of light greenstone containing pillow lava structures, which have been used to infer that this part of the Gjersvik Nappe is an inverted sequence, with the stratigraphic up-direction to the south (see Fig. 3). The rocks of pyroclastic and volcano-sedimentary origin associated with the greenstones mentioned in the previous paragraph are found to the south, towards Skiftesmyr, and are dominated by banded metatuffites. Directly around the

Skiftesmyr deposit there are also spilitic quartz-keratophyres with a possible dacitic protolith (Halls et al., 1977) (Heim, 1993), though these are also found in other areas of the Gjersvik Nappe.

Because most of the tectonic borders and structures in the Gjersvik Nappe are steeply dipping, nearly vertical in some cases, the geological map in and of itself gives an excellent overview of structures and tectonic units (see Fig. 3) (Heim, 1993). The structural geology and deformation history of the region is controlled by the Caledonian orogeny and can be thought of in terms of two major stages, the first of which is the formation of isoclinal folds and the imposition of early axial plane schistosity in the volcanic sequence. This resulted in thrust and slide horizons separating the plutonic and volcanic levels of the Gjersvik eruptive sequence, as well as resulting in zones of high tectonic strain along lithological boundaries with contrasting competency within the volcanic sequence. The plutons behaved as tectonic wedges, piercing and partially overriding the overlying volcanics, which explains the presence of some discordant contacts that have previously been interpreted as evidence of a non-stratiform ore genesis (Halls et al., 1977; Heim, 1993). This happened during the emplacement of the allochthon during Mid-Silurian times (Halls et al., 1977). The zones of high tectonic strain occurring locally at lithological boundaries within the volcanic sequence has caused penetrative alteration of the rocks, forming chlorite-albite-epidote schists devoid of any earlier volcanic fabric (Halls et al., 1977), which in combination with the flattening of adjacent units is thought to have resulted in a lenticulated style of deformation, a characteristic feature of highly deformed volcanostratigraphy and associated plutonics (Halls et al., 1977). This might provide an explanation as to the formation of the "pinch-and-swell" structure of the Skiftesmyr ore body (Buer & Heim, 1991), though this is more likely to be a result of intersecting fold axes at the locations of thickening (Langley, 1973).

The second stage of deformation in the region, superimposed on the earlier isoclines and schistosity, has created an open system of broad folds, which has resulted in the formation of an irregular pattern of dome and basin structures, and is believed to be caused by the equilibration between the basement rocks and the imposed load of the allochthon (Halls et al., 1977). The age of the rocks of the Gjersvik Nappe is hard to specify as they are more or less devoid of fossil evidence, though they are markedly similar to the rocks of the Støren group in the Trondheim region, which through the dating of fossils (*Dictyonema flabelliforme*) in an underlying schist (from the Gula Group) has been given a maximum age of Upper Cambrian –

18

Lower Ordovician (Tremadocian) (Halls et al., 1977). A minimum age for the rocks of the Gjersvik Nappe can be construed from the U-Pb dating of zircons from the intrusive bodies it contains. Roberts and Tucker (1991) (quoted in Cook & Hoefs, 1997, and Stephens et al., 1993) give a U-Pb zircon age of 456 ± 2 Ma for the Møklevatn Intrusion, which is assumed to

Legend:

- Granodiorite/trondhjemite
- Granodioritic two-mica gneiss of intrusive origin
- Gabbro
- Doleritic dike complex
- Dark and light greenstones, (Gjersvik Group)
  Pillow lavas
  Metabasalts/metagabbro
  Tuffs and tuffitic rocks
- Quartz-keratophyre (Gjersvik Group)

- Volcanic breccia (Limingen Group)
  Phyllites
  Magnetite-rich quartzite
  Tuffs and tuffitic rocks
  Amphibolitic metadolerites
- Marble/phyllite (Røyrvik Group)
- The Formofoss Nappe Complex
- The Tømmerås Mountain Complex

Figure 3: *Geological map of the Skiftesmyr area, digitally redrawn by the author based on maps and notes from Heim (1993), showing the rocks in the Skiftesmyr area and the location of the deposit relative to the nearby intrusives.*

be the latest major intrusive in the Gjersvik Nappe. Stephens et al. (1993) gave a U-Pb zircon age of 483 ± 5 Ma, which is likely closer to the maximum age of the rocks of the Gjersvik Nappe. This suggests that the ore forming magmatic activity continued for as long as 25 Ma (Cook & Hoefs, 1997).

1.6. VMS-type deposits

1.6.1. Introduction

Volcanogenic massive sulphide (VMS) is a term used to describe several different types of ore deposits, primarily with a Cu-Zn metallogeny, though there are sub-types in which Pb and Au are among the most important economic ores. Among nonferrous metallic deposits VMSDs rank second only to porphyry copper deposits in terms of economic importance (Ohmoto, 1996). Worldwide, VMSDs represent a major source of Zn, Cu, Pb, Ag and Au, as well as a significant source of Co, Sn, Se, Mn, Cd, In, Bi, Te, Ga and Ge, and some deposits also contain significant amounts of As, Sb and Hg (Galley et al., 2007).

1.6.2. VMS deposits of the world

Over 800 VMS deposits are known around the world, with tonnages ranging between 200,000 t to nearly 300 Mt. As with size, the ore grades also vary significantly, both in terms of the amount of ore present and also the types of ore mined, but one might say that an average VMSD would contain approximately 1.5% Cu, 3 % Zn and 1% Pb, with 50 ppm Ag and 0.5 ppm Au present (Ohmoto, 1996). Large VMSDs are generally divided into categories depending on size, these being giant (>100 Mt), very large (50-100 Mt) and large (25-50 Mt) deposits respectively (Galley et al., 2007). The average VMS type deposit is typically much smaller than this, with a tonnage of 1-3 Mt (see Fig. 4) (Ohmoto, 1996). Because of the genetic nature of VMS deposits it is not uncommon for several individual deposits to exist in the same area or tectonostratigraphic unit, often referred to as a VMS district or camp, e.g. the Iberian Pyrite Belt of Portugal and Spain, Abitibi in Canada, or in fact the Grong mining district. The Iberian Pyrite Belt is the largest known VMS district in the word, estimated to contain a total of 1575 Mt of ore, and it is also home to several of the world's largest VMSDs,

such as Neves Corvo (270 Mt) and Rio Tinto (250 Mt) in Portugal and Spain respectively. The single largest VMS-type deposit is the Windy Craggy deposit in British Columbia, Canada, with a tonnage of 297.4 Mt (Galley et al., 2007). The above mentioned deposits are all anomalous with respect to size, though there are others which in turn are anomalous with respect to high ore grades.
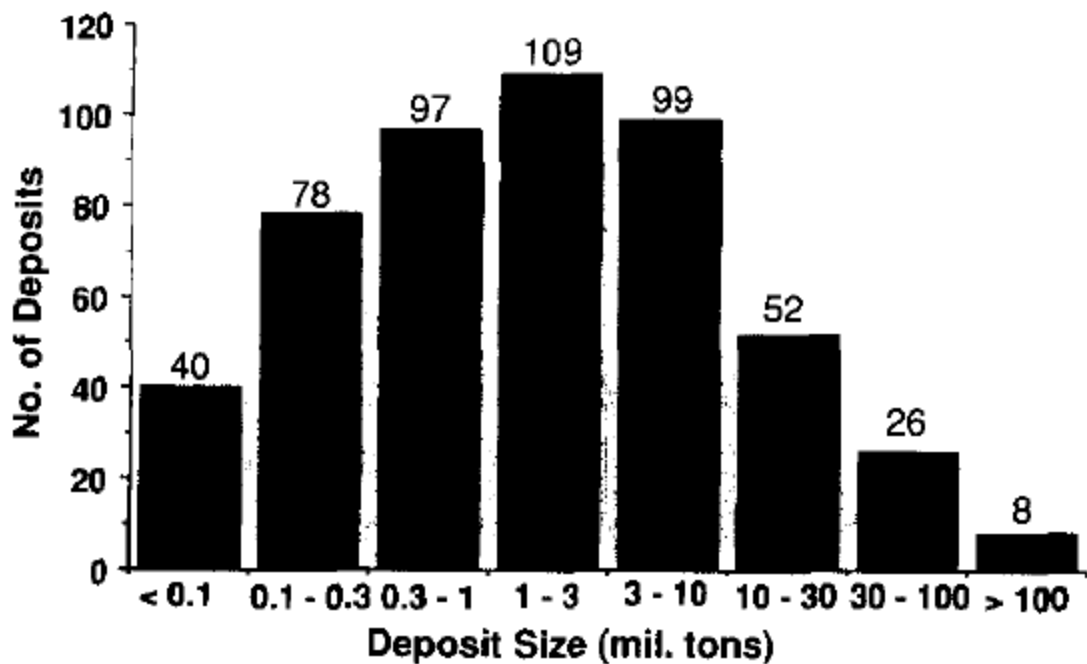
Figure 4: *Distribution of 509 worldwide VMS deposits based on tonnage. From Ohmoto (1996), based on data from Mosier et al. (1983).*

1.6.3. The formation of volcanogenic massive sulphide deposits

VMSDs are created as the result of a hydrothermal ore-forming process, in a process that we can observe to this day, namely as so-called "black smokers". Black smokers are hydrothermal vents on the ocean floor from which heated brine is vented into the sea (see Fig. 5). These hydrothermal fluids are rich in dissolved metals as a result of the high temperature, acidity and salinity of said fluids, all of which are factors that increase the amount of metals that can be transported in solution. Black smokers represent a direct analogy to Cyprus-type VMS deposits, as these are thought to have formed along mid-oceanic ridges, though all

21

VMSDs are formed by a similar process, albeit in differing geological settings. While mid-oceanic ridges, back-arc basins, intraoceanic arc rifts and continental arc rifts are typical settings for the formation of these deposits, intruding plutons or sea floor calderas initiate the same type of fluid circulation and thereby enable VMS-type mineralizations (Robb, 2005).

Though there are differences between the various types of VMSDs, most have a twofold ore distribution, with one ore zone as a stratabound, stratiform massive sulphide body, and another in the form of a stockwork, commonly referred to as a stringer zone, containing veins and disseminated sulphides. The massive sulphide ore body typically contains ~90% of the heavy metals present in the deposit, with less than 10% in the stringer zone, though the latter might be enriched in different metals as a result of ore mineral zonation, and as a result remain economically viable as an ore. The stockworks represent the channelways through which the hydrothermal fluids travel, while the massive sulphide body is thought to represent an accumulation of sulphides on the sea floor or in unconsolidated sediments, the latter formed, as mentioned, as an interaction between the hydrothermal fluids and cold seawater. In other words, the stockwork ores are epigenetic, while the massive sulphides are syngenetic (Ohmoto, 1996).

The source of the sulphur in VMSDs is sulphates from seawater, which is reduced to form sulphides (Robb, 2005), whereas the metals come from the surrounding volcanic rocks, dissolved by the convecting hydrothermal fluids percolating through them. Specific metal assemblages are as a result associated with specific volcanic rocks, as e.g. different types of basalts have relatively consistent metal contents. The Cyprus-type VMS deposits are for example typified by a Cu + Zn metal association, which reflect their formation by leaching of predominantly mafic volcanic rocks, whereas the felsic or mixed volcanic rocks associated with e.g. Kuroko-type deposits have a Pb + Zn + Cu metal association (Robb, 2005).

1.6.4. Classifications of VMS deposits

A generalized view of the different types of VMSDs, using genetic naming conventions:

- **Cyprus-type**: The Cyprus-type VMSDs have a Cu + Zn metal association, and are formed along mid-oceanic ridges as 'black smokers', similar to what can be observed

in the Pacific Ocean and elsewhere to this date. Heated brine is vented into the ocean through systems of cracks after having percolated through the surrounding mafic rocks (basalts), forming chimneys that are referred to as "black smokers". This type of deposit is typically hosted in an (or in a part of an) ophiolite sequence, and is named after the VMSDs of the Troodos ophiolite complex in Cyprus. Cyprus-type VMSDs are typically hosted by mafic-dominated assemblages, commonly ophiolitic (Galley et al., 2007; Piercey, 2009; Robb, 2005).
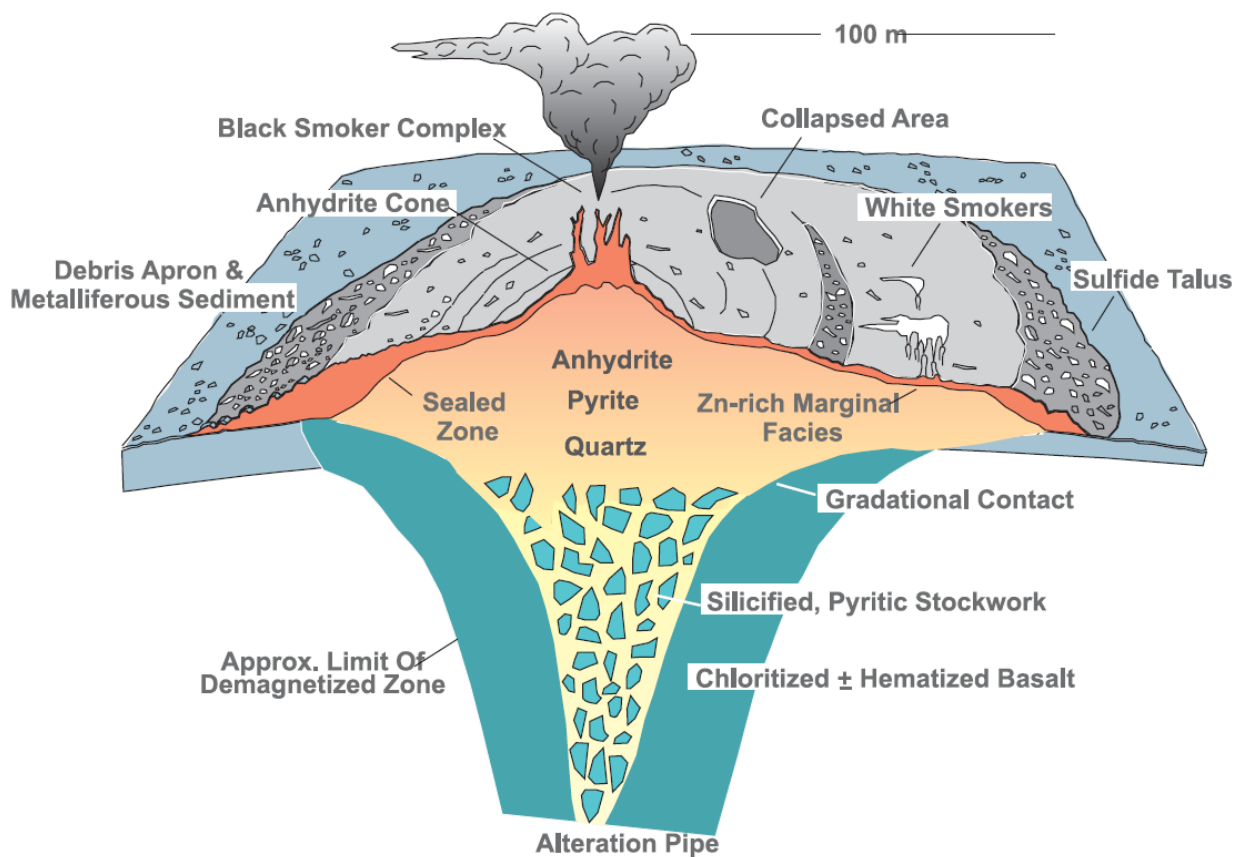
Figure 5: *Schematic representation of a modern black smoker and related VMS deposit from the Mid-Atlantic Ridge. The massive to semi-massive sulphide lens is underlain by a stockwork vein system and an associated alteration zone. From Galley et al. (2007).*

- **Kuroko-type**: The Kuroko-type VMSDs have a Pb (+Ba) + Zn + Cu metal association, and are formed by ocean arc volcanism. Kuroko-type VMSDs generally have felsic dominated footwall rocks, which explains the increased amount of Pb present in the mineralization compared to VMSDs hosted by mafic assemblages. Kuroko means "black ore" in Japanese, and was originally a term used to describe the

23

galena and sphalerite rich ore from massive sulphide deposits in Japan, but has later been used as a name for all Japanese VMSDs of Miocene age, and internationally as a specific example of a VMS-type deposit hosted in bimodal-felsic volcanic rocks. This is likely due to it being one of the most studied types of VMS deposit, and the first to be recognized as being of submarine exhalative origin (see Fig. 6) (Ohmoto, 1996).

- **Besshi-type**: The Besshi-type of VMS deposit occurs in a stratigraphic sequence dominated by clastic sediments, with some mafic igneous rocks, and is as such similar to both the Cyprus- (in being associated with mafic volcanics) and Escanaba-types of VMSDs, and there has been some controversy regarding the use of the term as a general name for any siliciclastic-mafic deposit as a result (Sundblad et al., 2006; Ohmoto, 1996). The name comes from the historic Japanese Besshi-deposit.

- **Escanaba-type:** Escanaba-type VMS deposit is a name given to massive sulphide deposits hosted by turbidites or hemipelagic sedimentary rocks, and comes from relatively recent studies of the Escanaba Trough and Middle Valley (northern Juan de Fuca Ridge) in the Gulf of California. The studies, inspired by the discovery of the hydrothermal vents at 21ºN on the East Pacific Rise (1979) and at the Galápagos Rise (1977), were undertaken with the goal of determining the mechanism controlling the formation of mineral deposits, alteration of the oceanic crust, chemical and thermal effects of the vents on the surrounding ocean and the interaction between thermal vents and their unique biospheres. The studies of thermal vents that followed lead to confirmation of the models currently used to explain hydrothermal ore formation. The primary difference between the Escanaba type of ore formation and the more common Cyprus- or mafic type is the rate of sedimentation. Mid-oceanic ridges can be classified as sediment starved or sediment dominated, the former being most common by far. The hydrothermal fluids at sediment starved ridges naturally then represent the interaction between said fluids and basalts, whereas at sediment dominated ridges such as the Escanaba Trough the sediments have a major effect on the composition of the hydrothermal fluids and the resulting hydrothermal deposits, resulting in a difference in ore minerals present and the potential for enrichment in metals not typically associated with VMS-deposits formed in different environments (Morton et al., 1994).

One can also classify the different types of VMS based on the host-rock assemblages of the footwall, which is beneficial as it places no constraint on the genesis of the ore, and as such is more general and less prone to misunderstandings related to the genesis of the specific ores (see Fig. 6) (Piercey, 2009; Galley et al., 2007):

- **Mafic-ultramfic:** These deposits are associated with mafic-dominated assemblages, such as ophiolites. Examples of deposits of this type are the VMS deposits of the Troodos ophiolite complex in Cyprus, the ophiolite-hosted deposits of Oman, the Løkken deposit of Trondheim, Norway, and the ophiolite-hosted deposits in Newfoundland, Canada. This type of deposit is as a result used synonymously with the Cyprus-type. These deposits are thought to occur at intraoceanic back-arcs or fore-arc basins, or at oceanic ridges (Piercey, 2009; Galley et al., 2007; Koski & Mosier, 2012; Shanks & Koski, 2012; Ohmoto, 1996).

- **Bimodal-mafic:** These deposits are associated with mafic-dominated assemblages, with up to 25% felsic rocks. The felsic rocks usually host the actual deposits. An example of this deposit type would be the Kidd Creek deposit in Canada. The inferred tectonic setting of this deposit type is at a rifted, immature intraoceanic arc (Piercey, 2009; Galley et al., 2007; Koski & Mosier, 2012; Shanks & Koski, 2012).

- **Siliciclastic-mafic:** Siliciclastic-mafic deposits are associated with mafic (or ultramafic) assemblages, with felsic rocks as a possible minor component, and siliciclastic rocks. This deposit type is thought to form at rifted continental margins, sedimented oceanic ridges or back arcs or intracontinental rifts. The Japanese Besshi deposit is a typical example, together with deposits such as Windy Craggy in Canada and Ducktown (USA). Sundblad et al. (2006) suggests that the Norwegian deposits at Røros and Sulitjelma might also be of this type. The Escanaba Trough and its massive sulphide deposits are considered to be a modern analogue of this type of deposit (Piercey, 2009; Galley et al., 2007; Koski & Mosier, 2012; Shanks & Koski, 2012). Halls et al. (1977) also note the similarity between the metablastesis of pyrite from Ducktown (Tennessee) and Sulitjelma.
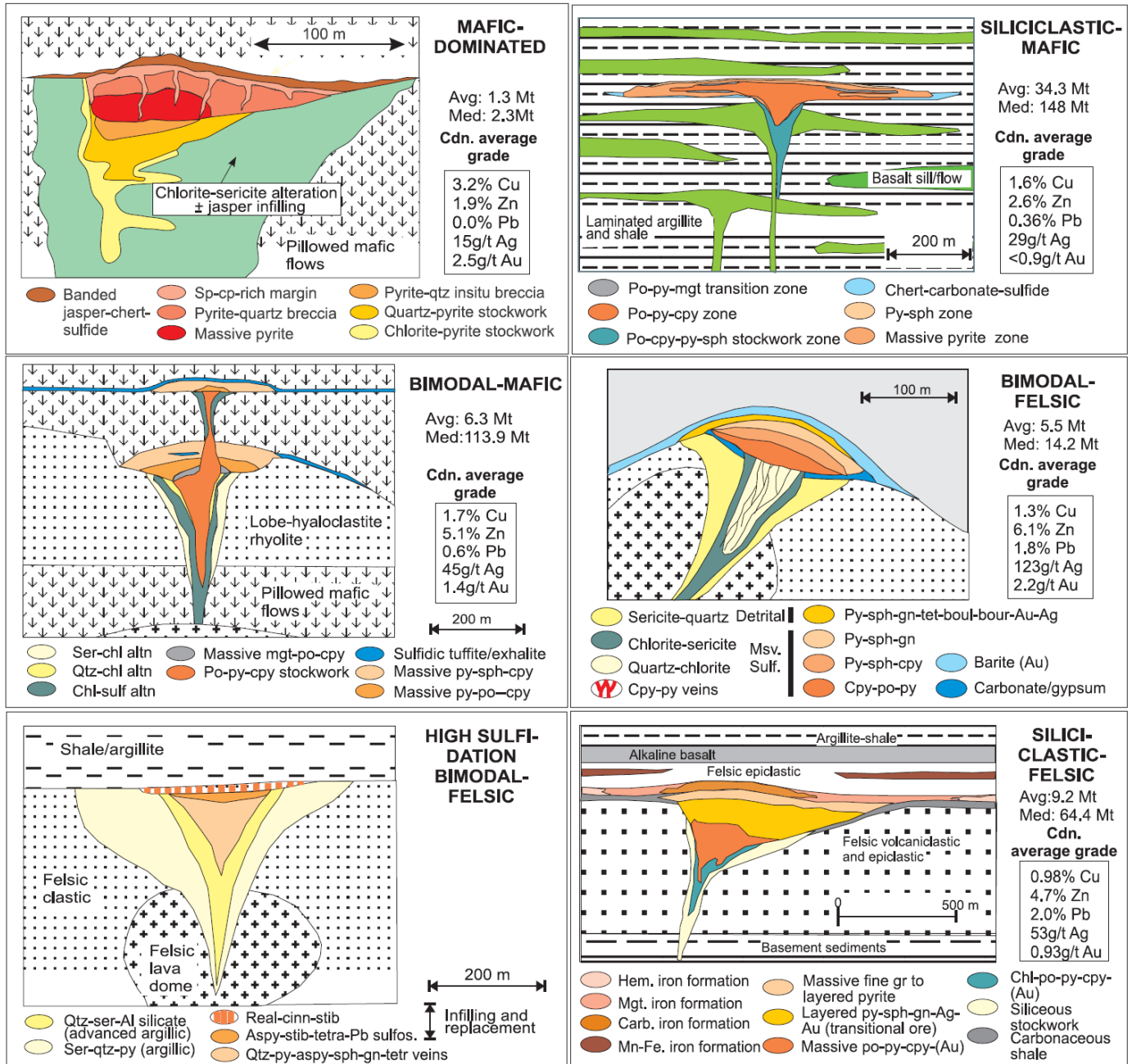
Figure 6: *The lithological representation of VMS deposits from Galley et al. (2007) based on host rock lithologies. The figure shows the idealized representation of the different deposit types, as well as average grades and tonnages. The information regarding grades and tonnages are from Canadian VMS deposits, and is as such not necessarily applicable to deposits worldwide, but does provide an indication as to the typical metals associated with the individual deposit types. The "high sulfidation bimodal-felsic" type has in my description been grouped with the bimodal-felsic deposits. It should again be noted that regardless of whether the lithological classification system is better suited to the description of VMS deposits, the representation as given here is still represents generalized perspective.*

26

- **Siliciclastic-felsic:** Siliciclastic-felsic, or bimodal siliclastic, deposits are dominated by siliciclastic rocks and abundant felsic rocks. They typically contain very little mafic rocks, generally less than 10%, and are found in a shale rich setting. They are thought to have formed at mature epicontinental margin arcs and back arcs. Examples of this type of deposit are Brunswick No. 12 in the Bathurst district in Canada, the Iberian Pyrite Belt (containing deposits such as Rio Tinto) and the Stekenjokk deposit in Sweden (Piercey, 2009; Galley et al., 2007; Koski & Mosier, 2012; Shanks & Koski, 2012). This deposit type is often referred to as a "Kuroko deposit" (see Table 1).

- **Bimodal-felsic:** These deposits are associated with assemblages where felsic rocks are more abundant than their mafic counterparts, with the possibility for minor amounts of sediments. Examples of bimodal-felsic deposits are found in the Skellefte district in Sweden, the Kuroko deposits of Japan and the Buchans district of Newfoundland. These deposits are thought to have formed at rifted continental margin arcs and back arcs (Piercey, 2009; Galley et al., 2007; Koski & Mosier, 2012; Shanks & Koski, 2012).

It is also important to specify that these types are generalizations, and that what is observed in nature does not necessarily always fit the proposed models, and that we as such are likely to see variations and subdivisions of these groups, particularly with the genetic classification as each deposit is bound to have some original feature. Problems surrounding the genetic classification of ores are shown in the table below, particularly with respect to the Kuroko-designation and the problems related to distinguishing between Besshi and Escanaba deposit types.

Genetic classification of VMS deposits	Classification based on lithologic associations	Examples of ancient deposits	Inferred tectonic setting
Kuroko	Siliciclastic-felsic	Bathurst District, Canada; Iberian Pyrite Belt (Rio Tinto), Spain & Portugal; Stekenjokk, Sweden	Mature epicontinental margin arc and back arc
Kuroko/Noranda	Bimodal-mafic	Noranda, Canada; Kidd Creek, Canada	Rifted immature intraoceanic arc
Kuroko	Bimodal-felsic	Kuroko, Japan; Skellefte district, Sweden	Rifted continental margin arc and back arc
Besshi	Siliciclastic-mafic	Besshi, Japan; Windy Craggy, Canada	Rifted continental margin, sedimented oceanic ridge or back arc, or intracontinental rift
Escanaba	Siliciclastic-mafic	Escanaba (modern analogue), USA; Besshi, Japan; Windy Craggy, Canada	As above
Cyprus	Mafic (-ultramafic)	Troodos ophiolite, Cyprus; Løkken, Norway	Intraoceanic back-arc or fore-arc basin, or oceanic ridge.

Table 1: *Examples of different types of classifications of VMS deposits, based on genetic and lithological criteria respectively, attempting to summarize the previous chapter and highlighting the weaknesses of the genetic classifications compared to the lithologic associations (Piercey, 2009; Galley et al., 2007; Koski & Mosier, 2012; Shanks & Koski, 2012).*

1.6.5. VMS deposits of the Norwegian Caledonides

The Norwegian Caledonides are home to multiple volcanogenic massive sulphide deposits, formed at various stages during the closing of the Iapetus Ocean and the collision between the Laurentian and Baltic paleocontinents. Ordovician deposits are also found on the Laurentian side of the collision in Canada and the USA, there in the Appalachian mountain range. In Norway the majority of the stratabound volcanogenic ores are found at the Köli structural level. As can be seen in Figure 2, the deposits can be grouped into five separate districts, namely the Nord-Troms district, the Sulitjelma district, the Grong-Stekenjokk district, the Trondheim district and the Rogaland district. The majority of the deposits can be found in the Central Norwegian Caledonides, which encompasses the Trondheim and Grong-Stekenjokk districts. Deposits of note are the Sulitjelma deposits, Skorovas, Joma, Gjersvik, Løkken and Røros. The Joma, Skorovas and Gjersvik deposits are all located in the same area as the Skiftesmyr deposit (see Table 2).

Deposit	Tonnage (Mt)	Cu (%)	Zn (%)
Joma	~20	1.3	1.7
Skorovas	~10	1.15	2.71
Gjersvik	1.6	1.6	0.90

Table 2: *Overview of grades and tonnages obtained from deposits in the vicinity of Skiftesmyr in the Grong mining district (Bernard, 1997).*

While there has been a lot of exploration activity and mining in the Grong area during the last 50 years, revision of previous findings in light of the new metal prices and improved technology continues to make the Grong mining district an interesting location for future mining and prospecting.

2. Methods

2.1. Sample collection and trenching

Samples collected to prepare thin sections from were gathered from trenches cutting across the mineralized zone of the Skiftesmyr deposit. The overburden was removed from the trenches using an excavator, a process proving to be somewhat difficult given the marshy and wet terrain, and then hosed down to clean the surface of the rock. The trenches were then measured, and photographs taken of the rocks using a 1 x 1 m grid. These photos were later used to produce the trench maps. Channel samples were collected along the length of the trenches, each sample 1 m long, using a hand-held gasoline powered saw. The channel samples were sent to the ALS laboratory for geochemical analysis. The mineralogical samples used to produce the thin sections described in this paper were collected adjacent to the channel samples (see Fig. 7).

2.2. Geochemistry

The geochemical analyses performed on the samples from the Skiftesmyr trenches were done in two phases. First, the channel samples were analyzed using ME-ICP61 (ICP-AES) at the laboratory of ALS Minerals, the results assumed to be comparative to the mineralogical samples due to them being collected next to each other. Selected samples have also been subject to trace element XRF-analysis, the samples selected primarily due to them either being part of the mineralized zone and hence warranting a closer look at trace elements present, or because they have been identified as metabasalt based on microscopic investigations, in which case trace elements can be used to infer the origin of the basalt by comparing it to the composition found in deposits with known geneses.

2.2.1. ME-ICP61

ME-ICP61 is the ALS Minerals naming convention used for a 33 element ICP-AES analysis. The samples, 0.25 g each, are dissolved using four different acids; HNO_3, $-HClO_4$, $-HF-HCl$ digestion and HCl, which dissolves most minerals. The sample method is described as four

acid near-total ICP-AES, "near-total" being used as, depending on the sample matrix, not all elements will be quantitatively extracted. After having been dissolved, the sample is then

Figure 7: *Pictures showing trenches with channel samples (top) and mineralogical sample (bottom). Note the white stain on the surface caused by weathering of sphalerite to hydrozincite (pictures were taken after trenches had been exposed for a year).*

topped off with dilute HCl and the solution containing the sample is analyzed using inductively coupled plasma-atomic emission spectrometry (ICP-AES) (ALS Global, 2009). The samples were also analyzed for gold using Au-AA23, where a 30 g sample is "fused with a mixture of lead oxide, sodium carbonate, borax, silica and other reagents as required, inquarted with 6 mg of gold-free silver and then cupelled to yield a precious metal bead. The bead is digested in 0.5 mL dilute nitric acid in the microwave oven, 0.5 mL concentrated hydrochloric acid is then added and the bead is further digested in the microwave at a lower power setting. The digested solution is cooled, diluted to a total volume of 4 mL with de-mineralized water, and analyzed by atomic absorption spectroscopy against matrix-matched

standards" (ALS Global, 2005). The analytical data provided from the geochemical investigations of the channel samples will be included in full in Appendix 3.

2.2.2. XRF

Samples analyzed by XRF for trace elements were cut down into appropriate size, and crushed in a swing mill. The swing mill was thoroughly washed prior to use to minimize any contamination, as well as between the individual samples. The powder was then weighed and mixed with wax pills (POLYSIUS PORLIFE® Mahlhilfe), with 9.0 g of rock powder and 9 wax pills for each sample. Once a homogenous mixture was achieved, the samples were pressed into pills. The XRF machine used was a Bruker S8 Tiger XRF at the Department of Geology (University of Tromsø).

2.3. Production of thin sections

25 thin sections were prepared from the 23 samples, with multiple thin sections made from two samples from the mineralized zone. The samples were cut to appropriate size (~3.5x~2.5x~0.5 cm), and subsequently polished at the Department of Geology at UiT.

2.4. Microscopy

The microscopical investigations of the samples were done using a Leitz Wetzlar petrographic microscope. The minerals were studied in plane- and cross-polarized light, henceforth referred to as PPL and XPL respectively, as well as reflected light for the opaque minerals. A camera mounted to the microscope was used to take pictures of the minerals. The thin sections were also scanned to provide an easy overview of the entirety of the thin section. These images are included in Appendix X. The naming convention used for the samples, both thin sections and geochemical, are on the form of TSK X – MY – Z (**T**rench **Sk**ifesmyr [trench number] – **M**ineralogical Sample [mineralogical sample number] – [number of thin section – only used if multiple thin sections are made from the same sample]). A complete list of abbreviated

mineral names from Kretz (1983), and other commonly used abbreviations are included in the appendices.

3. Observations

3.1. Observations in thin section

In this section observations from the thin sections will be represented in a summarized manner, dividing the samples into separate lithologies rather than representing each sample individually. Likely protoliths for the different lithologies will also be established, as well as a closer look at the ore minerals and how they are distributed throughout the samples, and which lithologies seem to be associated with the different types of sulphides.

3.1.1. Different lithologies present in the samples

The rocks of the Gjersvik Nappe are metamorphosed to greenschist facies, an observation that can readily be made from the abundance of chlorite and actinolite/amphibole in the samples, as well as the sericitization of feldspars, and is also supported by literature (e.g. Halls et al., 1977). The rocks are of volcanic and volcaniclastic origin, with only minor amounts of sedimentary rocks present. The sedimentary rocks associated with the Gjersvik Nappe are found in the Limingen Group, composed primarily of phyllites (see Figure 3). The phyllites contain some graphite, which is a potential cause of an electromagnetic anomaly observed along the Sandøla Valley. The volcanic rocks are extensively deformed and altered, and generally all primary igneous fabrics have been lost, but pillow lavas are found in some areas. The different lithologies found in the samples from the trenches are metabasalts, quartz keratophyres, pyroclastic rocks and quartzite, as well as the massive sulphides. There is also some evidence of felsic volcanic (rhyolite/rhyodacite) rocks that do not appear to be pyroclastic in nature, thus possibly representing the host rock of the felsic pyroclastic rocks (i.e. the quartz keratophyres), or dikes originating from a nearby felsic eruptive center.

3.1.1.1. Metabasalts

These rocks are characterised by their relatively low quartz content (0-25%), presence of plagioclase (in some cases only in the form of an aphanitic quartz and plagioclase matrix, thereby making a more exact estimate of the mineral assemblages present difficult), and large

amounts of chlorite (30-60%) and actinolite/amphibole (~30%) (see Fig. 9). This generally represents a typical mineral assemblage for basalts that have undergone greenschist facies metamorphism (Blatt et al., 2006). The presence of hornblende in some samples (see Fig. 8), indicate upper greenschist facies. Accessory minerals in the samples of this type are epidote and clinozoisite, as well as varying amounts of disseminated sulphides (see Fig. 8). Some of the samples also contain veins of quartz and/or carbonates. TSK 11 – M2 seems to represent a second type of metabasalt. It is primarily composed of plagioclase and chlorite, with some epidote, calcite and opaque minerals, with any amphiboles likely altered to chlorite. Based on mineral composition and visual estimation using a QAPF diagram, this likely represents a basaltic metaandesite (see Fig. 10), which together with the basalt and potential rhyodacitic pyroclastic material and/or lava flows indicate at least three stages of volcanic activity.
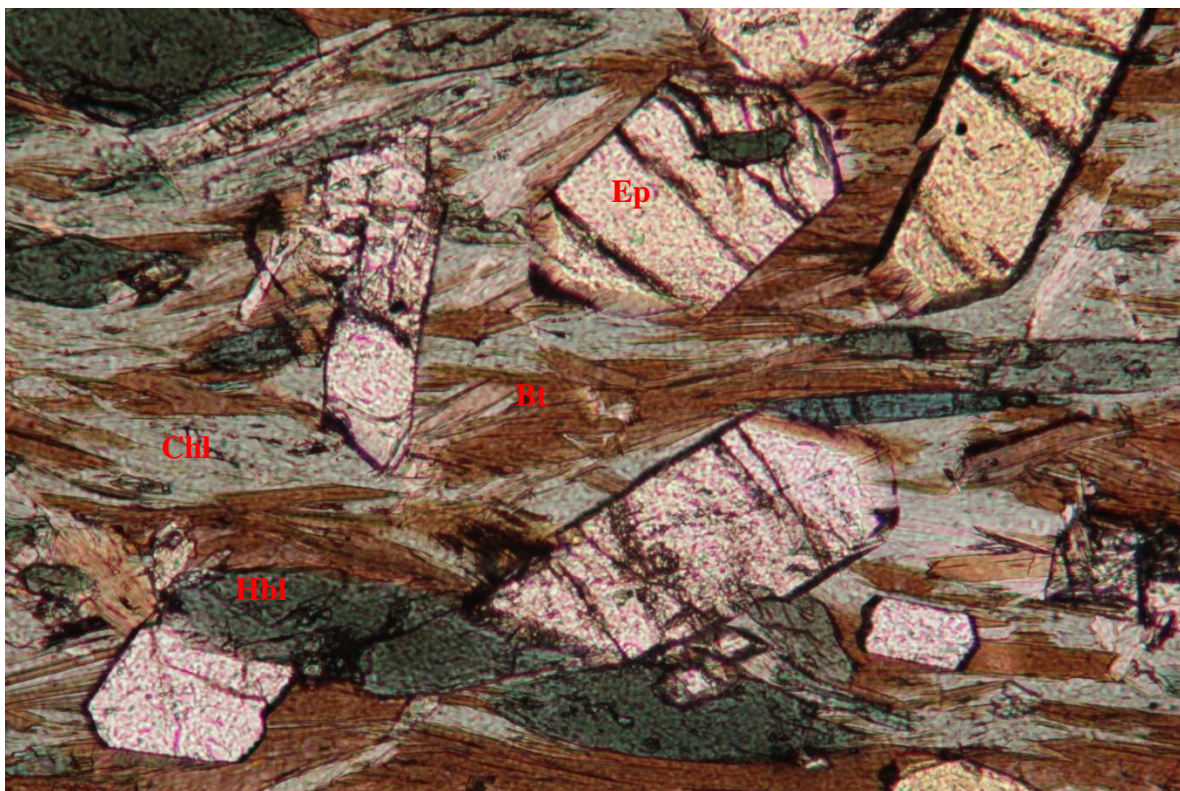
Figure 8: *Epidote crystals in biotite (partially chloritized) and chlorite groundmass. Epidote and clinozoisite seem to be the most abundant in mica rich layers such as this. Dark green minerals are hornblende. From TSK 10 – M8. Width of field: 1.8 mm.*
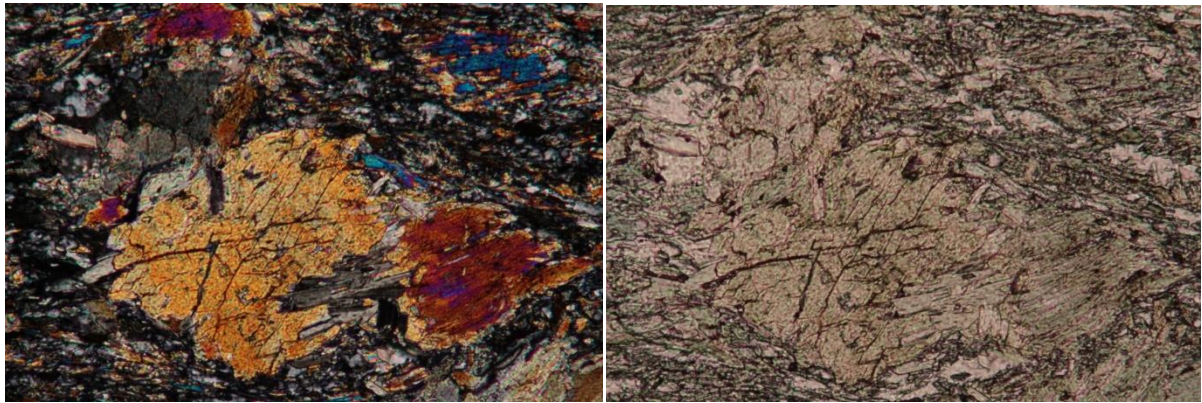
Figure 9: *Amphibole phenocryst in quartz-chlorite-rich matrix from metabasalt (TSK 14 - M6), in cross- (left) and plane-polarized (right) light. Field of view: 1.8 mm.*
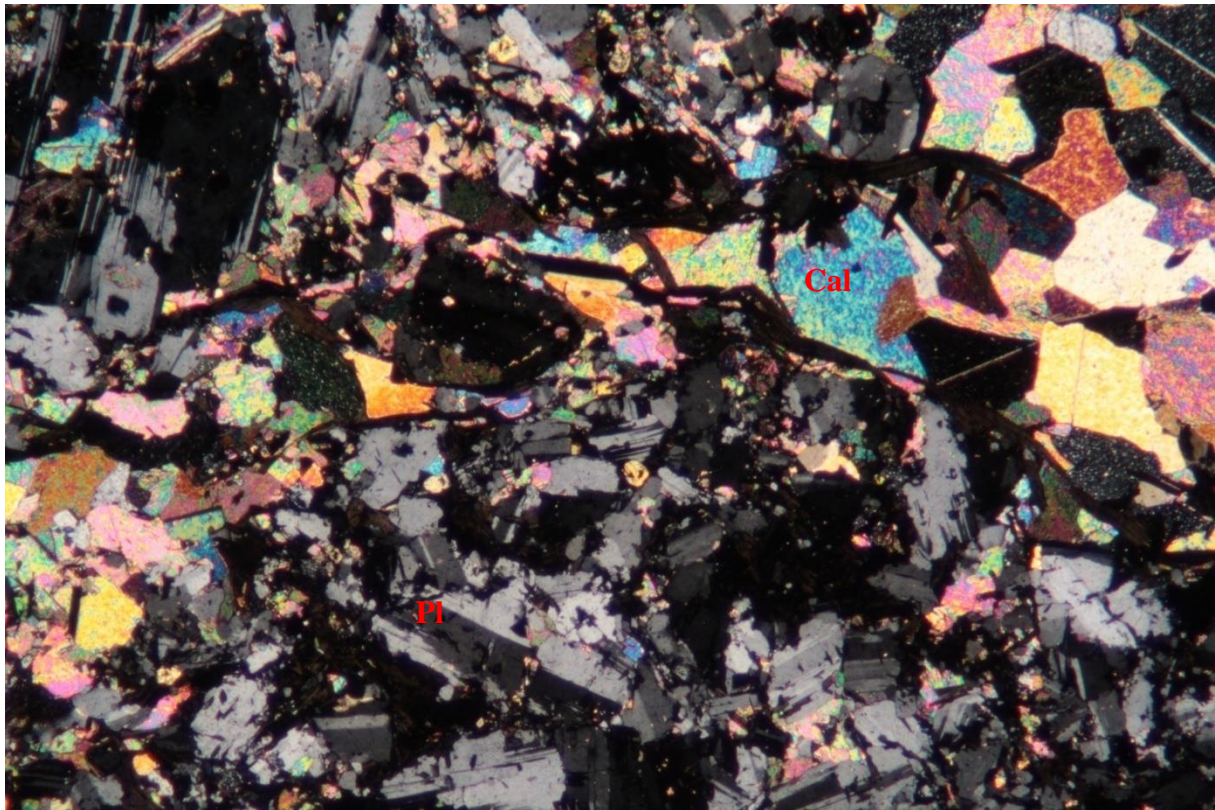
Figure 10: *Carbonate vein in basaltic metaandesite. Note how plagioclase makes up a large portion of the rock. Plagioclase is present together with lesser amounts of chlorite. From TSK 11 - M2. Width of field: 3.6 mm.*

3.1.1.2. Quartz keratophyres

Quartz keratophyres are leucocratic sodic felsic volcanic rocks, and can be classified as either quartz-albite-phyric or albite-phyric depending on which minerals constitute the porphyroclasts in the rock. Quartz keratophyres are distinguished from keratophyres by being felsic, whereas "true" keratophyres are of intermediate composition in terms of SiO_2-content. Both varieties may be aphyric (Schermerhorn, 1973). Any mafic silicates that have been present are now represented by dispersed chlorite.
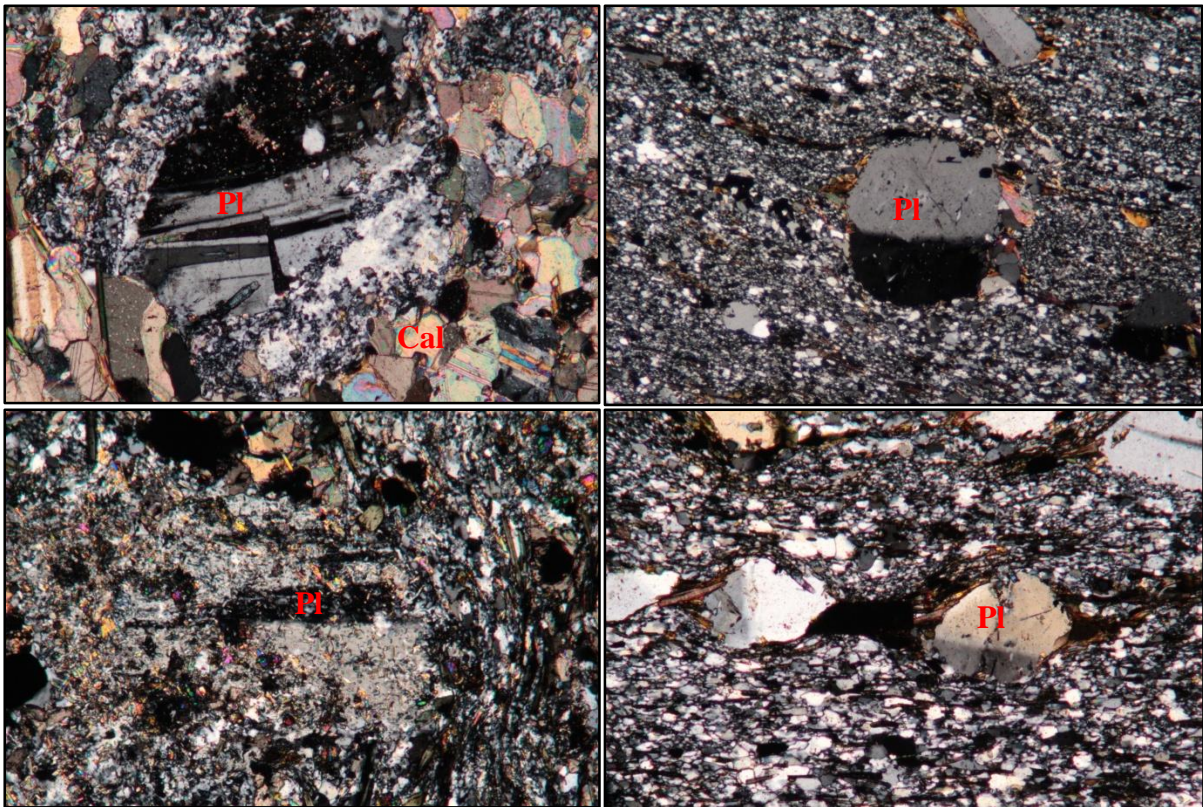
Figure 11: *Albite porphyries in fine grained quart-feldspar(-biotite-chlorite) groundmass. Top left: Albite-phyric quartz keratophyre, with plagioclase in association with carbonate vein from TSK 3 – M10. Width of field: 1.8 mm. Top right: Plagioclase porphyroblast in fine grained quartz-rich groundmass, with layering defined by biotite. From sample TSK 10 – M11. Width of field: 1.8 mm. Bottom left: Heavily sericitized plagioclase grain in matrix of quartz, biotite and white mica, the latter assumed to be the product of sericitization of other plagioclase grains. Sample TSK 5 – M5, width of field: 1.8 mm. Bottom right: Albite- twinned, rounded plagioclase fragments in quartz rich matrix, with bands of biotite and opaque minerals. Note the localization of biotite and opaque grains to plagioclase pressure shadows. TSK 10 – M11, width of field: 1.8 mm.*

Disseminated sulphides are present throughout the samples, generally very fine grained, with some larger grains occurring in or around quartz veins. The samples typically consist of a matrix of aphanitic quartz and microlitic plagioclase (likely albite) throughout which larger phenocrysts of plagioclase are dispersed (see Fig. 11). Most of the samples also contain chlorite. Due to the aphanitic nature of the matrix it is difficult to determine the exact proportions of quartz and plagioclase present in the samples. Generally, the quartz keratophyre samples contain 40-60% quartz, 10-30% plagioclase (most of the typically aphanitic matrix has been judged to be quartz, but it is as mentioned borderline impossible to positively identify due to grain size), chlorite (0-30%) (in some samples partially chloritized biotite) and accessory pyrite. Some of the samples also contain accessory amounts of calcite and garnets. The quartz keratophyres seem to have originated as tuffs due to the presence of larger feldspar pyroclasts (e.g. Figure 11), generally composed of chlorite and plagioclase. These tuffs are composed of material from rhyolite/rhyodacite felsic volcanics, subsequently metamorphosed under greenschist facies conditions (Sandstad et al., 1996).

3.1.1.3. Felsic dike

The only sample that fits this description comes from trench 1 (TSK 1 – M15), which cuts through the main surface mineralization. It is similar to the quartz keratophyres in composition, with 60-70% quartz, ~30% biotite/chlorite, with clinozoisite and disseminated sulphides as accessory minerals (see Fig. 12). There is also some white mica. It appears in hand samples as a light, almost white, rock with green chlorite bands and small spots of rust on fresh surfaces from the sulphides, though the weathered surface is extensively rust coloured due to its immediate proximity to the main sulphide mineralization. The quartz is inequigranular, and fine grained. It differs from the quartz keratophyres in lacking any pyroclasts or porphyroclasts, and also in containing no visible feldspar. There might be feldspar among the aphanitic quartz groundmass, but it is due to grain size hard to tell. Indications from geochemical analysis of the sample do make it likely however, as there are moderate amounts of Na and K present. There is also the possibility that this is not intrusive, but that it rather represents the quartz-phyric variety of quartz keratophyres.
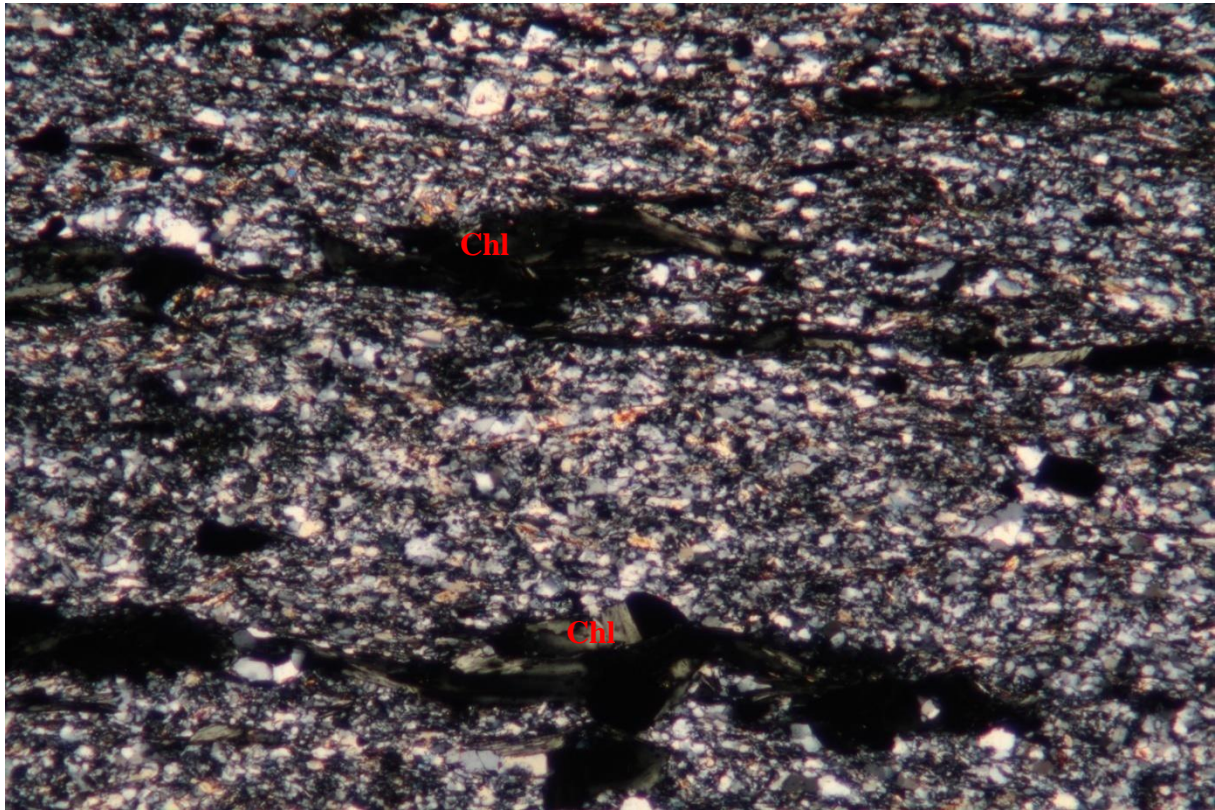
Figure 12: *Fine grained quartz with chlorite (dark, elongated grains) and opaque minerals from TSK 1 - M15. The banded appearance of the rock is defined by the chlorite. Width of field: 3.6 mm.*

3.1.1.4. Pyroclastic rocks

These rocks consists of tuffs and volcanic breccias of mixed felsic-mafic affinities. As mentioned, some of the pyroclastic rocks seem to share the characteristics of the quartz keratophyres, so the tuffs, tuffites and/or tuffitic rocks mentioned here will be the ones that have originated primarily from more mafic materials. The tuffs are distinguished by the presence of pyroclastic materials. In accordance with IUGS classifications, adopted from Schmid (1981), a tuff is a rock containing <75% pyroclastic fragments, a tuffite contains 25-75% pyroclastic fragments, and a rock containing >25% pyroclastic fragments can be described as tuffitic. In the case of the Gjersvik Nappe and the degree of deformation and metamorphism the rocks have undergone, it is however on occasion difficult to distinguish between the individual groupings, or even between tuffs and breccias. I will as a result refer to the rocks as pyroclastic, rather than make vague and unfounded assumptions regarding the percent-wise distribution of pyroclastic contents. Compared to the quartz keratophyres, the mafic pyroclastic rocks contain less quartz and plagioclase and more biotite, chlorite, epidote
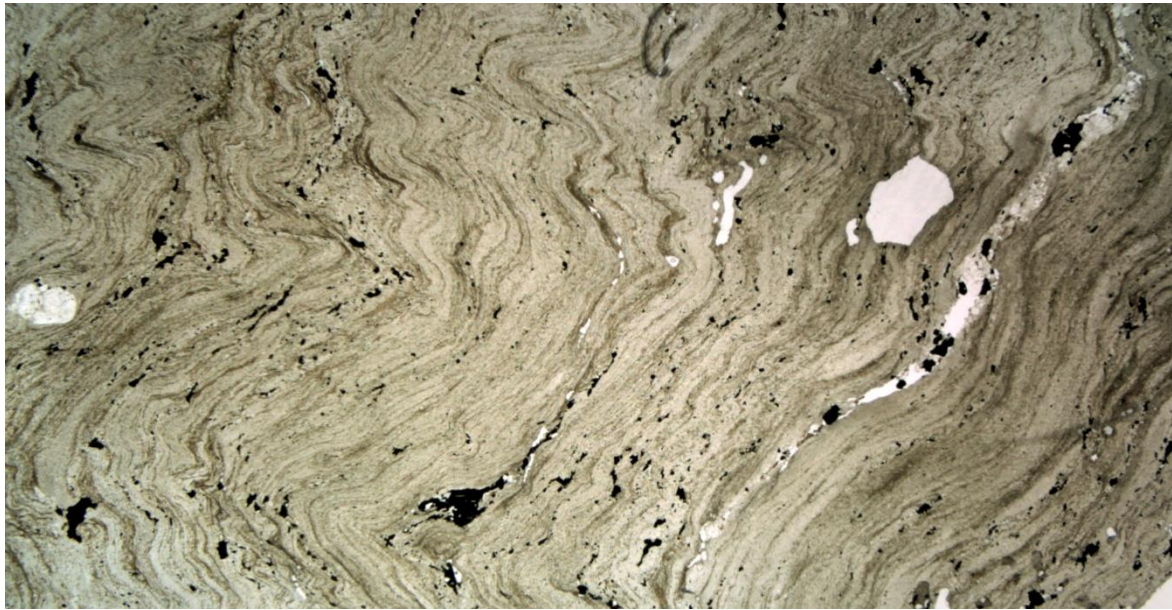
Figure 13: *Thin section TSK 14 - M3, scanned. Note the microscale folds and alternating bands of quartz and chlorite-biotite mica. Also note the localization of sulphides to fold hinges.*
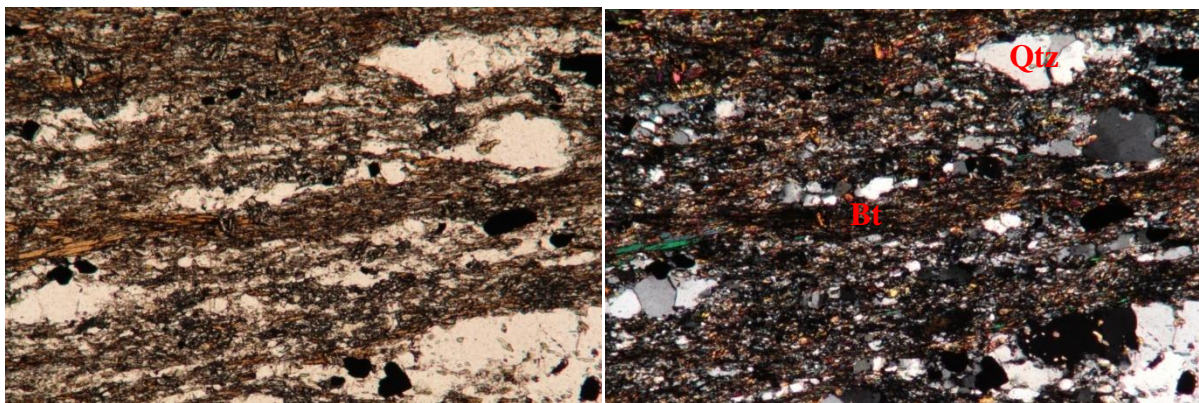
Figure 14: *Photomicrograph from TSK 14 - M3, showing layers of chlorite-biotite and quartz aggregates. Width of field: 1.8 mm. PPL (left), XPL (right).*

and disseminated sulphides. Generally, the mineral assemblages can be said to be quartz (15-30%), feldspar (0-5%), chlorite and biotite (25-70%), with smaller amounts of disseminated sulphides and epidote. The typical mineral assemblage for these pyroclastics is approximately 30% quartz, 5% feldspar, 50% biotite/chlorite (interpreted as remnants of mafic and ferrous silicates), 10% disseminated sulphides and 5% epidote (see Fig. 13 and 14). Some of the samples also contain carbonates. The disparate mineral assemblages are a result of the mixture between the mafic and felsic affinities of the pyroclastics. Some of the rocks initially thought to be of extrusive origin might actually represent intrusive basaltic lava flows. Halls

et al. (1977) describes similar rocks from the Skorovas area, there thought to represent a tectonic facies originating as metamorphosed and flattened mafic flows, thereby not of sedimentary or extrusive origin as initially thought.

3.1.1.5. Quartzite

One sample (TSK 10 – M10) contains ~90% quartz and ~10% sulphides/opaques, and is as such referred to as a quartzite. In trench 10, this quartzite forms a ~25 cm thick layer in the surrounding quartz keratophyre, extending across the width of the trench. It is not observed in adjacent trenches, but extends over 10 meters along the length of trench 5. The rock is roughly equigranular with relatively coarse grain size, with the grains showing some elongation as a result of strain. This is also evident from the direction of the disseminated sulphides and opaque minerals, which are localized in bands. The quartz associated with these bands often has a smaller grain size than the more monomineralic quartz layers (see Fig. 15). The rock could be of sedimentary origin, and as such represents a somewhat anomalous feature of the deposit, as it would be the only non-volcanogenic sedimentary rock found. It might also represent a zone of intense silicification (e.g. Galley, 1993), or a metamorphosed chert layer. Present in the thin section are also two large round chlorite aggregates, possibly pseudomorphs of pyroxene (or garnet, due to the shape) (see Fig. 16). This chlorite differs from the chlorite found in the other samples by being of an optically negative variety, indicating a composition favoring Mn and Cr over Mg (Nesse, 2000). Minor amounts of carbonates and biotite are also found related to the opaque bands.
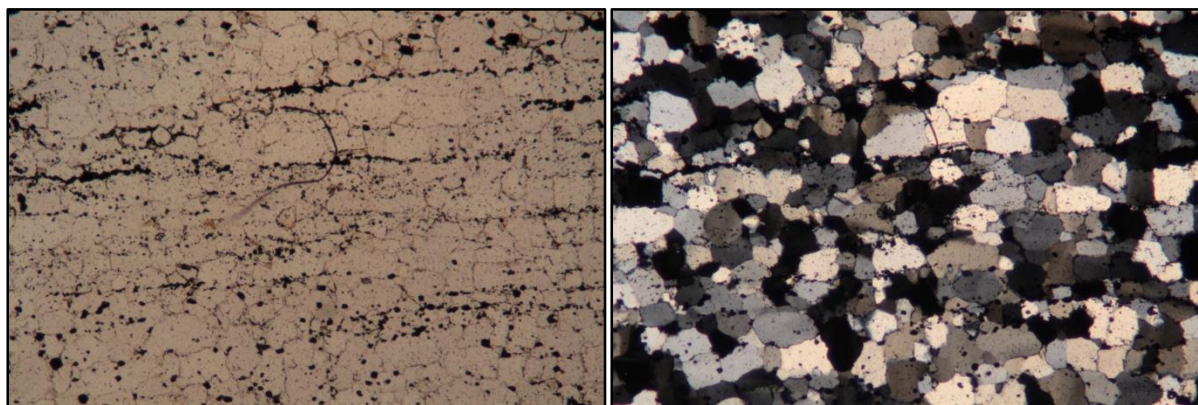
Figure 15: *TSK 10 - M10, quartzite. PPL to the left, XPL to the right. Note how the opaque minerals are localized in bands. Width of field: 3.6 mm.*
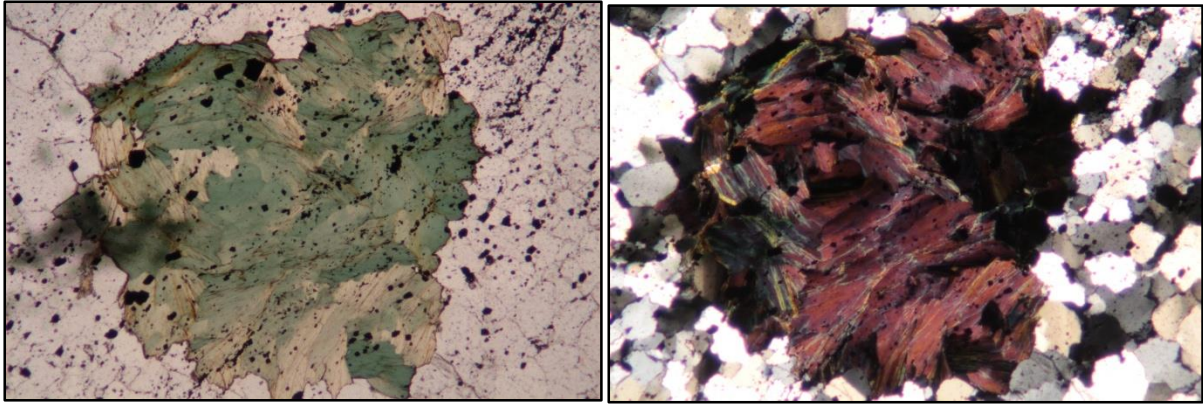
Figure 16: *One of the two large chlorite aggregates present in the sample. PPL to the left, XPL to the right. Note the anomalous interference colors, typical of optically negative chlorite varieties, which indicate a composition favoring Mn and/or Cr over Mg (Nesse, 2000).Width of field: 3.6 mm.*

3.1.1.6. Massive sulphides

This section contains descriptions of the massive sulphide bearing samples in PPL/XPL. Descriptions of the same samples using reflected light microscopy are located in chapter 3.2. The descriptions here will as such primarily encompass the non-opaque minerals. The samples included in this group contain 40-60% opaque minerals (sulphides), ~40% quartz and 10-20% micas (biotite, chlorite and muscovite). Some samples contain accessory epidote. Based on the non-opaque minerals present, the massive sulphides can be divided into three separate groups, namely those representing the main Cu-Zn ore zone (e.g. TSK 1 – M14), the massive sulphides that are enriched in precious metals but contain less Cu and Zn (e.g. TSK 7 – M5) and the opaque minerals that appear as banded pyrite-magnetite-quartz sediments (e.g. TSK 13 - M4), the latter being typical of reduced facies of iron rich exhalatives (Halls et al., 1977). The samples from the Cu-Zn rich sulphides are primarily associated with quartz and minor amounts of white mica, with the quartz being relatively coarse grained. The white micas often form large aggregates, which is likely a result of deformation around the more mechanically competent pyrite and quartz grains. The samples associated with the highest concentration of precious metals, i.e. Ag and Au, contain quartz, chlorite and accessory amounts of epidote, and shows a *durchbewegung* texture (see Fig. 22) (Vokes, 1969; Craig & Vaughan, 1994). The quartz here is very fine grained, almost aphanitic, and localized in aggregates and bands. The quartz dispersed between the sulphide grains has a slightly larger grain size (see Fig. 17). Epidote is found together with the quartz grains, and the chlorite is
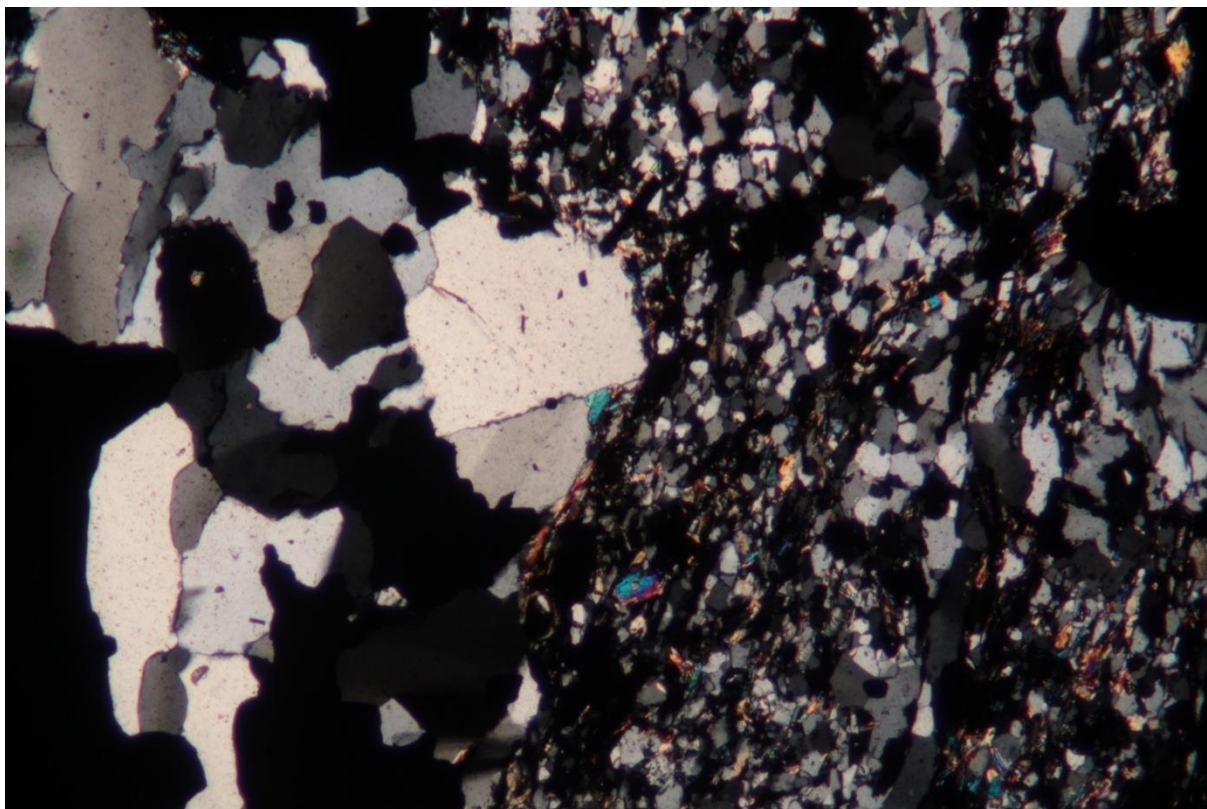
Figure 17: *Semi-massive sulphides from sample TSK 1 – M14-1 in XPL. Black areas represent the opaque minerals. Note the variation in quartz grain size, where the larger grains are associated with large pyrite grains, whereas the smaller grains and micas are associated with the interstitial groundmass. Width of field: 3.6 mm.*

generally found together with the sulphides, though smaller chlorite crystals are present in the quartz. Both of the above rocks, when viewed in hand samples rather than thin sections, can be seen to contain several clasts and quartz and chlorite rich fragments, with small (mm to cm scale) folds and bands, which are likely remnants of pyroclastic material. Similar features do not occur in the samples thought to represent banded pyrite-magnetite-quartz sediments, which are of exhalative origin. These samples are clearly banded in nature, with alternating bands of pyrite and quartz, with disseminated, fine grained iron oxides spread throughout, and also on occasion forming separate bands (see Fig. 24). They are likely to have formed in an environment distal from the focus of the magmatic activity.

3.2. Observations in reflected light

This section covers observations of the thin sections using reflected light microscopy. See section 3.1.1.6 for a description of the non-opaque minerals present in the samples from mineralized zone.

3.2.1. Samples from the mineralized zones

As covered in section 3.1.1.6., the samples from the mineralized zone can be divided into three separate groups depending on composition, namely the sample(s) enriched in base- and precious metals respectively, and the samples that consist of an iron oxide-pyrite-quartz association, which represents reduced facies of iron rich exhalatives. Due to the nature of the samples, i.e. them being channel samples from the surface of a trench, there is abundant evidence of oxidation and likely subsequent leaching of base metals. This is also evident from observations in thin sections, where chalcopyrite and sphalerite grains are pitted (careous) and partially removed, and several of the pyrite grains are skeletal in nature. The latter is likely a result of the reduction in molar volume following the oxidation of the sulphides, which also results in a very porous rock, thereby allowing further oxidation.

3.2.1.1. Base metal-rich massive sulphides

This group is comprised of the TSK 1 – M14 samples, with TSK 1 – M4 likely representing the contact between the base metal rich sulphides and the surrounding host rock. Pyrite is the dominant sulphide mineral, with sphalerite and chalcopyrite present as inclusions within the pyrite grains and along the grain boundaries between pyrite grains (see Fig. 18). The effects of surface weathering are evident, particularly among the sphalerite and chalcopyrite, which are extremely pitted and in some cases partially or completely removed. The grade of the ore from this sample is 0.47% Cu and 0.9% Zn, which reflects this leaching of base metals, as samples from the ore zone in drill cores show grades that are on average more than double what is observed here. Pyrite has also suffered from exposure to surface conditions, with skeletal pyrite grains evident (see chapter 4.3). The larger pyrite grains are less affected by the surface weathering than the smaller grains, which as mentioned display a skeletal texture, with occasional growth of goethite in the gaps left behind.
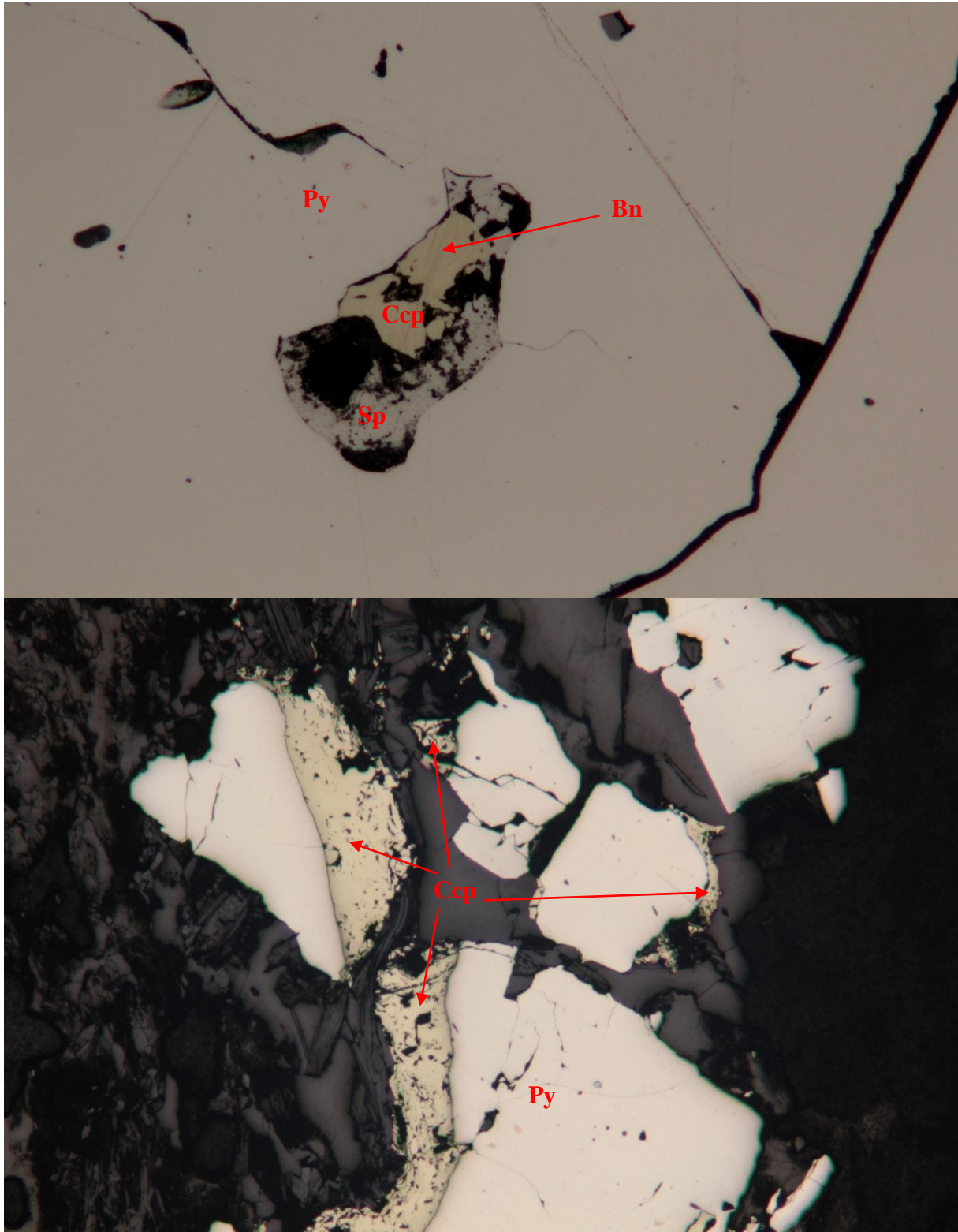
Figure 18: *Top: Chalcopyrite (yellow) and sphalerite (grey) inclusion in pyrite (white). Chalcopyrite contains bornite exsolution lamellae, probably formed at a junction between pyrite grains that has been removed by later crystal growth. TSK 1 – M4; width of field: 0.45 mm. Bottom: Chalcopyrite (yellow) forming at the boundaries of pyrite (white) grains. TSK 1 – M14 - 1; width of field: 3.6 mm.*
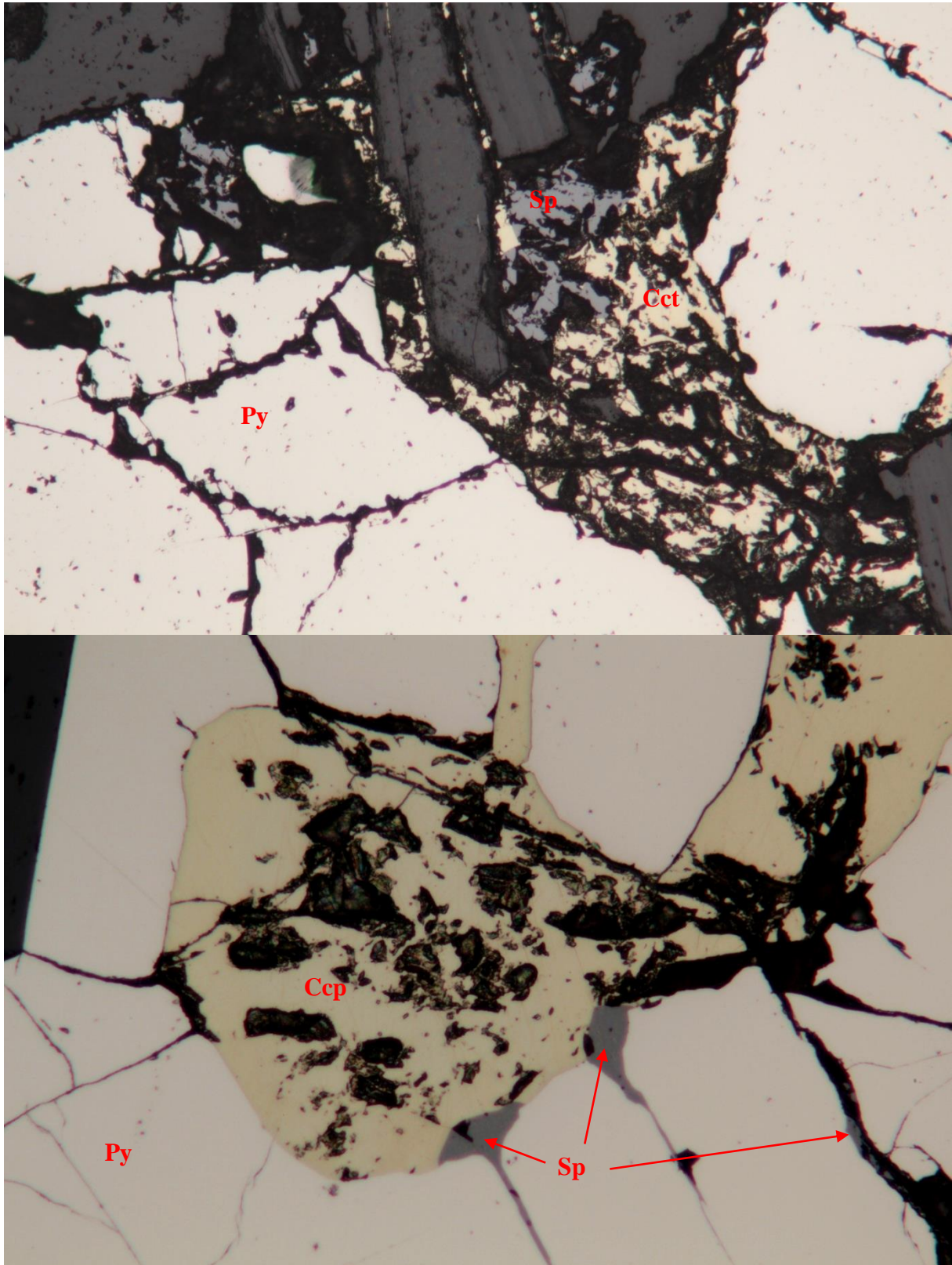
Figure 19: *Top: Careous chalcopyrite (yellow) and sphalerite (grey) between pyrite grains. Polishing pits are shown as black, and silicates as dark grey. TSK 1 – M14-2; width of field: 1.8 mm. Bottom: Chalcopyrite forming at a triple junction in pyrite. Note how sphalerite (grey) has filled in cracks in the pyrite. TSK 7 – M5; width of field: 0.45 mm.*
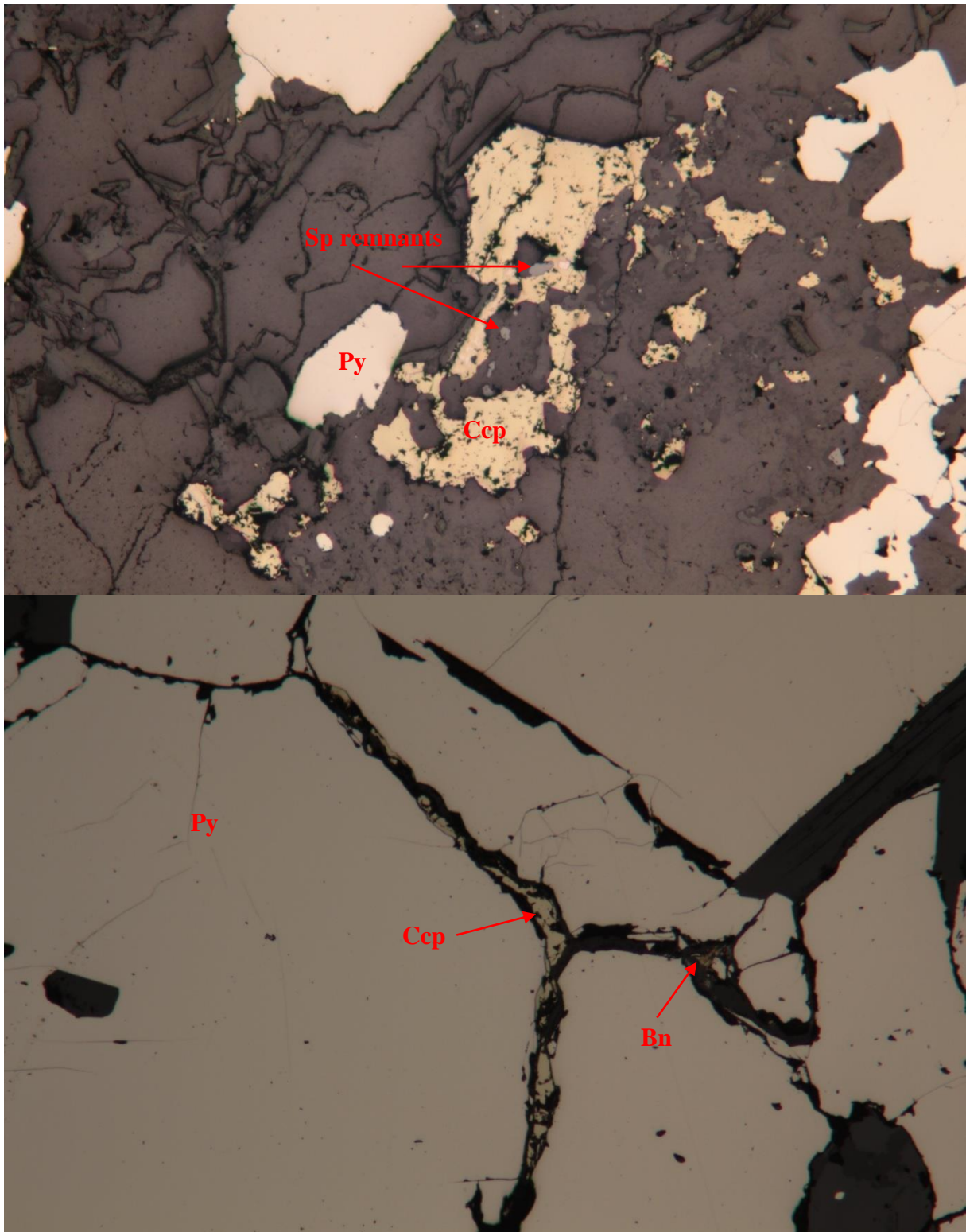
Figure 20: *Top: Chalcopyrite grain, extensively altered and nearly removed by surface weathering processes. Sample TSK 7 – M5; width of field: 3.6 mm. Bottom: Chalcopyrite along grain boundary in pyrite. Note the presence of triple (120°) junctions in the pyrite. This is typically referred to as "foam structure". Note the alteration to bornite along the crack to the right. Sample TSK 7 – M5; width of field: 0.9 mm.*
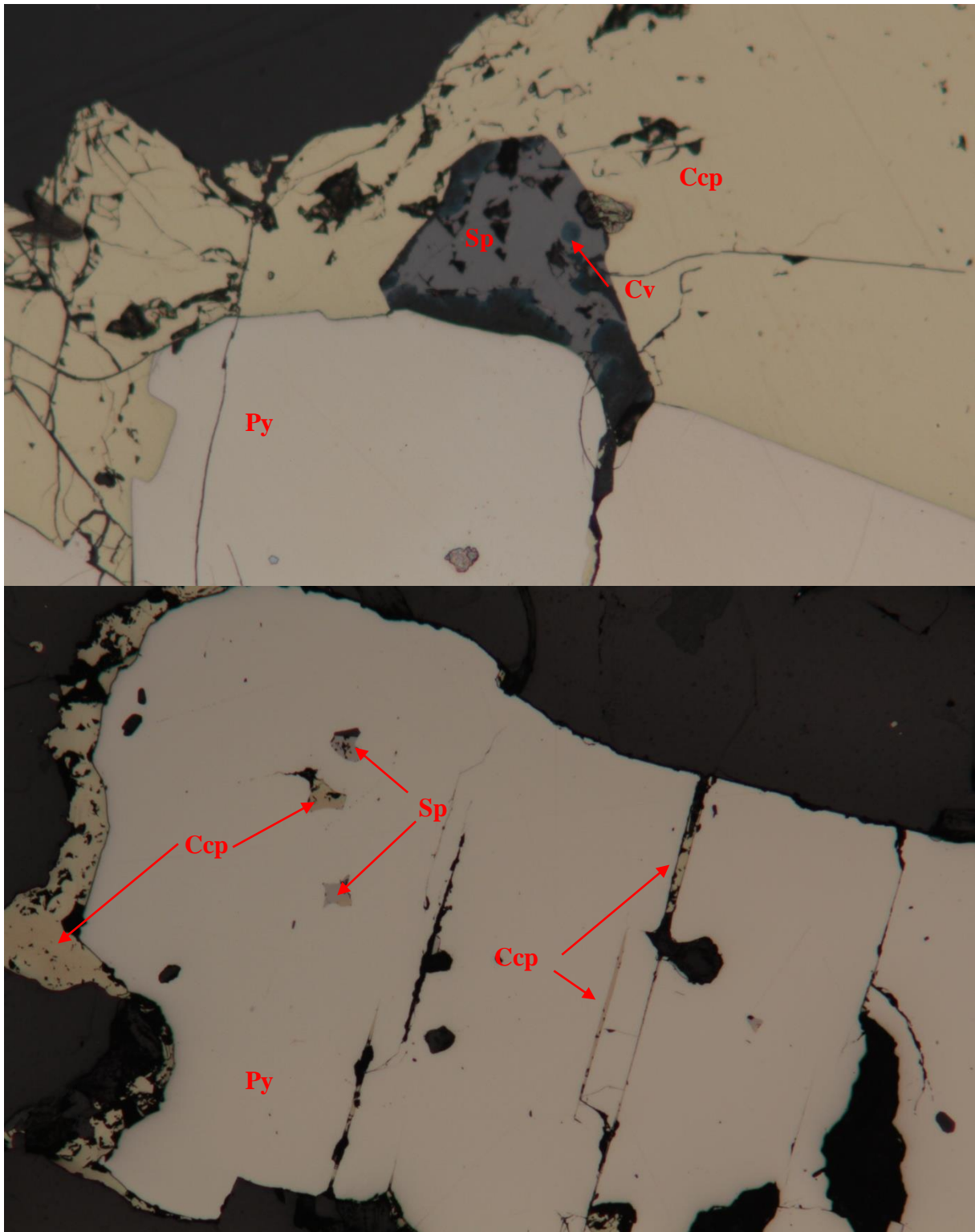
Figure 21: *Top: Chalcopyrite along pyrite grain boundary. Note the presence of covellite (blue) in the enclosed sphalerite grain. Sample TSK 7 – M5; width of field: 0.45 mm. Bottom: Extensional cracks in pyrite with chalcopyrite infilling, as well as chalcopyrite and sphalerite inclusions within the grain (likely at the location of previous triple junctions), and chalcopyrite along the grain boundary. TSK 1 – M14 – 1; width of field: 1.8 mm.*

The blackened and dark areas within partially skeletal grains are likely the result of crystallization of goethite and a result of relief caused by these voids. This also reveals some of the internal structures of the pyrite grains. The large grains that seem to have suffered only limited effects of the surface weathering are on average about 0.4-0.5 mm, and the smaller grains have a size of 0.1-0.2 mm. Several of the cavities between grains contain residual sphalerite and chalcopyrite. Chalcopyrite is in rare cases partially altered to bornite (e.g. Fig. 18).

3.2.1.2. Massive sulphides enriched in precious metals

While the samples with the highest grades of base metals also contain precious metals, the sample with the highest Au and Ag contents by far is TSK 7 – M5. The sample is composed of quartz, chlorite and sulphides (see Fig. 20 and 22), where most of the quartz and chlorite is located in aggregates that have been interpreted as *durchbewegung* textures (Vokes, 1969; Craig & Vaughan, 1994). The sample has likely been subjected to cataclastic deformation, with the sulphides having recrystallized after the deformation. The sulphides, which are primarily composed of pyrite, form larger aggregates outside the lobes and aggregates of quartz and chlorite, and the pyrite shows a foam texture with triple junctions between the different grains at ~120°, which is a typical annealing texture in pyrite. This indicates that there has been recrystallization of pyrite occurring after the deformation in charge of producing the *durchbewegung* texture. Chalcopyrite occurs frequently within the sulphide rich areas, more so than even in the samples that have yielded higher grades for Cu. This is likely the result of a combination of factors, amongst them dilution of the sample material by the quartz and chlorite aggregates, as well as the small sample size utilized for the ME-ICP analysis. Sphalerite is not as abundant, and only occurs as inclusions in pyrite, and locally next to larger chalcopyrite grains. The chalcopyrite is in a few areas partially altered to covellite, and some chalcopyrite also shows bornite exsolution lamellae. The sphalerite locally shows signs of chalcopyrite disease. This is a common phenomenon in VMS deposits and other sulphide bearing metal deposits, and indicates that the Cu mineralization occured later than the Zn mineralization (Ohmoto, 1996). The rarity of chalcopyrite disease in the observed thin sections is likely due to metamorphic re-equilibration, where chalcopyrite has migrated to grain boundaries or similar features (Craig & Vokes, 1993). Bornite exsolution lamellae and replacement of chalcopyrite with covellite and chalcocite are also present (see

49

e.g. Fig. 18, 21 and 23). Bornite exsolution lamellae are the result of compositional or structural adjustments as the minerals cool, either from initial crystallization or from the maximum temperature during metamorphic recrystallization (Craig & Vaughan, 1994). The replacement of chalcopyrite with covellite or chalcocite is a common observation in weathered ores. This happens when iron is preferentially removed from chalcopyrite, forming bornite, and later chalcocite, covellite and digenite. Chalcocite may also form as a result of the alteration of chalcopyrite. These processes are typically associated with supergene enrichment of base metals. The iron is often reprecipitated as goethite, or removed, leaving a careous, i.e. corroded or pitted, texture (Craig & Vaughan, 1994), as the alteration of sulphides to oxides will result in a decrease of molar volume. In the thin sections observed, goethite most often appears black, also in reflected light, due to oxidation and the small size of the individual grains.
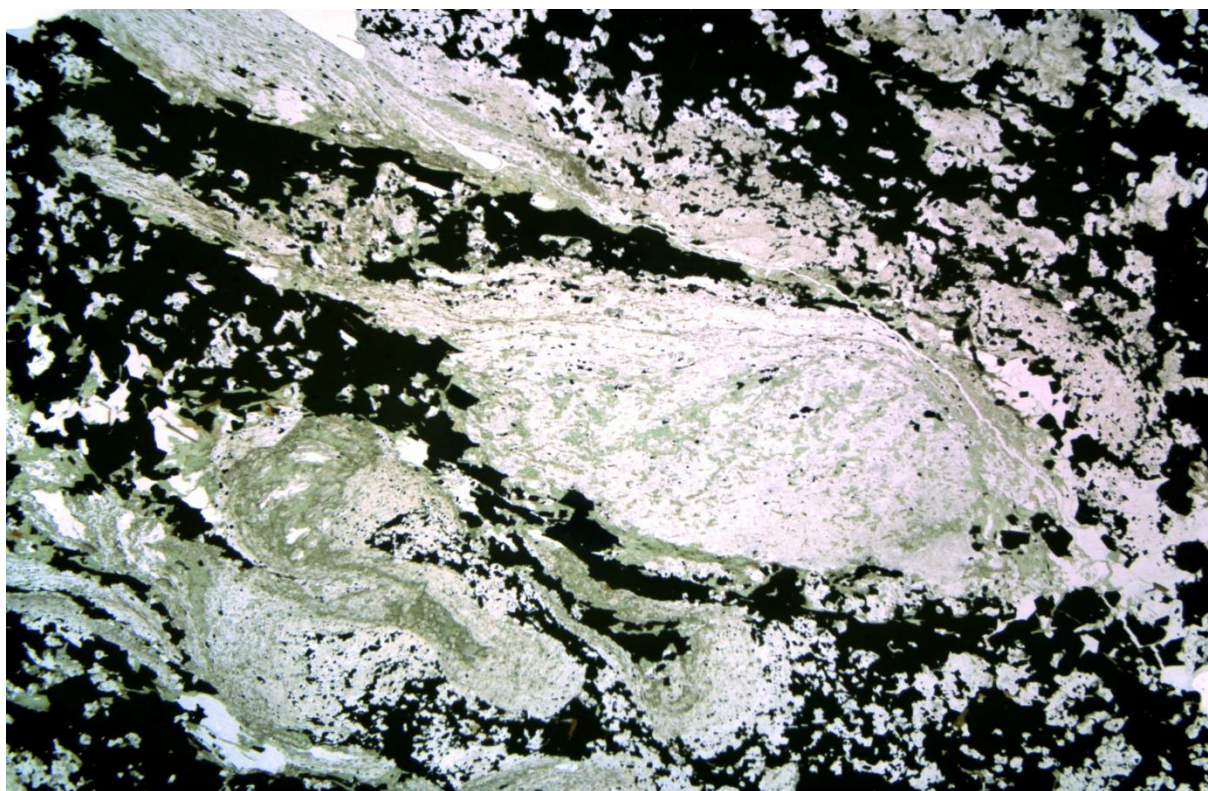
Figure 22: *Durchbewegung texture from sample TSK 7 - M5. Dark areas represent sulphide minerals, white areas are composed of quartz and white mica, and green areas are chlorite. The picture is from a scanned thin section, and represents the entire thin section (width of field: ~3 cm). Durchbewegung textures are observed when the rock is deformed, and silicates are "rolled up" to form spherical aggregates while the sulphides deform by cataclasis. The sulphides later recrystallize, which is evidenced by the formation of a foam structure within the sulphide-rich aggregates.*

50
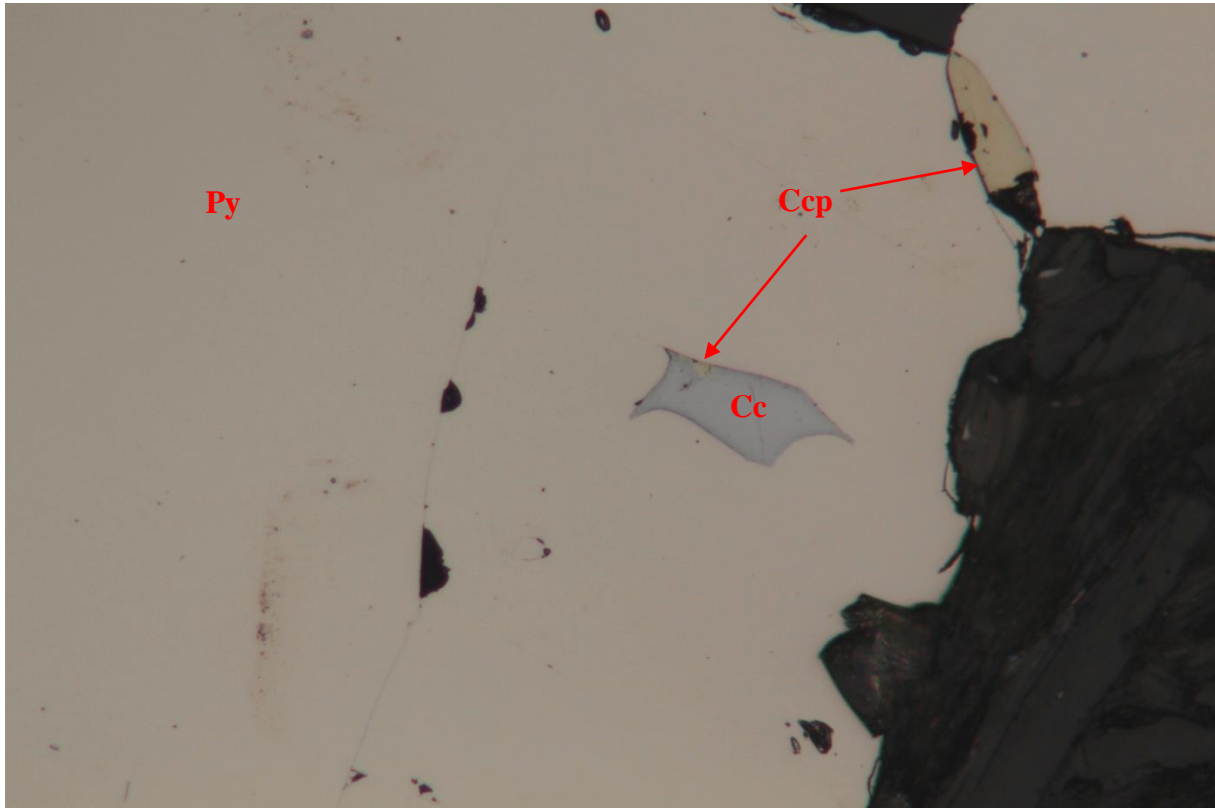
Figure 23: *Chalcocite with minor remnants of chalcopyrite in pyrite grain. Note the chalcopyrite at the boundary between the two pyrite grains. TSK 1 – M14 -2; width of field: 0.45 mm.*

3.2.1.3. Iron-rich exhalatives

The massive opaque minerals present in these samples, TSK 13 – M4 – 1 & 2, are pyrite, while the bands of more fine grained materials are composed of pyrite and iron oxides, likely magnetite and/or goethite. The massive pyrite grains, which have a size typically ranging between 0.5 and 1 mm, are surrounded by a mass of pyrite that has no distinct grain size, boundaries or shape. While the pyrite is easily distinguished, also in hand samples, the fine grained iron oxides, which includes some small pyrite grains, appears as dark and diffuse bands in the rock. Minor amounts of sphalerite are also present. The banded appearance of the rock, as well as the variations in grain size from layer to layer, indicate that it originated as an exhalite (see Fig. 24).
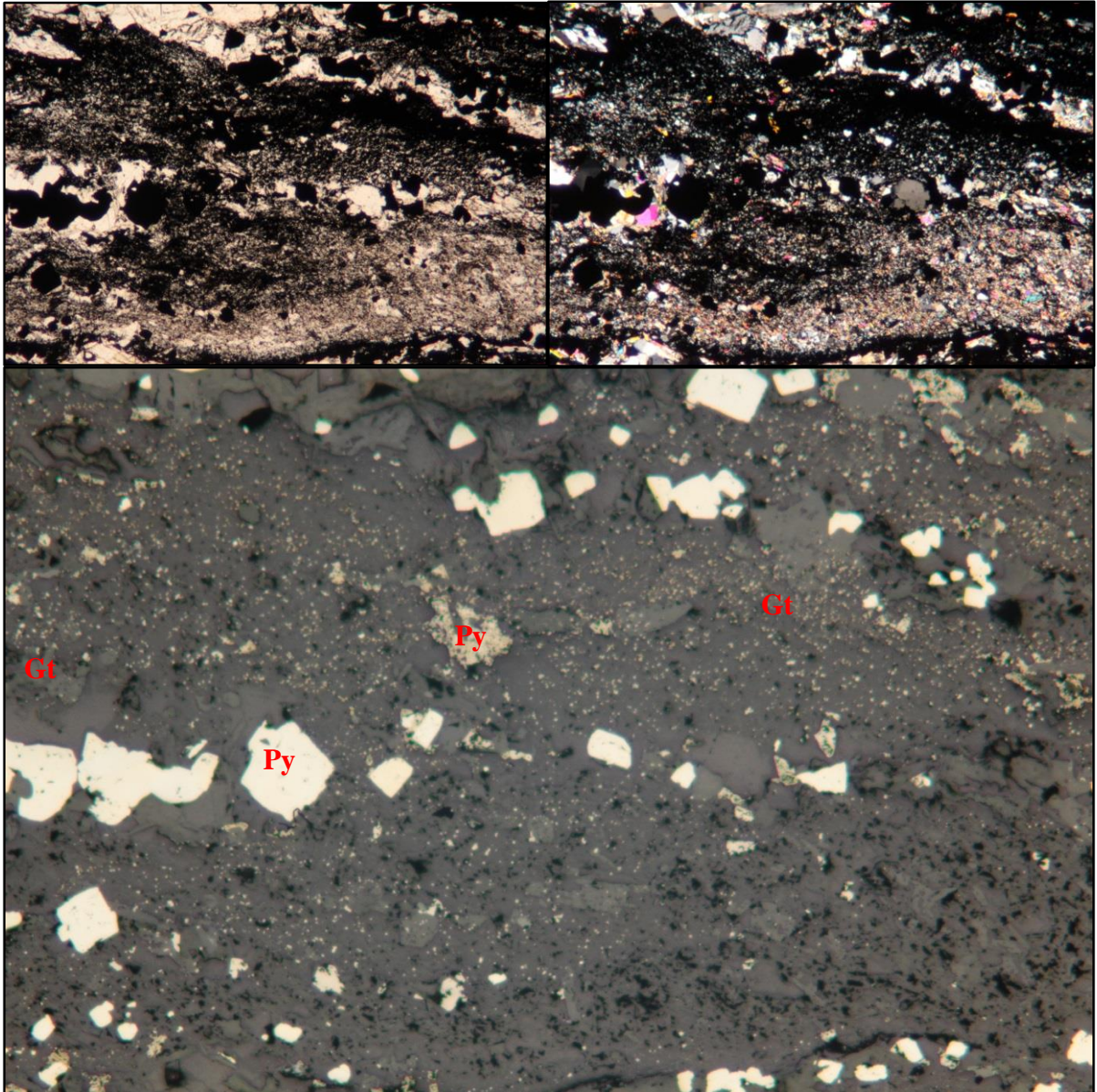
Figure 24: *Iron-pyrite-quartz rich exhalatives from TSK 13 – M4 – 1, with the same section shown in PPL (top left), XPL (top right) and reflected light (bottom). Note the larger pyrite grains, with more fine grained pyrite (white, with weathered grains slightly yellow) and magnetite and goethite (grey) in the bands of fine grained opaque minerals. Width of field: 3.6 mm.*

3.2.2. Disseminated opaque grains in host rocks

The host rocks and other lithologies present also in some cases contain a variable amount of disseminated sulphides and opaque minerals, generally either magnetite/goethite or pyrite. Chalcopyrite and sphalerite are also present as singular grains in some of the samples, though this is not a common occurrence. Some of the grains also show evidence of having been

subjected to surface weathering processes, as is to be expected from trench samples gathered in marshy terrain, in which case some of the sulphides are partially replaced by oxides such as goethite. The presence of sulphides, of which pyrite is the most dominant by far, seems to diminish with increased distance from the mineralized zone, suggesting that the deposition of the sulphides in the host rocks is related to them being percolated by sulphide bearing hydrothermal fluids either during the initial formation of the deposit on the sea floor or remobilization during metamorphic activity.

3.3. Geochemistry

3.3.1. Volcanic and volcanogenic rocks

The geochemical data was primarily acquired using ICP-AES (ME-ICP61) and XRF analyses, as described in chapter 2. The main objective of the interpretation of the geochemical data is the determination of the protoliths of the volcanic and volcanogenic rocks, i.e. metabasalts, tuffs and quartz keratophyres observed in thin section, an important step in being able to describe the genesis of the Skiftesmyr deposit. This will be accomplished using data acquired from trace element XRF analysis of the appropriate rocks. Due to the degree of alteration and metamorphic facies of the sampled material, as well as the effects of surface weathering, plots using Si, such as SiO_2 vs. total alkali, have not been used, as SiO_2 is known to be mobile during alteration (Floyd & Winchester, 1978). Similar problems arise from the use of Ba, Sr, Cr and Ni in plots, where Ba and Sr are particularly mobile during weathering and metamorphism, and Cr and Ni are very sensitive to olivine and pyroxene fractionation (Pearce & Cann, 1973). Ba, Sr, Cr and Ni do provide some useful information that might be of assistance in giving an indication as to how and where volcanic rocks were formed, though they are, together with SiO_2, unsuitable as primary diagnostic elements in the determination of rock type. High contents of Ba is for instance typically associated with volcanic arc basalts, whereas the contents in ocean-floor basalts is generally much lower. The same applies to Sr, though both these elements are affected by greenschist facies metamorphism, and are particularly mobile in association with carbonates. Cr and Ni contents are generally lower in volcanic arc basalts than in ocean-floor basalts, though high contents of Cr, Ni and MgO are also indicative of the presence of e.g. olivine phenocrysts in the original and unaltered basalt. The presence of olivine phenocrysts will result in a reduction of the absolute amounts of Ti,

53

Zr, Y, Nb and Sr present in the sampled material (Pearce & Cann, 1973), essentially diluting the amount of trace elements present. This should be taken into consideration when interpreting the results, as it would cause a systematic error in the representation of the data.

Characterizing the mafic volcanic rocks has been done in accordance with the methods proposed by Pearce and Cann (1973). This method entails first plotting Y/Nb against known mafic volcanic rocks in order to determine the alkalic character of the samples (see Figure 25). This gives an indication of whether the samples are alkalic, transitional or tholeiitic in nature, and compares the Y/Nb ratio to known examples of "within-plate"- (this grouping includes ocean island basalts (OIBs) as well as continental basalts), ocean-floor- and island arc basalts, and is therefore a good indication of the petrologic character of the sampled materials.
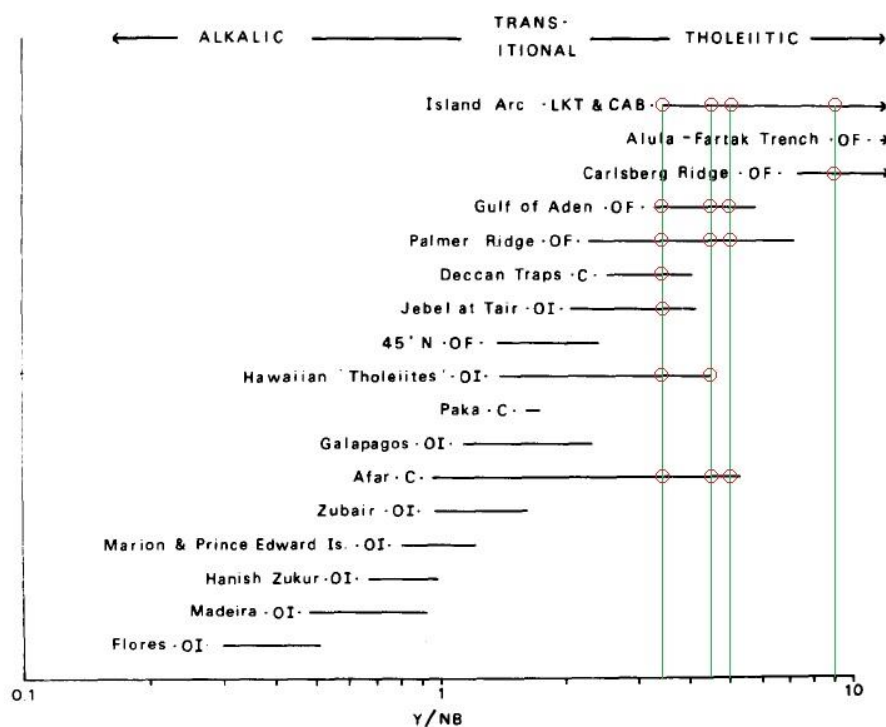
Figure 25: *Determination diagram for distinguishing the petrologic character of the basalts, modified from Pearce & Cann, 1973. Y/Nb for alkalic basalts is <1 for WPBs and <2 for OIBs. Y/Nb for tholeiitic rocks is >2 for WPBs and >3 for OIBs. The green lines indicate samples of Skiftesmyr metabasalts, with red circles emphasizing the intersections with known basalts from around the world. As can be seen from the diagram, the best fit for the Skiftesmyr samples is LKT and CAB tholeiitic island arc basalts.*

The second step is to produce a ternary plot of Ti, Zr and Y to more accurately discriminate between ocean island and continental basalts (WPB), ocean-floor basalts (OFB), low-K tholeiites (LKT) and calc-alkaline basalts (CAB), with the distinction between WPB and the rest being the most important (see Figure 26). Once it has been determined that the samples have not originated as WPBs, the next step is to identify whether or not the sample is altered, weathered or been subject to metamorphism. This is to be able to choose the elements to be plotted in order to give the best possible representation, with respect to element mobility in different situations. In this case, a plot of Zr and Ti will be used, as plotting Ti, Zr and Sr, while offering a more comprehensive interpretation of the geochemical data, will be less accurate due to Sr mobility during metamorphism, alteration and weathering. The plot of Zr vs Ti will provide a good representation of whether the samples originated as OFBs, LKTs or CABs (see Fig. 27).
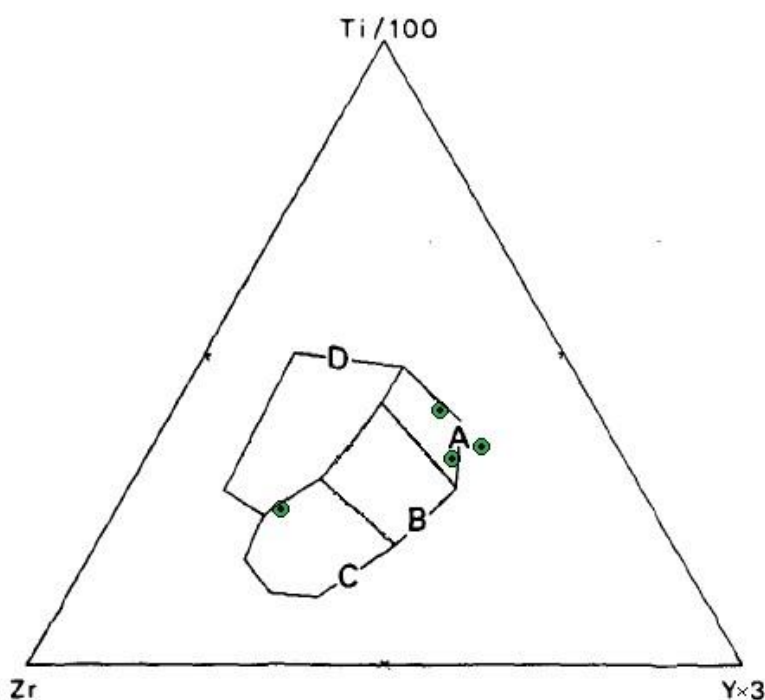
Figure 26: *Ternary plot of Zr, Y and Ti, modified from Pearce and Cann (1973). The primary purpose of this diagram is distinguishing between WPBs and island—arc and seafloor basalts (LKTs and CABs). WPBs plot in field D, LKTs in fields A and B and CABs in fields C and B. Sampled metabasalts from Skiftesmyr are represented as green dots, with the majority plotting firmly in field A, i.e. representing low-K tholeiites. Sample TSK 11 – M2, which plots in field C, is also distinct from the other samples in being of andesitic composition. The geochemistry as such reflects the observations made in thin sections.*

55
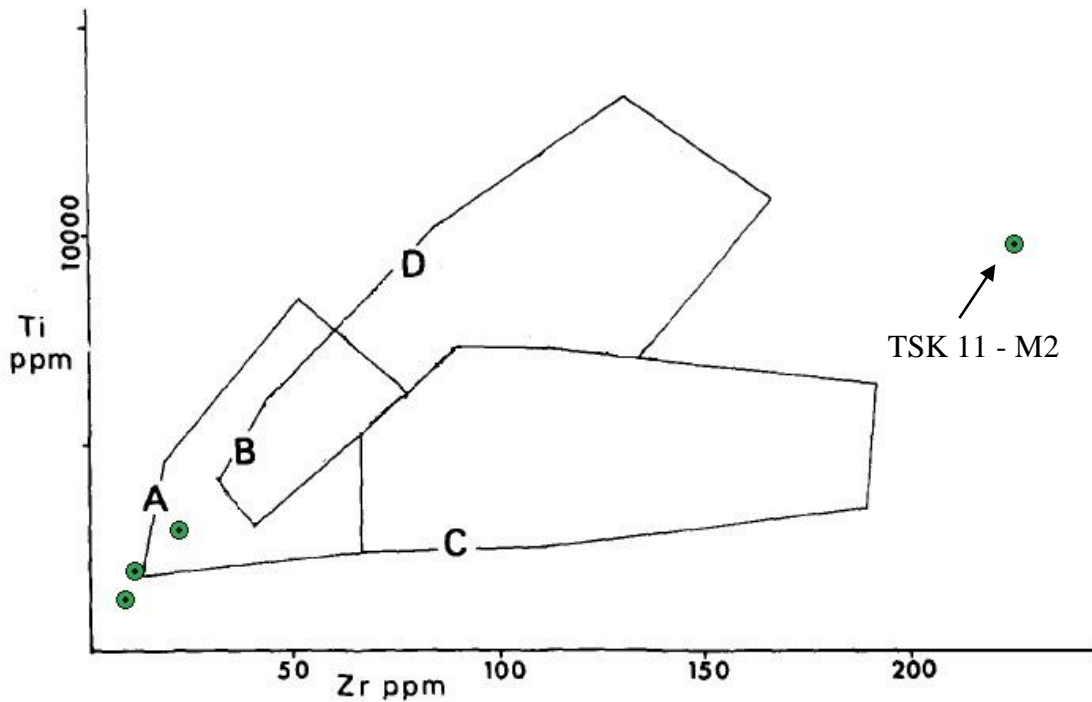
Figure 27: *Discrimination diagram using Zr and Ti from Pearce and Cann (1973). This diagram was chosen preferentially over a ternary Zr, Sr and Ti plot due to it being less influenced by element mobility during greenschist facies metamorphism. Fields A and B represent LKTs, C and B represents CABs and OFBs are plotted in fields D and B. As is evident from the figure, most of the samples plot in field A, indicating that they are low-potassium tholeiites, with sample TSK 11 – M2 as somewhat of an outlier, as in the previous figure. The location of sample TSK 11 – M2 is consistent with data obtained for CABs in Pearce and Cann (1973), though it should be noted that the main density of CAB samples plot in field C.*

The tholeiitic, or subalkaline, trend observed in most of the samples is caused by fractional removal of olivine during crystallization, leading to an increase in the Fe content relative to Mg. Tholeiitic basalts are also reduced, as opposed to calc-alkaline basalts, which are oxidized (Blatt et al., 2006). The tholeiitic and calc-alkaline trends are typically displayed in an AFM diagram, a ternary plot of $Na_2O + K_2O$, MgO and $FeO + Fe_2O_3$, as displayed in Figure 28. Due to the effects of metamorphism and spilitization (a seafloor metasomatic alteration of primary basalts resulting in an increase in e.g. Na) on the igneous rocks of the Skiftesmyr deposit, in addition to variations in Fe content due to sulphide disseminations, such a diagram has some inherit flaws when applied in this situation. To reduce these inaccuracies, total Fe has been recalculated to FeO for samples with relatively large amounts

of sulphide disseminations, though the reader should still be aware that this representation is, at best, meant to give a rough indication of the types of igneous rocks present and the trend of fractionation, and to corroborate the observations previously made in this section.
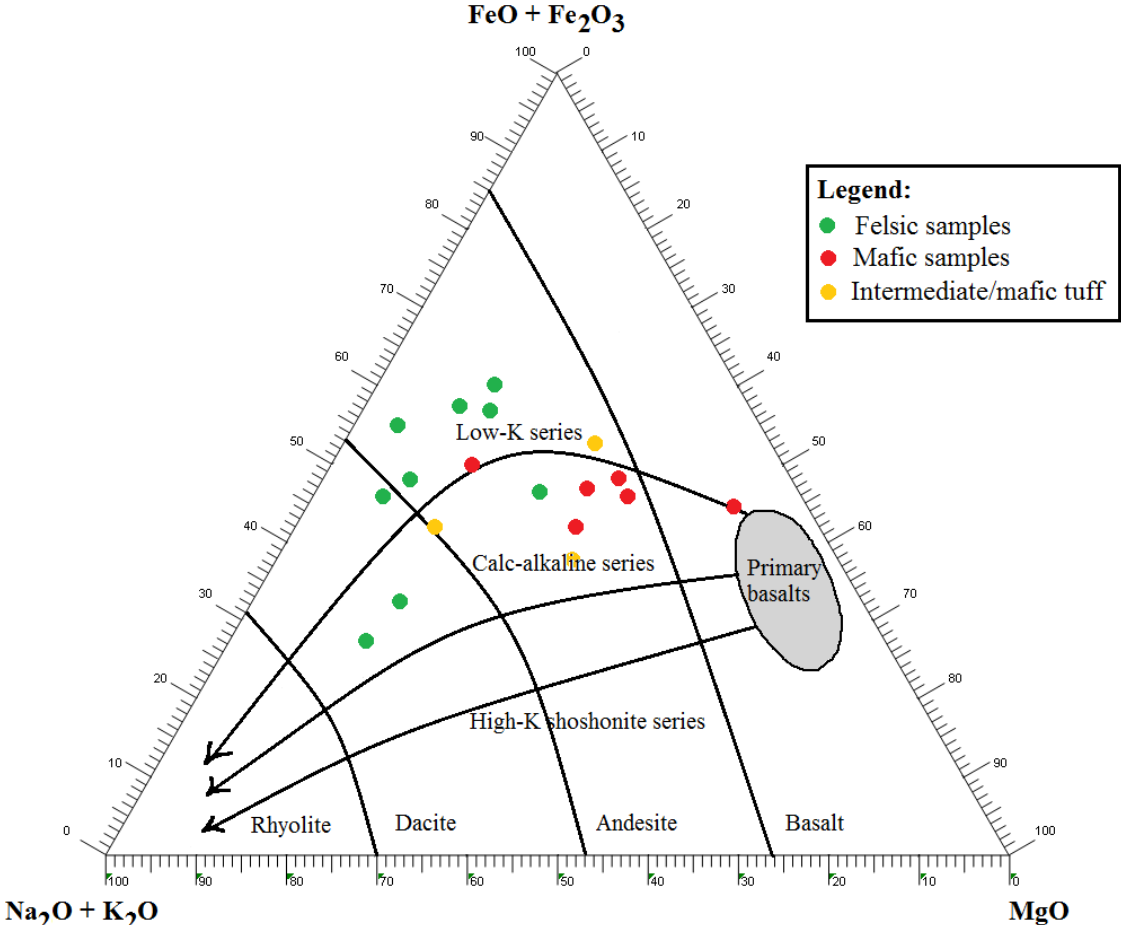
Figure 28: *AFM diagram showing the calc-alkalic trends, modified from Blatt et al. (2006). The compositional ranges are approximations. The Skiftesmyr samples are marked as red, green and yellow dots, with the red dots representing mafic samples (predominantly metabasalts), the green dots representing felsic samples (primarily quartz keratophyres) and the yellow dots representing intermediate/mafic tuffs. A low-K trend is evident, confirming previous observations.*

While figures 25-27 have been optimized as well as possible with respect to the metamorphic grade and degree of alteration and weathering observed in the samples, Floyd and Winchester (1976) propose some more immobile element discrimination diagrams, utilizing Ce and Ga as well as Ti, Zr, Y and Nb, tailored for use with metamorphosed and altered samples (see Fig. 29-30).
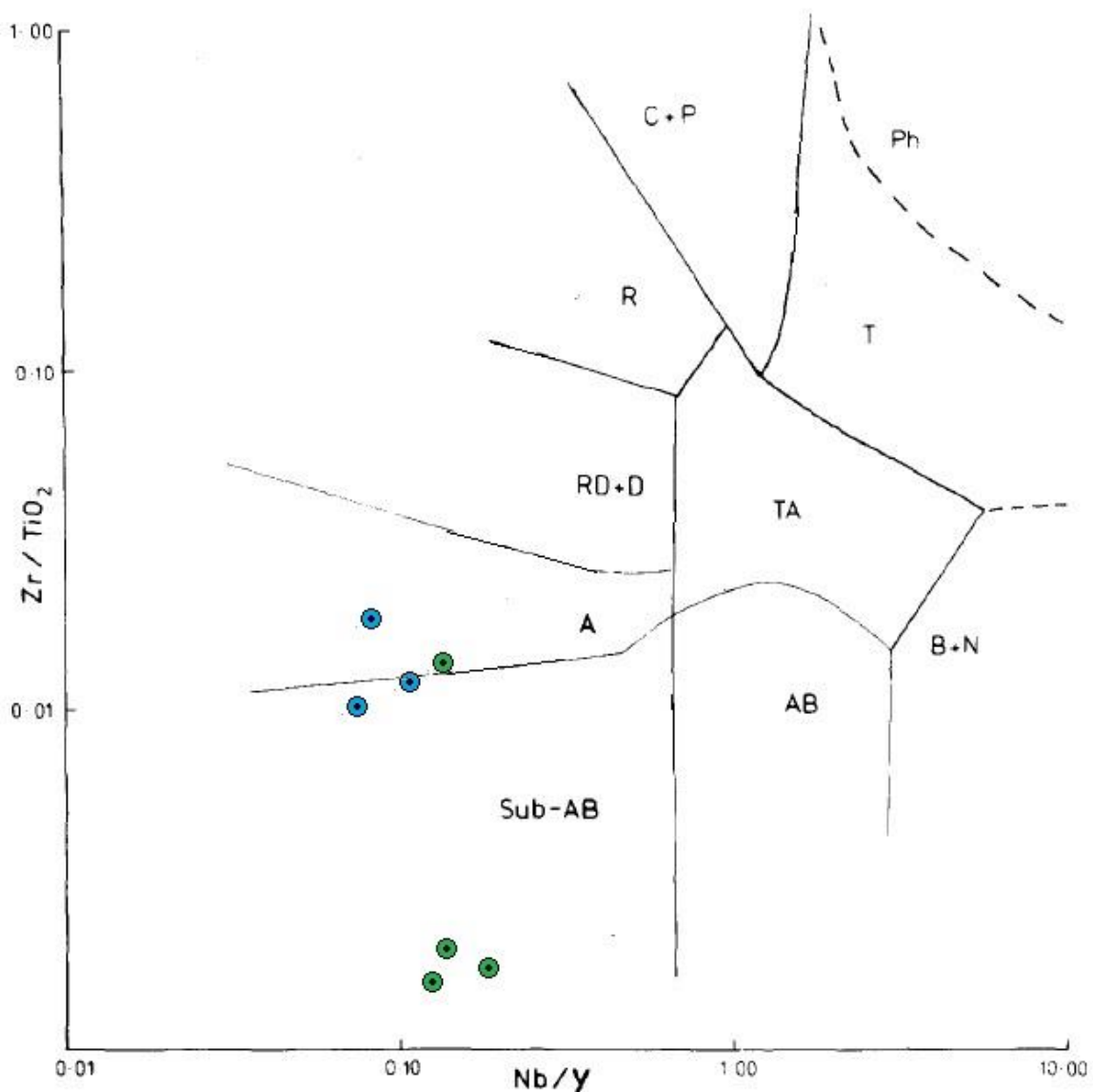
Figure 29: *Discriminative plot of Nb/Y and Zr/TiO₂ from Floyd and Winchester (1978).*
Metabasalts are shown as green dots, whereas the felsic samples (predominantly quartz
keratophyres) are shown as blue dots. The diagram is based on various samples from
greenschist, amphibolite and granulite facies meta-volcanic suites from around the world.
The relatively high Cr-contents in several of the samples might however indicate the
possibility of a systematic error in the Zr/TiO₂ ratio. This is particularly true for some of the
metabasalts. Rock group subdivisions (applies to diagrams 29-31): AB = alkali basalts,
hawaiities, mugearites, trachybasalts; Sub-AB = sub-alkaline basalts (tholeiitic and high-
alumina); B + TB + N = basanites, trachybasanites, nephelinites; A = andesites; D + RD =
dacites and rhyodacites: R = rhyolites; TA = trachyandesites; T = trachytes; Ph =
phonolites; C + P = comendites and pantellerites.

58
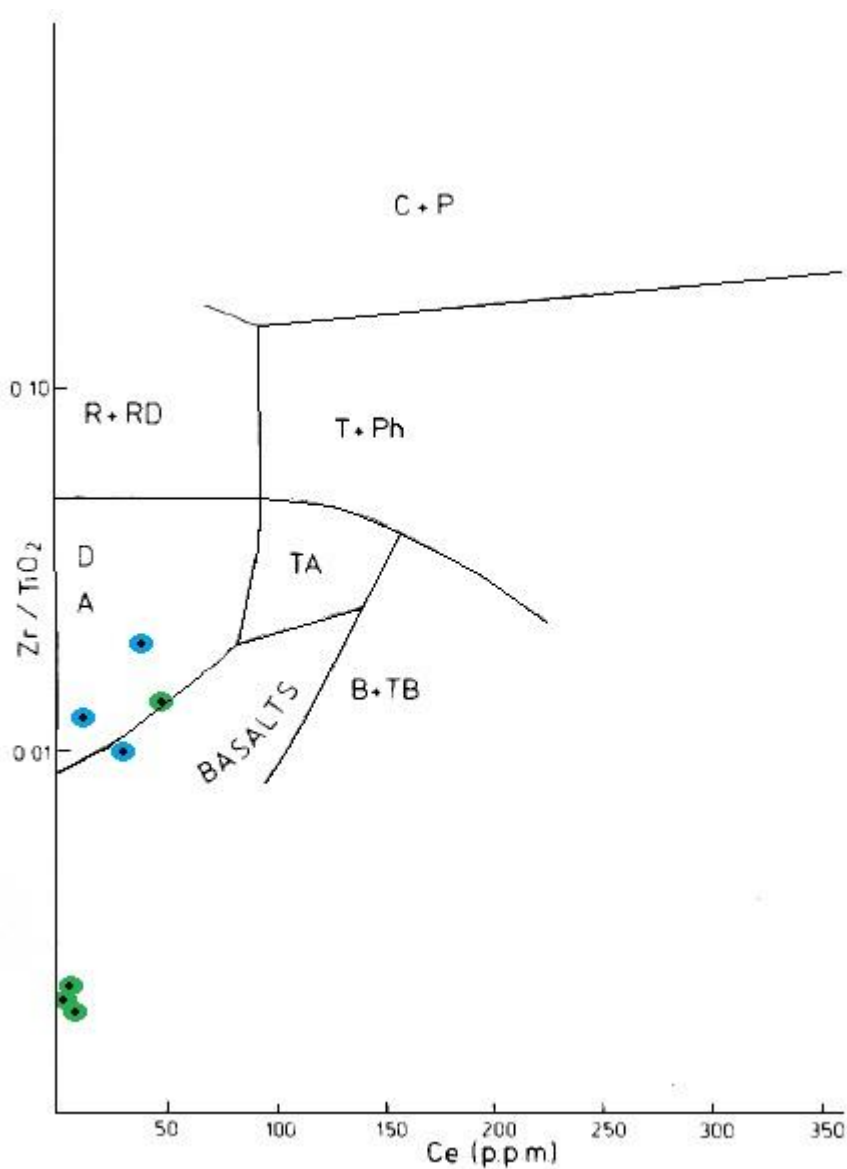
Figure 30: *Discrimination diagram of Zr/TiO$_2$ – Ce from Floyd and Winchester (1978).*
Metabasalts are shown as green dots, and felsic samples (predominantly keratophyres) are
shown as blue dots. The division of subgroups of rock types is the same as in Figure 29. The
immobile elements chosen for these plots, specifically the Zr/TiO$_2$ ratio, has been shown to
remain essentially constant throughout metamorphic processes and spilitic alteration, due to
a sympathetic increase in the respective elements. The metabasalt plotting at the
basalt/andesite border is TSK 11 – M2, which was earlier classified as a basaltic andesite
based on its mineralogical composition.
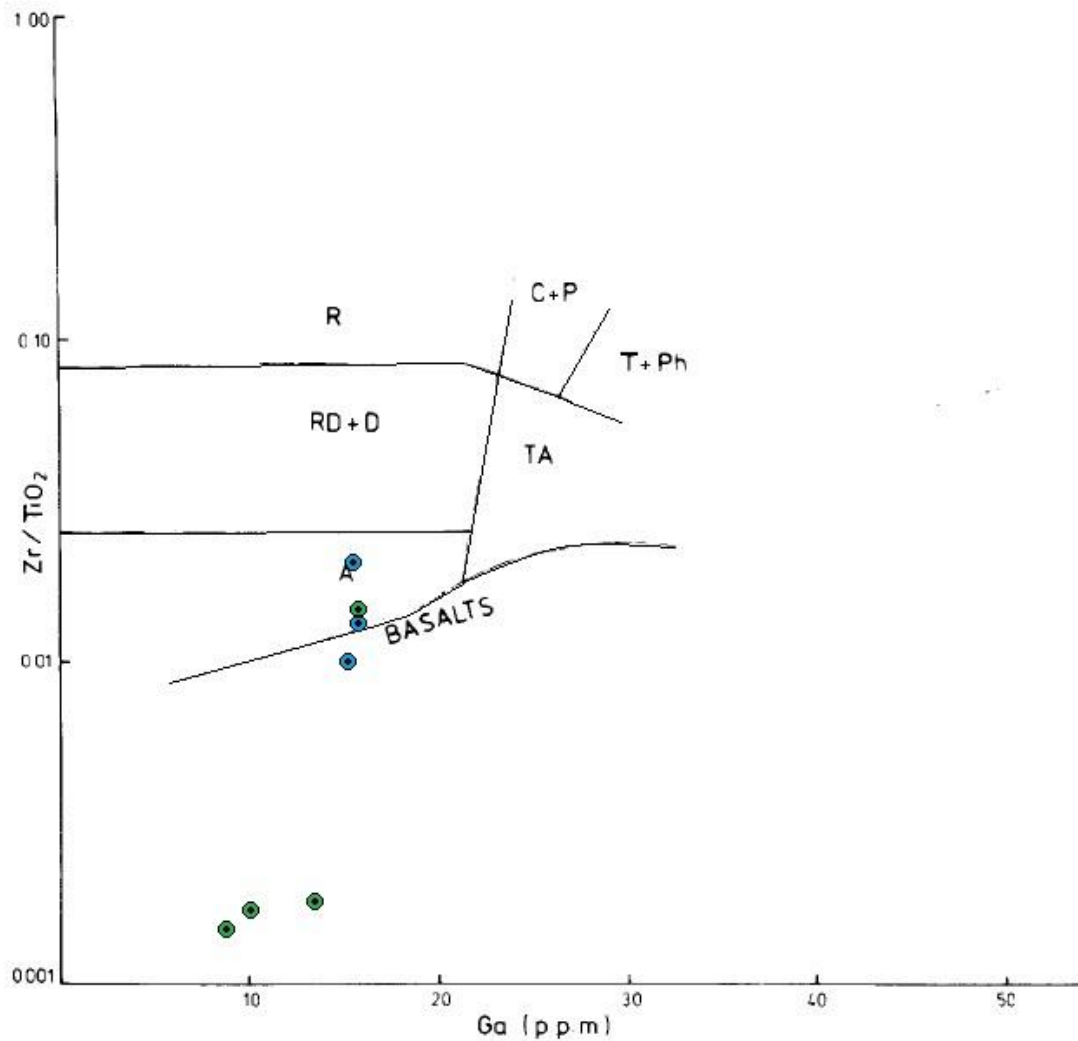
Figure 31: *Diagram showing variations in Zr/TiO$_2$ – Ga in the volcanogenic samples from Skiftesmyr. The diagram is from Floyd and Winchester (1978), and is made for use with rocks from greenschist, amphibolite and granulite facies meta-volcanic suites. The naming conventions for the subdivisions of rock types are the same as Figure 29. Metabasalts are represented as green dots, whereas felsic samples (quartz keratophyres and the hypothesized felsic dike) are shown as blue dots. The metabasalt plotting in the andesite field (A) is TSK 11 – M2. As in figures 29 and 30, the quartz keratophyres also have a composition consistent with an andesitic protolith, which does not correspond with the literature from the area, where they are referred to as rhyodacitic, which might indicate a different formation, or alternatively e.g. TiO$_2$ mobility. Cr-contents, if high, might indicate an olivine rich initial composition, which would explain relatively low TiO$_2$-contents, but this is not the case for the felsic rocks. TiO$_2$ mobility could be indicated by e.g. titanite localized in bands, but this has not been observed in thin sections of the samples.*

By comparing metabasalts from various VMS-type deposits from around the world, several from Norway and the Grong mining district included, Pearce and Gale (1977) proposed similar diagrams for determining the nature of igneous rocks with a specific focus on ore deposits and depositional environments. Figure 32 shows a plot of Ti/Y vs. Zr/Y, and while the main purpose of the figure is to distinguish between plate margin and WPBs, an interesting feature revealed in that the samples from Skiftesmyr basalts actually plot closer to Cyprus-type deposits than samples taken from nearby deposits in Trøndelag (Løkken, Gjersvik and Joma).
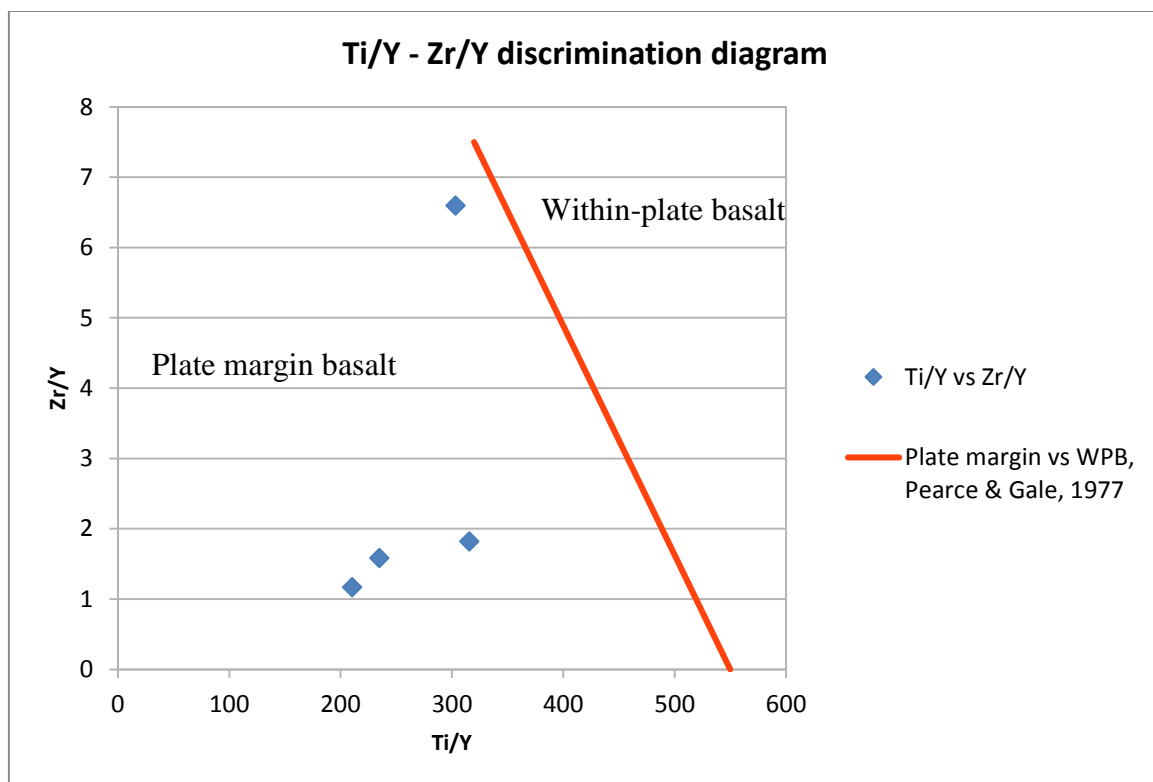
Figure 32: *Ti/Y – Zr/Y discrimination diagram for metabasalts, modified from Pearce and Gale (1977). Samples are shown in blue, and the division between plate margin (left) and within-plate basalts (right) is represented by the red line. As can be seen, the samples plot firmly within the plate margin field, thus substantiating previous findings. The diagram is analogous to the Zr – Y – Ti diagram shown in Figure 26, though somewhat simplified. Most importantly, comparison with data from Pearce and Gale (1977) show that the majority of the samples (excluding TSK 11 – M2, which is the sample with the highest Zr/Y ratio) plot closer to samples from Cyprus-type VMSDs than other deposits, even those in Trøndelag (i.e. Joma, Gjersvik and Løkken).*
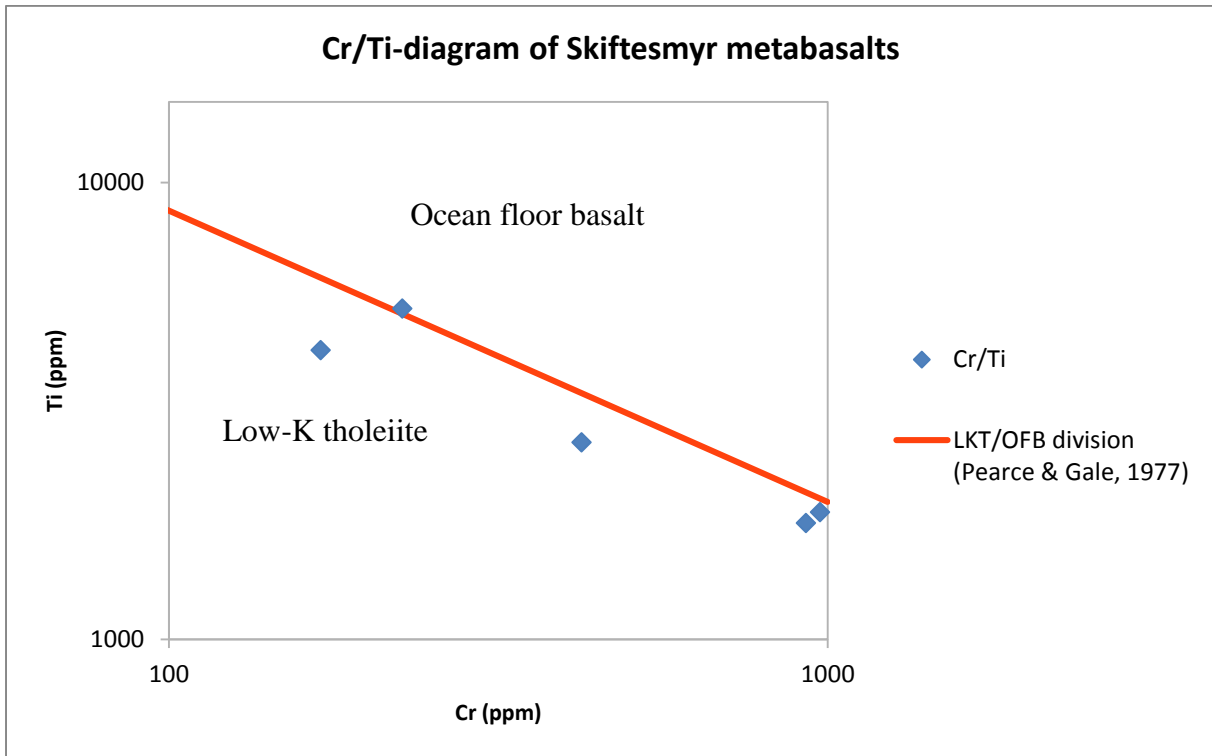
Figure 33: *Cr – Ti diagram of Skiftesmyr metabasalts, modified from Pearce and Gale (1977). The red line indicates a division between low-K tholeiites and ocean-floor basalts. As can be seen, the samples consistently plot as LKT-type basalts, though the elevated Cr contents may be a source of some error in terms of the proximity to the dividing line.*

The Cyprus-type deposit samples analyzed by Pearce and Gale (1977) are from the Troodos Massif (Cyprus), Lasail (Oman) and Betts Cove (Newfoundland). TSK 11 – M2 (the sample with the highest Zr/Y ratio) is once again the exception. Figure 33 is included for the sake of comparison, but as has already been established, the elevated Cr-contents of the Skiftesmyr metabasalts, in some cases reaching over 900 ppm, make such a comparison less than ideal. The figure also exemplifies how increasing Cr-contents affect the amount of Ti present, as a linear trend (roughly comparable to the division line between LKT and OFB) can be observed.

Figure 34 is similar to Figure 27, but has been included on the merit of containing mean compositional data for other deposits. This should in no way should be interpreted as self-sufficient evidence of a specific deposit genesis, but can provide an indication as to the source rock for the metals in the deposit.
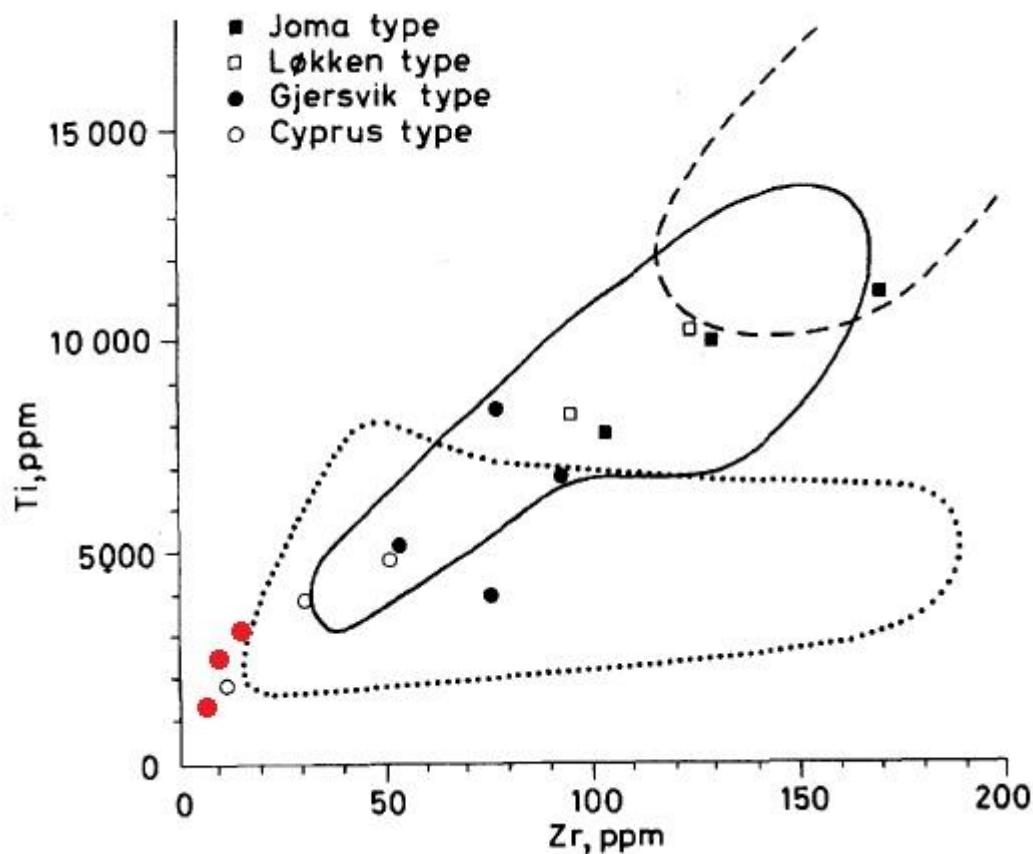
Figure 34: *Zr-Ti composition of samples of metabasalts from VMS deposits from Pearce and Gale (1977). Skiftesmyr samples are shown in red. The dotted line indicates a field of island arc basalts and andesites, the continuous line OFBs, and the dashed line WPBs.*

3.5.2. Ores and ore element relationships

Sample number	Cu (ppm)	Zn (ppm)	Pb (ppm)	As (ppm)	Ag (ppm)	Au (ppm)
TSK 1 – M4	2980	850	22	10	0,8	0,028
TSK 1 –M14	4680	8160	348	292	9,1	0,216
TSK 7 – M5	866	245	205	17	37,7	4,5
TSK 13 – M4	988	1355	24	33	0,9	0,016

Table 3: *Ore elements in mineralized samples from Skiftesmyr trenches. Pb and As are included as they are commonly associated with respectively Ag and Au mineralizations, e.g. gold hosted in arsenopyrite.*
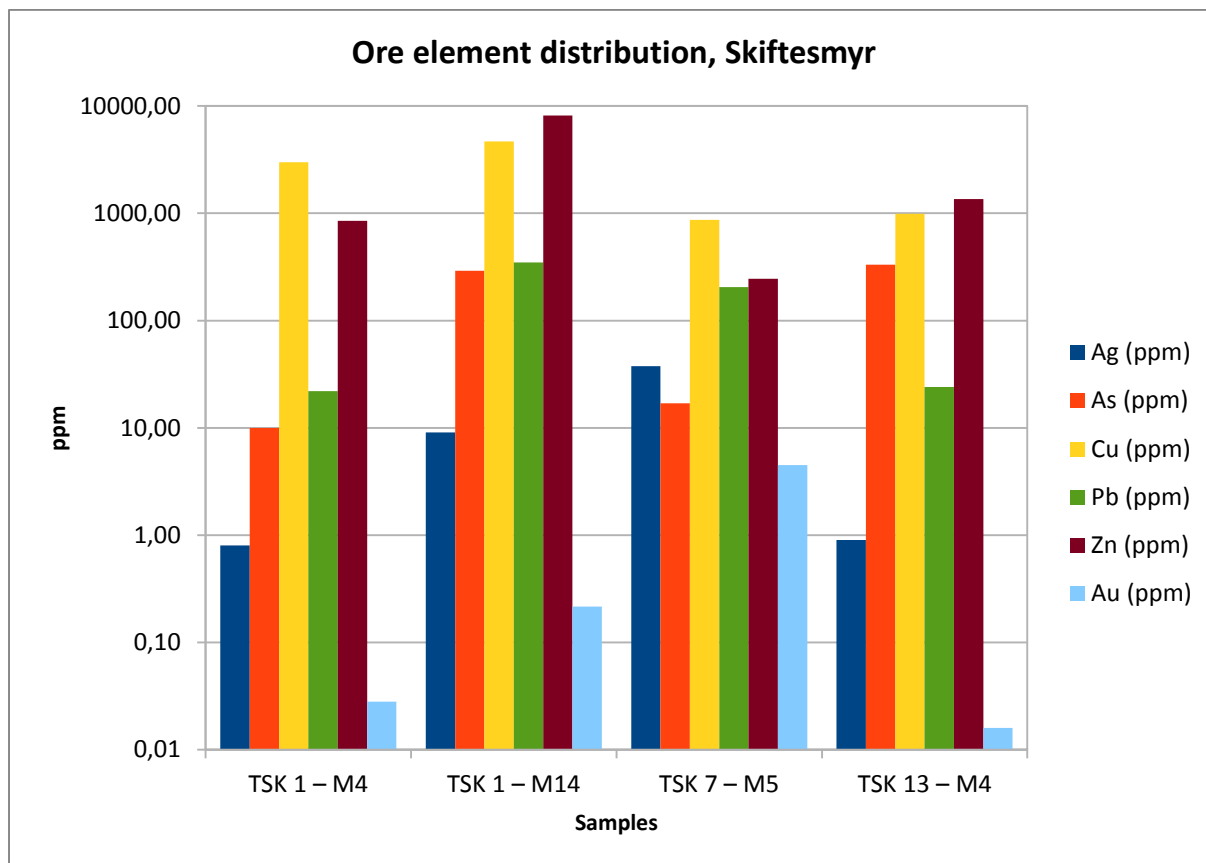
Figure 35: *Graphical representation of data presented in Table 3, showing ore element distribution in mineralized samples. Note that the Y-axis is on a logarithmic scale to enhance the contrast between precious and base metals.*

As is evident from Table 3 and Figure 35, the process of determining ore element associations, in particular with respect to precious metals, has been difficult. Based on observations of the geochemical data, the strongest correlation is between Au and Ag, which might indicate that the precious metals occur together in the form of electrum. Gold mineralization in a VMS-type depositional environment is often controlled by the copper mineralization, with the gold occurring as inclusions in and between chalcopyrite grains, or as a result of hydrothermal veins. Silver, on the other hand, is typically associated with Pb-Zn rich assemblages, though auriferous VMSDs may also be associated with Zn (Huston & Large, 1989).

It should of course also be noted that these samples are from trenches, and as such have been subjected to surface weathering. This might have had an effect on the distribution of ore elements, and as such comparing concentrations might not yield accurate results, as the different minerals are affected to a varying extent by these weathering processes. Other

factors, such as grain size, might also make a difference. This is observed in e.g. TSK 7 – M5, where larger chalcopyrite grains show less evidence of weathering, and sphalerite is only present as small, skeletal remains at grain boundaries, indicating that sphalerite weathers more readily compared to chalcopyrite at conditions applying to the Skiftesmyr deposit.
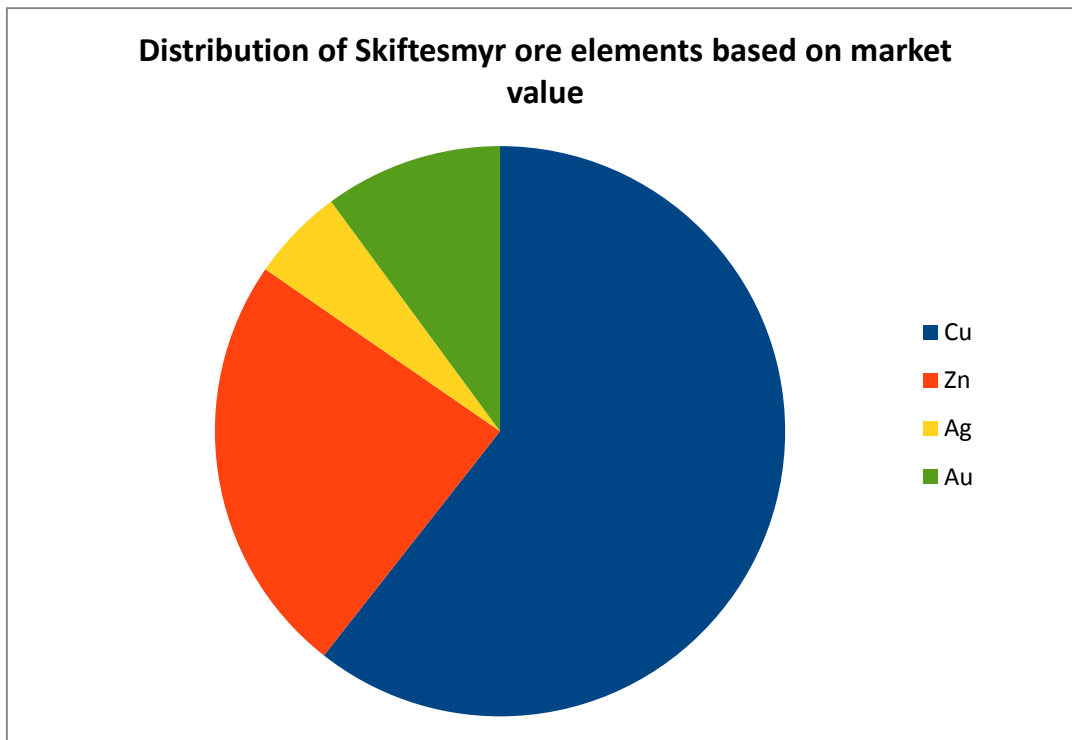
Figure 36: *Distribution of ore elements based on market value as of October 2013, showing their relative economic importance (made using data from Bernard, 1997; Haugen, 1982; Lindeman, 1992; and Lindeman, 1992B).*

The highest concentration of base metal ore elements is found in sample TSK 1 – M14, with 0.47 % Cu and 0,82% Zn. Pb is only present in small amounts, which is typical not only for these samples, but also for the deposit as a whole. Cu and Zn are the most common ore elements, and are of the greatest economic importance, followed by Ag and Au. The metallogeny of the deposit can as such be described as Cu>Zn(>Au>Ag) with respect to economic importance (see Fig. 36). Zn>Cu and Cu>Zn type metallogeny is common in several deposit types with host rocks dominated by mafic volcanics.

3.4. Field relationships and trench mapping

Due to the marshy nature of the terrain, most of the detailed geological information on the Skiftesmyr area is restricted to limited outcrops and trenches. The trenches exhibit a trend of (from north to south) mafic tuffs and metabasalts, followed by quartz keratophyres and felsic rocks, and finally into mafic to intermediate tuffs in the south. The ore is typically associated with the quartz keratophyres, which form the footwall of the deposit (see Fig. 37). This is consistent with the stratigraphic sequence being inverted, i.e. that the stratigraphic up-direction is to the south. The lenticular shape of the ore deposit is possibly a result of pyrite behaving as a competent phase during deformation, as described from the Skorovas deposit in Halls et al. (1977), or as proposed by Langley (1973) the result of the intersection of different fold axes. Trench mapping reveals two separate mineralized horizons roughly parallel to each other along strike, with the main mineralization to the south-southeast (see map attached in Appendix 2).

Mafic volcanics
(no samples representing this segment)

Mafic/intermediate tuffs
Laminated and folded, containing disseminated sulphides.

Mineralized zone
Two separate mineralized horisons. Massive to semi-massive sulphides.

Quartz keratophyre and felsic igneous rocks
Rhyodacitic tuffs and flows, or silicified andesites as indicated by geochemical analysis. Contains some disseminated sulphides.

Mafic volcanic
Metabasalts and mafic tuffs with minor sulphide dissemination.

Figure Q: *Idealized stratigraphy of the deposit.*

Furthest to the south, mapping in the field (e.g. Heim, 1993) reveals that the sequence composed of tuffs and volcaniclastic material is overlain by more mafic volcanics, likely similar to what has been observed further north. Whether these rocks represent a continuation of the volcanic activity is uncertain, as they might be thrusted into this position (see Fig. 3).

4. Discussion

4.1. Genesis of the deposit

4.1.1. Metallogeny

Observations in the field (e.g. Heim, 1993) and earlier geochemical analysis of rocks and ore from Skiftesmyr (e.g. Lindeman, 1992; Haugen, 1982; Bernard, 1997), as well as analysis and observations of geochemical data made in this paper show that the metallogeny of the Skiftesmyr deposit is Zn>Cu (with respect to grades; Cu>Zn>Au>Ag with respect to economic importance). The ore is however as demonstrated herein and by e.g. Heim (1993) and Sandstad et al. (1996) hosted by felsic volcanics, a trait typically accompanied by Zn-Pb-Cu metallogeny and ample presence of elements such as As, Sb, Cd, Sr and Ba (Galley et al., 2007). This is however not the case for the studied samples, and data from drill cores also show that Pb is also not present in significant amounts (<0.1%) in parts of the deposit not subjected to surface weathering conditions (Buer & Heim, 1991). The metallogeny of the Skiftesmyr deposit in other words corresponds to what would typically be expected from deposit types where the base metal content comes from the leaching of mafic rocks, i.e. mafic, bimodal-mafic or siliciclastic-mafic based on the lithological classification system proposed by Galley et al. (2007).

4.1.2. Volcanostratigraphy

As mentioned in chapter 3.4., and corroborated by e.g. Heim (1993), a volcanostratigraphy can be constructed based on trends observed as a part of field work, during trench mapping and later petrographic investigations of samples from aforementioned trenches. What can be observed can generally be summarized as a continuation between metabasalts and mafic volcaniclastic material at the bottom, followed by felsic volcaniclastics (i.e. the quartz keratophyres which comprise the footwall of the mineralization) and finally volcaniclastic material of mixed intermediate/mafic affinities towards the border with the Limingen Group in the south (see Fig. 37). Petrographic investigations show that the mafic metabasalts are primarily basaltic, but that basaltic andesite is also present. This is corroborated by

geochemical analysis of the sample material (e.g. Fig. 29-31). The discrepancy between literature and petrographic observations and the geochemical analyses with respect to the felsic sample material primarily referred to as quartz keratophyres will be discussed in chapter 4.1.4.

4.1.3. Igneous rock classification and determination of magmatic affinity and tectonic setting using trace element geochemistry

The methods and plots used to decide the nature of the igneous rocks from Skiftesmyr has been explained and described in chapter 3.5, where the plots that will be referred to in this section are also found. A complete list of geochemical data from both ME-CP (ICP-AES) and XRF analyses can be found in the appendices.

The plots used are from Pearce & Cann (1973), Floyd & Winchester (1978) and Pearce & Gale (1977), and have been chosen based on their use of elements that are immobile during metamorphism, alteration and weathering. Graphical representations of e.g. SiO_2 vs total alkali have not been used, as SiO_2 is known to be mobile during alteration (Floyd & Winchester, 1978), e.g. silicification (Gibson et al., 1983), and alkali elements are often subjected to e.g. spilitization (Galley, 1993). Based on the research of e.g. Pearce & Cann (1973), Floyd & Winchester (1978) and Hallberg (1984), the elements chosen to determine the magmatic affinity of the igneous rocks from Skiftesmyr are Ti, Zr, Y, Nb, Ga and Ce. An AFM diagram of Na_2O+K_2O, MgO and $FeO+Fe_2O_3$ modified from Blatt et al. (2006) has also been used to determine fractionation trends (see Figure 28), though as previously established this has an inherit weakness with respect to e.g. spilitization.

The classification of the igneous rocks is done using methods proposed by Floyd & Winchester (1978), chosen as they are intended for use with altered and metamorphic rocks. As can be seen in Figures 29-31 the metabasalts and quartz keratophyres plot firmly in the fields of sub-alkaline basalt and andesite respectively, with the exception of TSK 11 – M2 which plots at the intersection between the basalt and andesite fields. The latter lends credence to petrographic observations, where this sample was classified as a basaltic metaandesite, and the former confirms the classification used for the metabasalts. That the quartz keratophyres consistently plot as being andesitic rather than rhyodacitic represents a

major inconsistency between the observations made through the course of this study and the literature (e.g. Heim, 1993; Sandstad et al., 1996) available for the Skiftesmyr area. Some possible explanations for this phenomenon will be discussed further in chapter 4.1.4.

Comparing the petrologic character of the igneous rocks from Skiftesmyr to known examples from around the world using Y/Nb ratios clearly indicate their tholeiitic character (Pearce & Cann, 1973). While e.g. Figure 25 shows this clearly, it is not ideally suited for determining whether the rocks have originated at island arcs or on the ocean floor, though island arc provides the best fit using this specific method. The tholeiitic fractionation trend is also corroborated by the use of the AFM diagram (Figure 28).

The metabasaltic rocks are with the exception of sample TSK 11 – M2 consistently shown to represent low-K tholeiites, and Figure 27 indicates that they formed as island arc basalts. TSK 11 – M2, determined in thin section to be basaltic metaandesite plots as a CAB (calc-alkaline basalt), though Figure 27 does not provide any conclusive evidence for tectonic setting. When compared to other data gathered by Pearce & Cann (1973), it is comparable to other results gained from CABs formed in an island arc setting, though it should be noted that the comparison is tentative. One might as a result conclude that the Skiftesmyr metabasalts have formed in an ocean arc setting.

4.1.4. Quartz keratophyres and felsic samples

The different lithologies have as mentioned been determined using a petrographic microscope, though in one case the literature and observations in thin sections disagree with the geochemical findings, namely with respect to the quartz keratophyres. These rocks are in the literature described as rhyodacitic tuffs (e.g. Heim, 1993; Sandstad et al., 1996), which corresponds with the findings in thin sections – the samples of these rocks generally contain large amounts of quartz and feldspar, as well as a smaller chlorite component. The geochemical analyses and interpretations utilizing diagrams proposed by Pearce & Cann (1973) and Floyd & Winchester (1977) however indicate that these rocks have a composition closer to andesite (compositions vary between basalt and dacite for the felsic samples) (see Figures 29-31). There might be several explanations for this that do not exclude the possibility that these rocks are in fact rhyodacitic tuffs, such as that they actually represent a mixture of

felsic pyroclastic material and eroded mafic materials, thereby bringing their total composition to an intermediate position. Nor are these diagrams ideally suited for use with pyroclastic material due to the innate risk of contamination from other sources (Pearce & Cann, 1973), sedimentary or otherwise. Rocks elsewhere at the same stratigraphic level might as a result be rhyodacitic tuffs. While quartz keratophyres in literature are commonly referred to as rhyodacitic tuffs, this is as previously mentioned not necessarily the case, as "quartz keratophyre" is a descriptive term rather than one referring to a specific protolith (Schermerhorn, 1973). Schermerhorn (1973) defines quartz keratophyre as a "leucocratic sodic felsic quartz-albite-phyric (...) or albite-phyric (…) volcanic rock". This opens for an interpretation where the quartz keratophyre does not represent a rhyodacitic tuff, but perhaps rather a spilitized and silicified andesite or basaltic andesite. Such an explanation is corroborated by e.g. Gibson et al. (1983), where a similar situation is described from the Noranda VMS camp (i.e. VMS district) in Canada, and in part referred to by other authors (e.g. Schermerhorn, 1973; Halls et al., 1977; Galley, 1993; Galley et al., 2007) in the context of the spilite-keratophyre suite. Spilitization is as mentioned previously a process of *in situ* Na-K metasomatism caused by the interaction between sea water and ocean floor basalts (Galley, 1993). This leads to albitization and elevated amounts of Na_2O and K_2O in the rocks, and is why determining the magmatic affinity of basalts using silica versus total alkali plots in some cases leads to flawed results. Silicified andesites have a composition comparable to that of quartz keratophyres in literature (Schermerhorn, 1973; Gibson et al., 1983) with respect to silica contents and in being albite(-quartz)-phyric. The silicification alteration process can, according to Gibson et al. (1983), occur either as mottled epidote-quartz alteration or as silicification, i.e. similar to the mottled epidote-quartz alteration but without epidote, and is often related to chloritization. Silicification is characterized by quartz mantling chlorite-actinolite and epidote-filled amygdules and fractures (Gibson et al., 1983), and feldspar phenocrysts and microlites with a pilotaxitic texture are typically preserved. The exception would be in the most siliceous samples (>72% SiO_2). Chlorite is almost completely replaced by fine-grained quartz and lesser amounts of epidote and calcite (Gibson et al., 1983). This might also help explain the presence of some of the more quartz-rich samples from Skiftesmyr, i.e. TSK 1 – M15 and TSK 10 – M10 (respectively classified as a felsic dike and quartzite) (see Fig. 13 and 16), indicating that they rather than being sedimentary or a felsic intrusive might represent areas of more intense silicification. The increase in grain size in the "quartzite" compared to the fine grained quartz groundmass found in other samples might as a result be explained by a more complete replacement of chlorite, thereby allowing grain

growth to continue uninhibited by interstitial chlorite grains. The assumption that these rocks are silicified andesites or basaltic andesites rather than rhyodacites, in addition to being corroborated by geochemical analysis, also better explains the relatively high content of chlorite found in these rocks. Both spilitization and silicification represent greenschist facies metasomatic reactions, with spilitization typically occurring at temperatures in excess of 200°C and silicification at temperatures of approximately 350-425°C (Galley, 1993). Gibson et al. (1983) and Galley (1993) also conclude that silicification can play an important role in the formation of volcanogenic massive sulphide deposits in that it will reduce the permeability and porosity of the rocks, thus creating an impermeable layer under which a reservoir of metal-rich hydrothermal solutions can be formed (see Fig. 39). Fracturing, either related to rifting, hydraulic over-pressuring (Galley, 1993) or synvolcanic faults (Gibson et al., 1983), would then allow this fluid to rise onto the sea floor or into overlying porous sediments to precipitate sulphide minerals. This would, according to Gibson et al. (1983), result in a relatively thin layer of pyritic exhalite reflecting an unfocused discharge of solutions involved in alteration reactions, which would cease as the impermeable silicified layer was formed. A similar feature can be described from Skiftesmyr, where the northernmost mineralized horizon, represented in the samples by TSK 13 – M4 (classified as an iron rich exhalative through the course of petrographic investigations), could be interpreted to be the result of an initial unfocused discharge. It should be noted that the silicified layer mentioned above (see Fig. 39) is caused by infilling, and not by replacement, as is the case for the Noranda "felsic" volcanics (Gibson et al., 1983). It should however also be noted that this only represents one possibility, and that the geochemical data might be inaccurate due to contamination from other sources, or that the samples might have systematically reduced Ti-contents as a result of spilitization of the rhyodacitic tuffs (Galley, 1993). The high chlorite content might also be the result of later chloritic alteration during ore formation, or a result of regional metamorphism and tectonic emplacement. It should also be noted that the example locality for silicification used, i.e. Noranda, Quebec, is described as fresh and not noticeably affected by regional metamorphism after ore deposition, and that primary igneous features are still visible as opposed to Skiftesmyr. Another possibility is of course that rhyodacitic tuffs and silicified andesites/andesitic tuffs are both present together with basalts, and that rhyodacitic tuffs are more prevalent elsewhere at the same stratigraphic level.

4.1.5. Deposit genesis

Comparison and compilation of the data presented and discussed above indicates that the deposit has formed in association with mafic volcanic rocks in an ensimatic setting in relation to an island arc (see Fig. 40). When the data is plotted on the diagrams proposed by Pearce & Cann (1973), the results essentially exclude an origin as ocean-floor, within-plate or ocean-island basalts, and strongly favor an origin as LKT- and CAB type basalts related to island arc formation (see Fig. 25-27). Discriminating between mafic and ultramafic rocks cannot be done using Ti/Zr ratios (note e.g. the lack of picrite or komatiite basalt on figures 29-31), but this distinction can be made, although tentatively, by ultramafic igneous rocks generally having higher Cr-contents (Hallberg, 1984). This process, typified by abnormally high contents of Cr, Ni or MgO, may occur during the early stages of volcanicity, where the basalts contain relatively large amounts of olivine or pyroxene phenocrysts, which reduced the absolute amounts of Ti, Zr, Y, Nb and Sr (Pearce & Cann, 1973). Looking at the Skiftesmyr basalts (with the exception of TSK 11 – M2, the basaltic andesite [see Fig. 34]), a trend of high Cr-content is evident, also when compared to the data compiled by Pearce & Gale (1977) for other deposits in the area (i.e. Joma, Gjersvik and by extention Skorovas, and Løkken), where Cr-contents are much lower. The one exception would be ores of the Cyprus-type from the Troodos Massif (Pearce & Gale, 1977), typically associated with mafic and ultramafic rocks and formed in e.g. back- or fore-arc basins. While determination techniques for dividing between basalts formed in island arc and back- or fore-arc basin environments are limited with respect to geochemical analysis, observation of samples from the Troodos Massic (Pearce & Gale, 1977) indicate a depletion in LREEs. This is corroborated by observations from modern back-arc environments such as the Scotia Basin (Mariana Trough), where the ratios of LILE (large-ion lithophile elements) to HFSE (high field strength elements), in the case of Taylor & Martinez (2003) exemplified by the Ba/La ratio, are higher in back-arc basin than island arc basalts. An increased Ba/La ratio is generally associated with more mature island arc systems, as the increase in Ba is thought to represent a greater contribution of melt from the subducted slab (Taylor & Martinez, 2003). As previously established, e.g. Ba is known to be mobile during alteration and metamorphism, and this method as a result has limited application when used on rocks subjected to such conditions. Saunders & Tarney (1984) show that low-K tholeiites related to island arcs are often formed in the earliest stages of arc development, and that a gradual transition into more calc-alkaline suites occurs as the island arc matures. This is consistent with observations made by Halls et al. (1977) and in

Sandstad et al. (1996) for e.g. the Skorovas and Gjersvik deposits, suggesting their formation in relation to an immature arc. It is also consistent with the volcanostratigraphy observed from Skiftesmyr, where LKTs are found stratigraphically below the footwall, followed by the footwall of the mineralization (quartz keratophyres) which might be interpreted as calc-alkaline. The quartz keratophyres, felsic rocks and hanging wall mafic and intermediate tuffs generally also have an increase in Ba-content.

The combination of factors mentioned above indicate that the Skiftesmyr deposit formed in a back-arc environment, or rather an environment intermediate between a back-arc basin and an island arc due to the overlying tuffs. The deposit may have formed as a result of silicification and a subsequent focused discharge of hydrothermal fluids, as explained in Chapter 4.1.4 and suggested by the geochemical evidence (see Fig. 39), or with contemporary rhyodacitic volcanism occurring at the island arc. The heat source causing hydrothermal activity is uncertain, as none can be determined in the field, and might as such have been removed during tectonic emplacement. Possible heat sources could be an intrusive body under the deposit as one would commonly expect, or possibly a dike emanating from the magmatic activity at the island arc. Another possibility is an upwelling of the asthenosphere as a result of the rifting forming the back-arc environment (see Fig. 38). Post-arc rifting such as this has been described from the Gjersvik Nappe by Stephens & Gee (1985). Classification of the deposit in accordance with the naming conventions presented in chapter 1.6.4 is somewhat difficult due to the uncertainty regarding the origin of the quartz keratophyres. If the quartz keratophyres, as literature suggests, originated as rhyodacitic tuffs, possibly also as lavas or dikes of the same composition, the deposit would be classified as bimodal-mafic, similar to deposits in the Noranda VMS camp. One should however note the discoveries presented in Gibson et al. (1983) regarding some of the Noranda rhyolites being silicified andesites. Following this train of thought, the other possibility is that the quartz keratophyres of the Skiftesmyr deposit (at least in the footwall samples) represent silicified andesites, resulting in classification as an intermediary between the bimodal-mafic (or rather bimodal in the sense of mafic + intermediate lithologies, rather than mafic + felsic) and mafic-ultramafic lithological associations groups. Based on the geochemical analyses, the latter is more likely, and also explains the elevated Cr-contents. Sandstad et al. (1996) mention a likely connection between the genesis of the Skiftesmyr deposit and the Tromselv deposit to the north, though the Zn>Pb>>Cu (wt%) metallogeny of the deposit (NGU Ore Database, Tromselv) indicates otherwise (see Fig. 37).
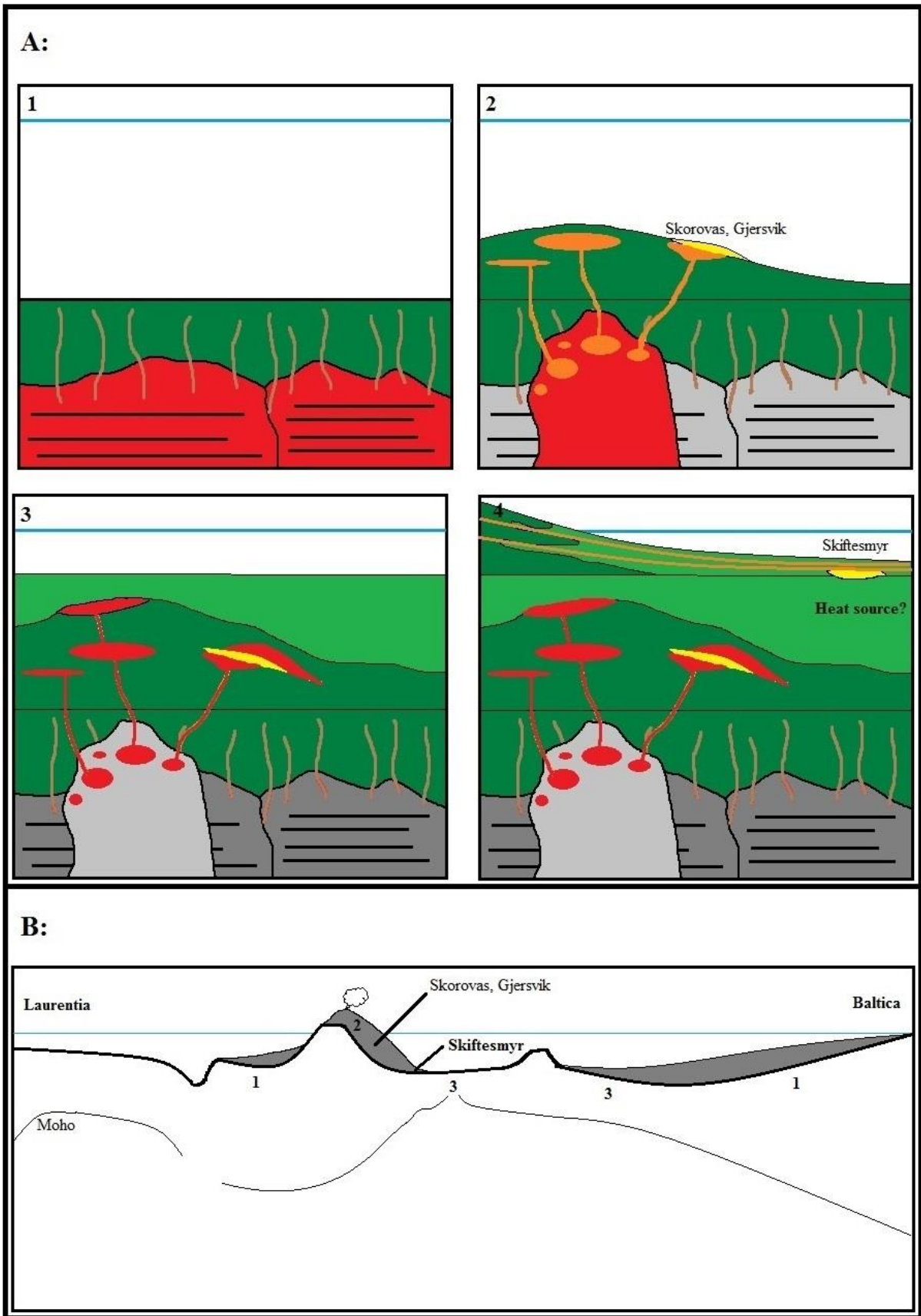
Figure 38: *A schematic representation of the evolution of the Gjersvik nappe and its volcanic rocks, and the relative formation of VMS-type deposits and mineralizations (based on figures from Sandstad et al., 1996 and Craig & Vokes, 1993). (continued on next page)*

A:

1) The lower (and oldest) volcanic unit, composed of basalts with an IAT (island arc tholeiite) geochemical signature (Sandstad et al., 1996).

2) Formation of an immature island arc. The Gjersvik and Skorovas deposits are related to this stage of volcanic activity (Halls et al., 1977; Sandstad et al., 1996).

3) Submarine basalts, possibly deposited during rifting of the island arc. It is possible that the Skiftesmyr deposit is related to this stage, i.e. deposition on the "sea floor", rather than as shown in the following stage.

4) Formation of the Skiftesmyr deposit and transport of tuffs which now comprise the hanging wall of the mineralization. Sandstad et al. (1996) propose that the Tromselv deposit further north also was deposited during this stage of volcanic activity, but as has already been established, the metallogeny of the Tromselv deposit indicate formation in relation to more felsic materials on account of e.g. Pb content. This might indicate that the Tromselv deposit formed in direct relation to a more mature island arc, and also adds credence to that the Skiftesmyr deposit was formed during stage 3 in the figure above (partially on account of the anomalous Cr content associated with ocean floor basalts).

B:

A representation of where the Skiftesmyr deposit formed in relation to the typical locations associated with other deposit types, in the context of the Caledonian orogeny. Location 1 represents a typical location for the formation of Red Sea type deposits (sedimentary exhalative, or SEDEX), and the Joma deposit could represent an example. Location 2 shows the location at which Kuroko-type deposits form, with Tromselv as a possible analogue with respect to deposits in the Grong area. Location 3 represents typical locations at which Cyprus-type deposits form.

FORMATION OF HYDROTHERMAL CELLS
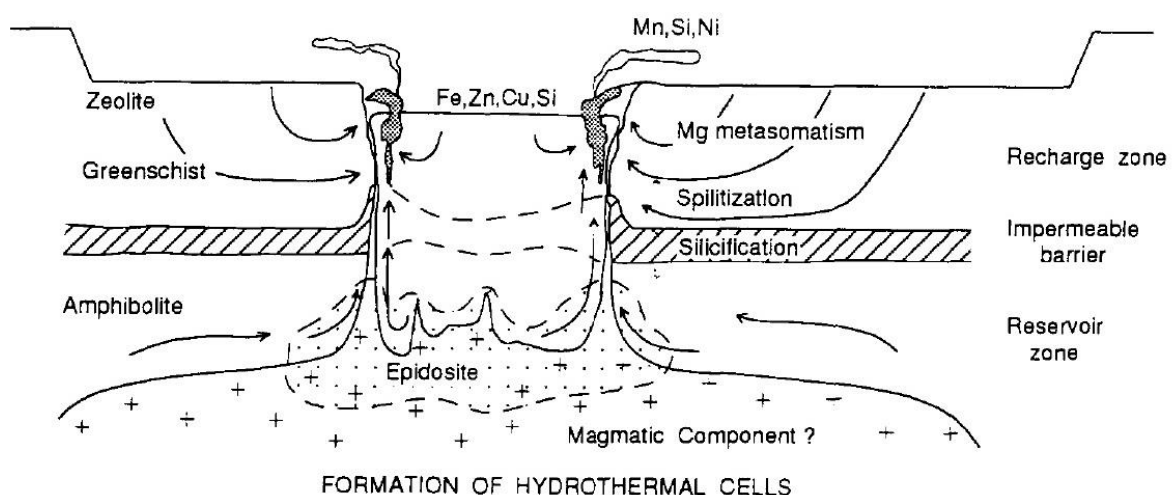
Figure 39: *In addition to silicification by replacement in e.g. andesites, as described by Gibson et al. (1983), silicification also occurs by infilling, as shown here. From Galley (1993). The figure shows the process from the perspective of a collapsed caldera, but similar processes will occur even if there is only a single vent.*
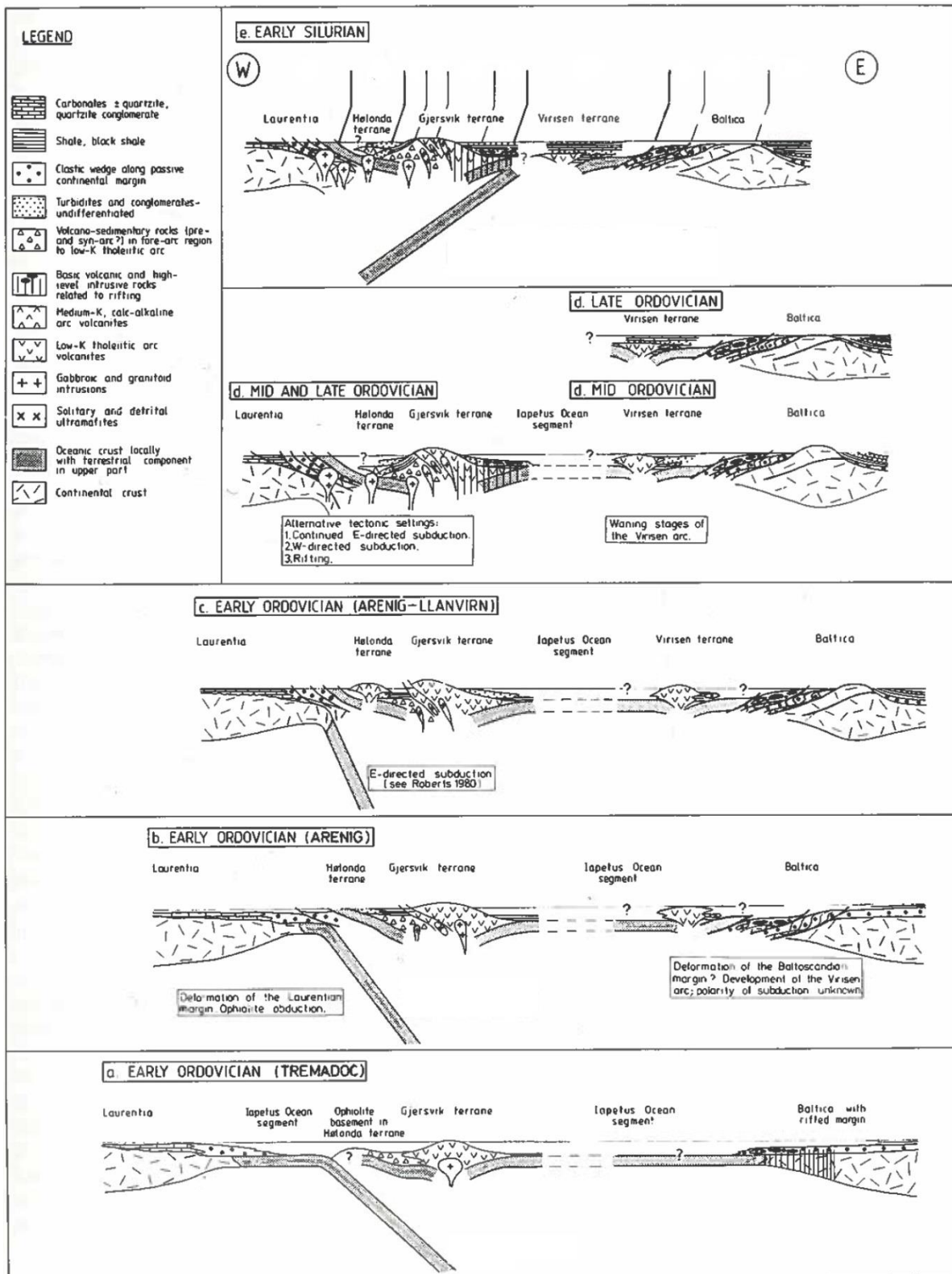
Figure 40: *A tectonic model for the formation of the Gjersvik terrane, showing the progressive elimination of the Iapetus Ocean during early Ordovician to early Silurian times. Note the change in the direction of the subduction zone. This model has been proposed on account of the cessation of intrusive activity under the Gjersvik terrane during the mid and late Ordovician. Modified from Stephens & Gee (1985).*

The connection between the mafic-ultramafic lithological association and mature back-arc environments is highlighted in e.g. Koski & Mosier (2012). As can be seen from Fig. 38, this provides the best fit for the Skiftesmyr deposit, and helps explain how it is different from other deposits in the area.

4.2. Ores and ore minerals

4.2.1. Ores and ore minerals

The grain size of pyrite as mentioned varies greatly between samples as a result of recrystallization. The ore minerals are typically located along grain boundaries or between grains, and less frequently as inclusions in pyrite. In the samples with the highest grades of Cu and Zn, e.g. TSK 1 – M4, TSK 1 – M14 and TSK 7 – M5, the larger grains of ore minerals are typically 0.1-0.5 mm in size (see Fig. 18-21). It should however be noted that surface weathering and subsequent leaching will reduce the grain size and remove a large percentage of the ore minerals. This representation of grain sizes observed in thin section might as such not be typical of the Skiftesmyr deposit. Literature suggest (e.g. Bernard, 1997) that the Skiftesmyr ore provides excellent recovery during beneficiation processes and is simpler to mill and process than equivalent ores from e.g. Skorovas and Joma, where the ore minerals are more fine grained (Nissen, 1992). This is due to the large grain size and likely also the location of the ore minerals at boundaries and intersections rather than as inclusions. The texture and interlocking of surrounding pyrite grains, which varies between mottled or careous textures in some samples and curving to straight boundaries with no interlocking grains in others, also indicate that liberation of ore minerals should be fairly easy (Craig & Vaughan, 1994). Another factor that plays an important role, particularly with respect to the production of Cu-concentrates (Craig & Vaughan, 1993), is that the extent to which sphalerite grains are affected by chalcopyrite disease is very limited. The difference in ore mineral (i.e. chalcopyrite and sphalerite) grain size observed between Skiftesmyr and e.g. Skorovas, Gjersvik and Joma is likely attributed to the different origins of the deposits.

The mineralized strata interpreted as Fe-rich exhalative (i.e. TS 13 – M4) do not contain high base metal concentrations. Such exhalite horizons do however represent useful tools for

exploration, as they indicate the presence of conditions suitable to VMS-type mineralizations (e.g. Galley et al., 2007), and are also valuable as marker horizons as they often cover a large area.

4.2.2. Precious metals

The greatest grades of precious metals are obtained from sample TSK 7 – M5. In order to develop a model for depositional controls for precious metals or discover trends in their distribution throughout the deposit one would need more samples from the ore zones, preferably from drill cores to exclude the possibility of supergene enrichment. A hypothesis based on trends for similar deposits (e.g. Noranda and Cyprus-type VMSDs) would suggest that Au would be associated with Cu-rich portions of the massive sulphides and in the stringer zone (Huston & Large, 1989). Based on the appearance of TSK 7 – M5, it is not unlikely that it represents a part of the stringer zone of the deposit (See Fig. 20 and 22).

The precious metals, e.g. Ag and Au, are most abundant in sample TSK 7 – M5, which is composed of quartz rich aggregates and sulphides, the latter group primarily composed of pyrite and some chalcopyrite. The grades of 4.5 ppm Au and 37.7 ppm Ag obtained from analysis of this sample is decidedly higher than the other samples, as well as being higher than the average for the deposit as a whole, though it should be mentioned that similar grades are observed in drill cores. Such high grades of gold and silver should, as previously mentioned, be associated with high grades of copper and zinc respectively, due to e.g. temperature constraints on precipitation, though that is not observed in the sample. This is likely to some extent the result of weathering and the presence of quartz-rich aggregates, essentially diluting the grades of the sulphides and weathering processes, which as previously mentioned seem to have resulted in preferential removal of sphalerite for this specific sample. The base metals to which precious metal deposition is related vary from deposit to deposit, but one can generally divide the precious metal associations into two groups; namely (1) an Au-Zn-Pb-Ag association commonly found in the upper part of Zn-rich massive sulphide lenses, and (2) an Au-Cu association commonly found in relation to the lower parts of the sulphide lenses or in the stringer zone (Huston & Large, 1989). The type of auriferous VMSD ores typically associated with Zn and Pb is also often Ba-rich, indicating deposition on or near the surface in a siliciclastic environment, such as the Kuroko deposits in Japan. Precious metals found in

association with copper are as mentioned generally found in the stratigraphically lower parts of the deposit, often together with chalcopyrite, other copper sulphides and pyrite. In the case of Cyprus-type (i.e. mafic, with reference to Table 1) deposits gold and silver can occur erratically distributed throughout the ore, but generally conform to the expected copper association (Huston & Large, 1989). These different precious metal metallogenic associations are likely partially controlled by temperature, with gold in Zn-rich portions of deposits being transported as $Au(HS)_2^-$ at low temperatures (150-275° C), and as $AuCl_2^-$ at higher temperatures (275-350° C) (Huston & Large, 1989, and references quoted therein). Diagrams showing the correlation between ore elements for the mineralized samples are included in Appendix 4, as they show very little with the exception of a relatively strong correlation between Ag and Au and are otherwise inconclusive, likely as a result of surface weathering.

4.2.3. Alternate uses for waste rocks and tailings

Due to the prevalence of sulphide disseminations, the waste and host rocks are not likely to be of value given current beneficiation and processing technology. Pyrite can potentially be used in the production of sulphuric acid, and due to problems related to acid mine drainage and the requirements and obligation to limit environmental impact during and after operations, selling a pyrite concentrate, even at a loss, might provide long term economic gain.

4.3. Alteration

Based on observations in the field and through the course of petrographic investigation it is possible to propose a division of alteration types for the different samples. The mafic rocks below the footwall (i.e. basalts and basaltic metaandesite) contain chlorite, epidote and carbonates, as well as some disseminated sulphides. The alteration of the footwall rocks (i.e. felsic samples and keratophyres) can be divided into two different alteration types, namely albite-chlorite and a quartz-sericite(-albite-chlorite) with disseminated sulphides. The latter comprise the immediate footwall of the mineralization. Albitization can be the result of spilitization, or the albite could (see chapter 4.1.4 and Fig. 38 and 39) be the result of silicification of andesite and as such be a primary feature, though spilitization is still likely to have occurred due to the conditions in which the Skiftesmyr deposit formed.

In order to distinguish between hydrothermal (in this case VMS-related) and diagenetic (i.e. metasomatic, spilitic or metamorphic) alteration in the samples, Large et al. (2001) propose the use of an alteration box plot, which shows different trends in alteration. Due to the extent of the alteration in the Skiftesmyr samples, likely both as a result of greenschist-facies conditions on the sea floor as a result of metasomatism (i.e. spilitization) and later upper greenschist-facies metamorphism during tectonic emplacement, a least-altered box has been adopted from the work of Large et al. (2001) (see Fig. 41).
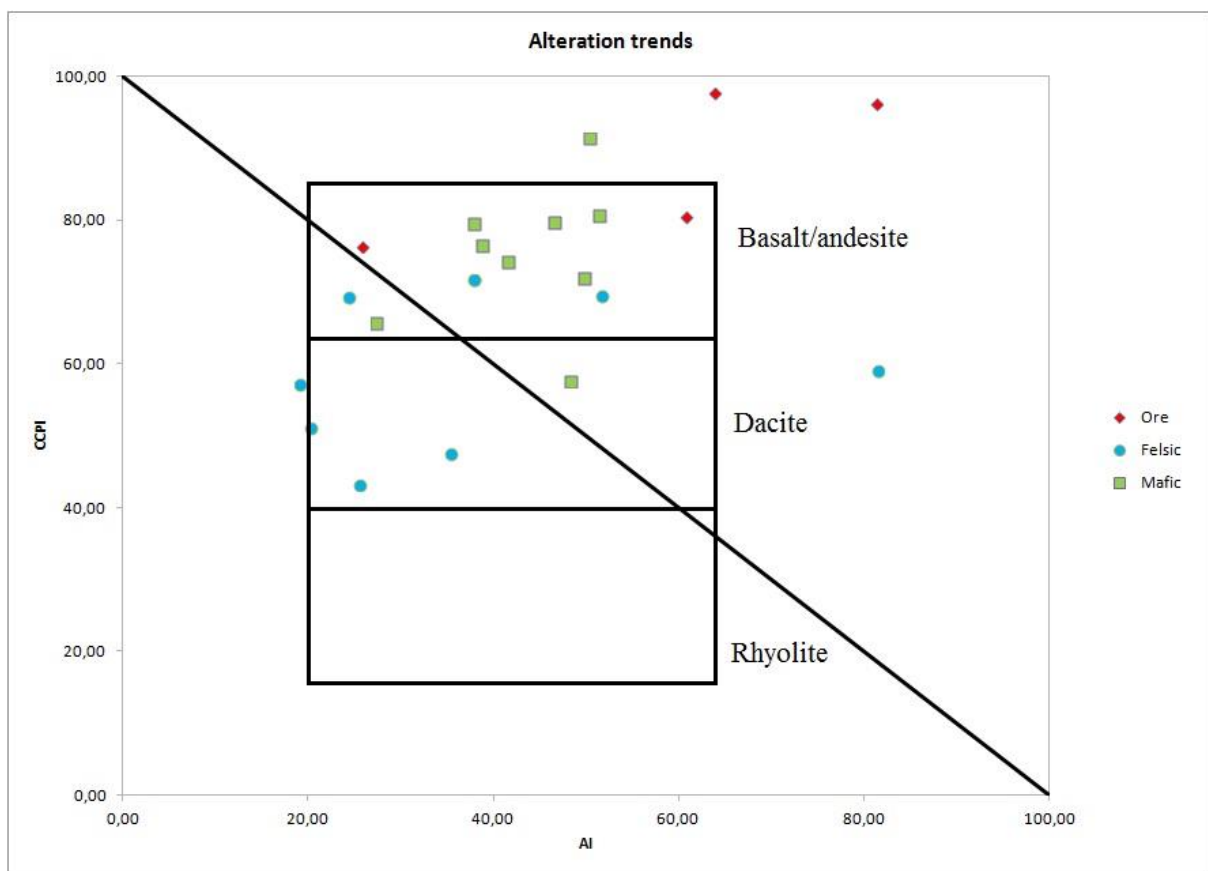
Figure 41: *Plot of AI and CCPI (see text below for explanation), with least-altered boxes for different sample compositions from Large et al. (2001). The black line distinguishes between diagenetic (below) and hydrothermal (above) alteration trends. Modified from Large et al. (2001).*

Alteration zones are also very important with respect to exploration, as certain types of alteration are typically associated with ore mineralization. The ability to distinguish between hydrothermal and diagenetic alteration trends, of which the former is of great importance with

respect to localizing a deposit, is therefore a valuable tool for exploration. The alteration box plot can as such be used to differentiate between altered rocks that are and that are not of interest, thus saving time and effort, and also to determine a vector towards an ore system, both in green- and brownfield exploration.

The alteration box plot is a plot of AI (Alteration Index) versus CCPI (Chlorite-Carbonate-Pyrite Index), with "least-altered boxes" determined either through petrographic investigations in cases where the sample material is relatively fresh and unaltered, or as shown in Fig. 41 and 42, where the least-altered box is selected based on previous work with similar (e.g. basalts, andesites, dacites and rhyolites), but variously altered rock types.

The alteration index is calculated in the following way:

$$AI = \frac{100 \, (K_2O + MgO)}{(K_2O + MgO + Na_2O + CaO)}$$

This is often referred to as the Ishikawa alteration index on account of it being defined in Ishikawa et al. (1976) (quoted in Large et al., 2001). The key reactions measured by this index involve the breakdown of Na-plagioclase and volcanic glass and subsequent replacement by sericite and chlorite. These alteration processes can be illustrated by the following reactions:

$$3NaAlSi_3O_8 + \ K^+ + 2H^+ = KAl_3Si_3O_{10}(OH)_2 + 6SiO_2 + 3Na^+$$
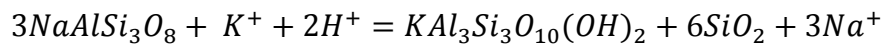
Albite → Sericite + Quartz

and

$$2KAl_3Si_3O_{10}(OH)_2 + 3H_4SiO_4 + 9Fe^{2+} + 6Mg^{2+} + 18H_2O$$
$$= 3Mg_2Fe_3Al_2Si_3O_{10}(OH)_8 + \ 2K^+ + \ 28H^+$$
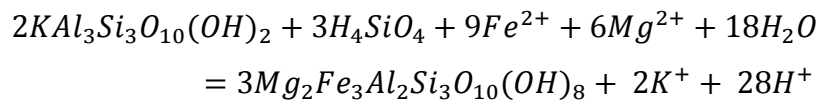
Sericite → Chlorite

The first reaction represents sericite replacement of albite in the outer parts of the alteration system, and the second is more prevalent in closer proximity to a massive sulphide mineralization, where chlorite-rich assemblages are dominant (Large et al., 2001).

The chlorite-carbonate-pyrite index is calculated in the following way (total Fe recalculated to FeO):

$$CCPI = \frac{100\,(MgO + FeO)}{(MgO + FeO + Na_2O + K_2O)}$$

Figure 42 (below) shows AI and CCPI plotted using the least-altered box for basalts and andesites (as per the results from geochemical analysis of the MetPro samples).
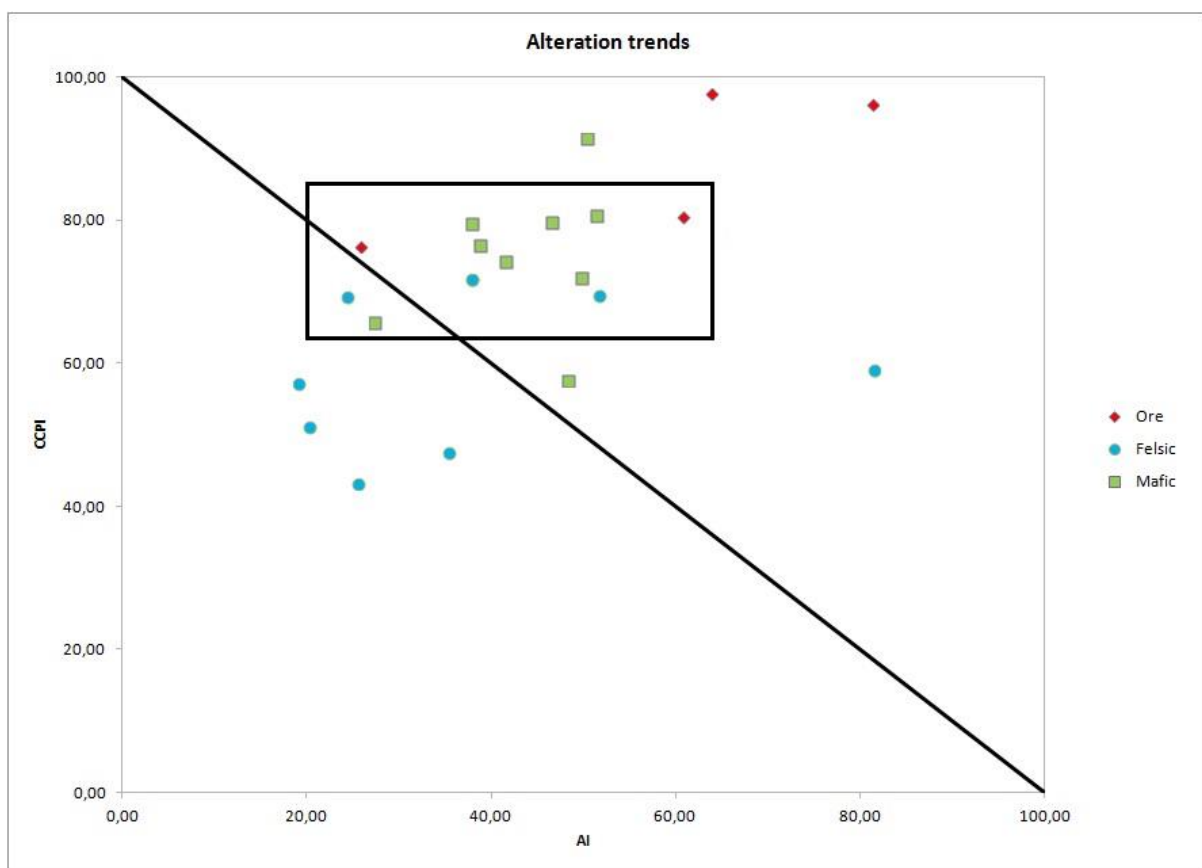
Figure 42: *Plot of AI and CCPI showing alteration trends, with least-altered box for basalts and andesites (from Large et al., 2001). The black line distinguishes between diagenetic (below) and hydrothermal (above) alteration trends. Modified from Large et al. (2001).*
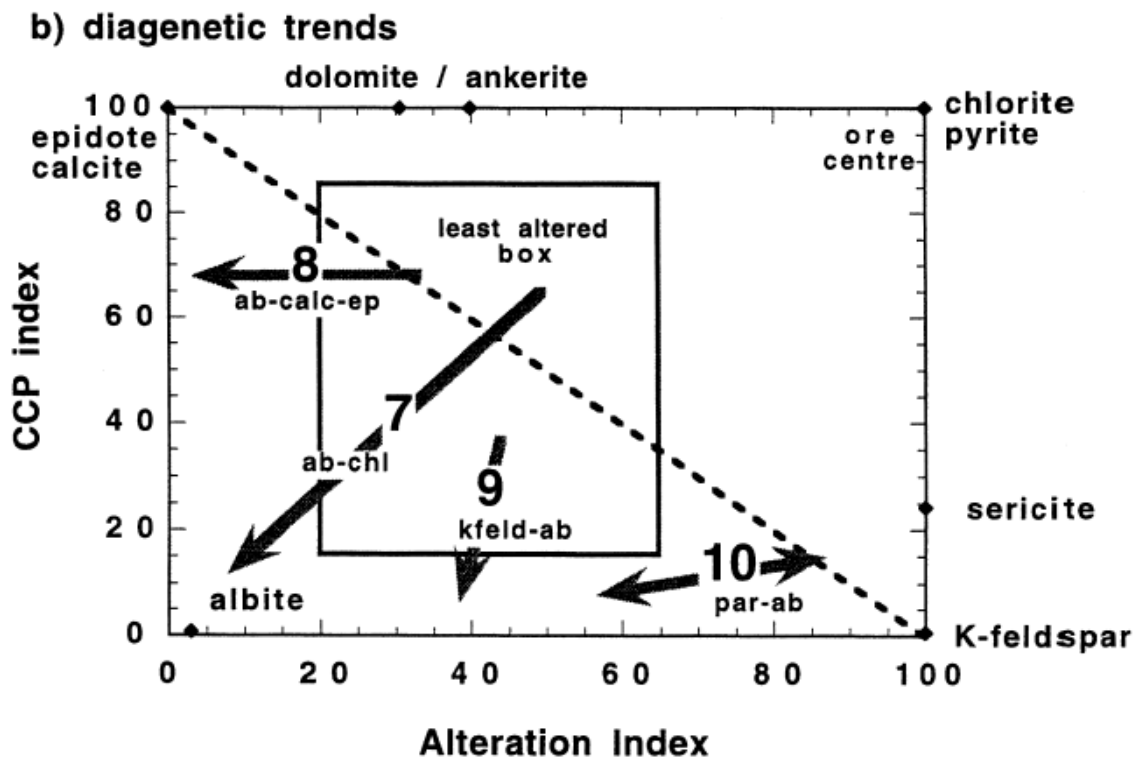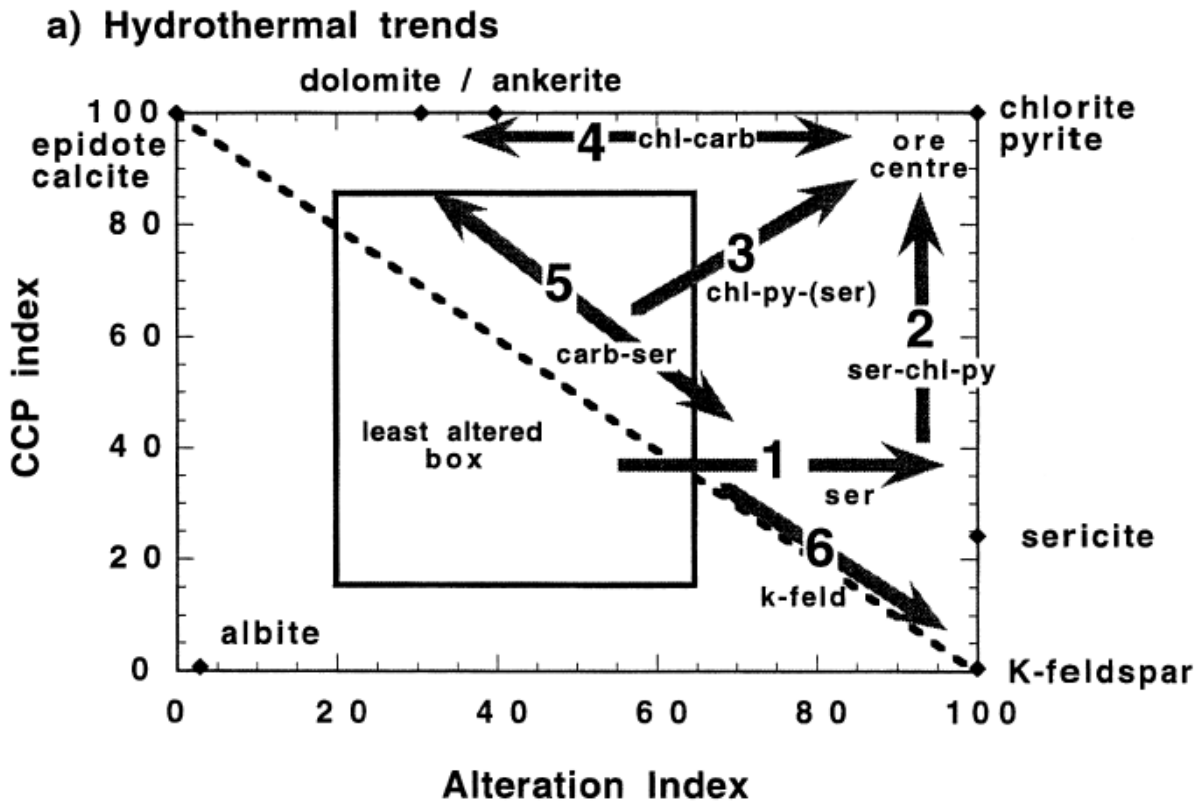
Figure 43: *Alteration trends for hydrothermal (top) and diagenetic (bottom) alteration, from Large et al., 2001. See text for detailed description of trends in accordance with numbers on the figure.*

Alteration trends as seen in Fig. 43 (Large et al., 2001):

Hydrothermal trends (Fig. 43a):

1. Weak sericite alteartion at the margin of a hydrothermal system in felsic volcanic host rocks.
2. Intense sericite-chlorite ± pyrite alteration typically found in the footwall of a VMSD within both felsic and mafic volcanics.
3. Chlorite ± sericite ± pyrite alteration typically found in the chlorite-dominated footwall in both felsic and mafic volcanic rocks.
4. Chlorite-carbonate alteration typically developed in immediately adjacent to massive sulphide lenses.
5. Sericite-carbonate alteration, typically found in the immediate hanging wall to a massive sulphide mineralization.
6. K-feldspar-sericite, an uncommon trend occasionally seen in the footwall in felsic volcanic rocks.

Diagenetic trends (Fig. 43b):

7. Albite-chlorite, typical of seawater interaction at low temperatures (e.g. spilitization).
8. Epidote-calcite ± albite, a common alteration trend found in intermediate to mafic volcanic rocks.
9. K-feldspar-albite, an early diagenetic trend of K-feldspar replacing albite.
10. Paragonitic sericite-albite, an uncommon diagenetic trend found in hanging-wall volcaniclastic rocks.

Comparing Fig. 42 with Fig. 43 and the alteration trends described above, a set of trends are evident. The felsic samples show a clear trend of chloritization (corresponding to diagenetic trend number 7) (see Fig. 43b), whereas the mafic samples seem to follow a trend more closely related to chlorite ± sericite ± pyrite alteration (hydrothermal trend number 3) (see Fig. 43a). This corresponds well with observations from field work and thin section studies. Plots of samples from the ore zone also show how the alteration box plot could be used in exploration activity, where samples in the proximity of the ore zone plot towards the upper right corner of the graph.

85

4.4. Surface weathering

4.4.1. Features of surface weathering and supergene enrichment

Surface weathering of VMS and other deposit types often results in an "iron cap" or leached capping, which is often referred to as a gossan, or being gossaneous. In the field, this is observed as a rust stained, porous and crumbling surface layer. This is the result of oxidation and the leaching of iron and base metals. The oxidation of sulphides into iron oxides is associated with a reduction in molar volume, which in turn leads to increased porosity, thereby allowing more meteoric water to seep through the rocks and reacting with the sulphides to form a solution of sulphuric acid. As mentioned, this process typically results in a depletion of base metal content, which explains the reduction in grades obtained from the trench samples as opposed to the data obtained from geochemical analysis of drill cores, though precious metals are often retained, or even enriched in such environments. This has led to gossans being considered attractive targets for Au, Ag, Ni and PGEs, though generally in the form of laterites. The grades of Au and Ag observed in the trench samples from Skiftesmyr are not anomalous, and similar grades are readily observed from the drill cores. It is as such unlikely that they represent such an enrichment, and are likely simply retained while most of the base metals have been leached from the rock. Gossans are typically associated with hydrated iron oxides, such as goethite, and can be represented as a sequence, with gossans on top, overlying an oxidized zone, which ends at the water table. The oxidized zone and the immediately underlying zone of supergene enrichment of sulphides often represent an economic ore, particularly in porphyry deposits. These weathering zones form on top of the primary hypogene ore. Because of the enrichment of "copper oxides", such as malachite and azurite, and Cu-enriched sulphides, such as bornite, covellite, digenite and chalcocite, such zones of supergene enrichment often represent the most economic ores of several Cu(-Mo)-porphyry deposits, forming a continuous blanket on top of the hypogene, and often low grade, ore. This blanket of enriched ore may contribute to the overall viability of the mining operation (Robb, 2005). Examples are the Chuiquicamata deposit of northern Chile, or the Kalmakyr deposit in Uzbekistan (Zvezdov et al., 1993). Evidence of supergene enrichment is also known from Skiftesmyr, though it has not been intersected by the drill cores, and the extent is as such not known.
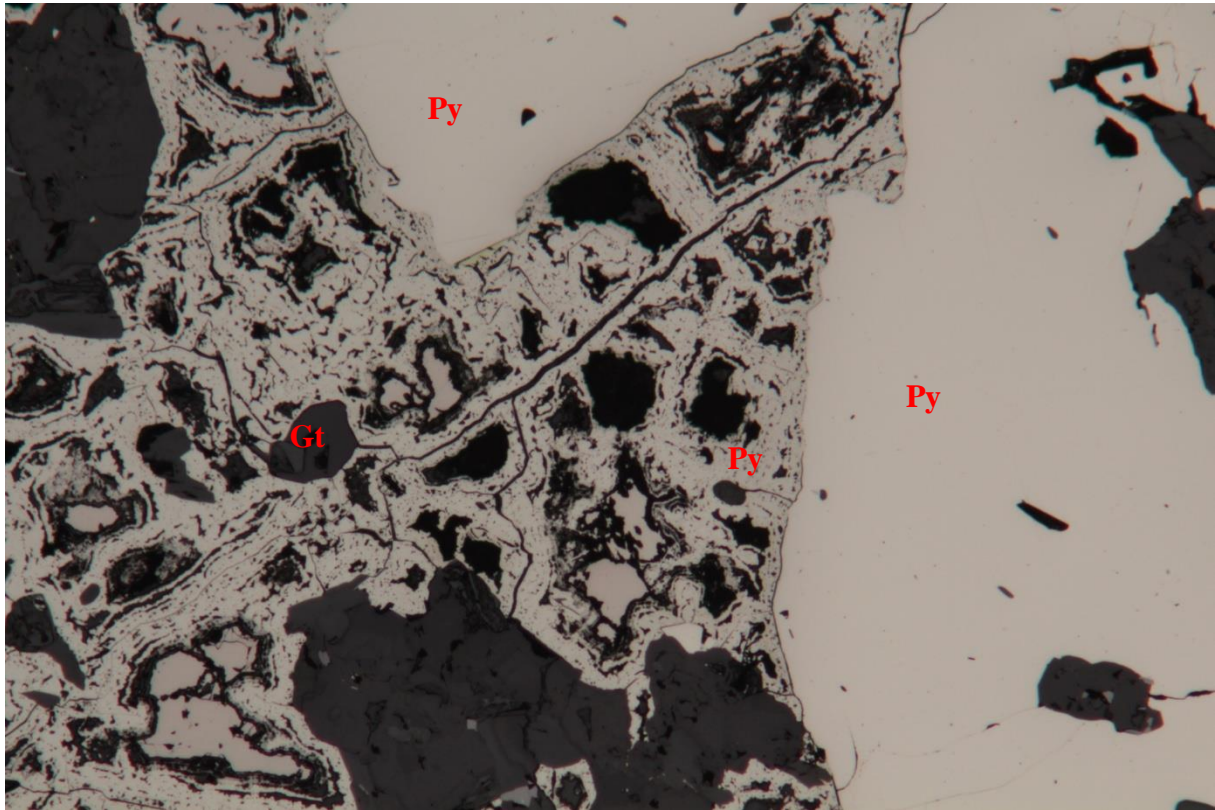
Figure 44: *Skeletal grains in pyrite from TSK 1 - M4. Width of field: 0.45 mm. Note how larger grains are less affected by the weathering processes. Black fields represent polishing pits, porosities and/or replacement of pyrite by goethite. The latter can present as opaque in PPL and XPL, and black in reflected light when it is not crystalline. The formation of skeletal grains by removal of Fe and replacement of pyrite by limonite-type Fe-oxihydroxides can also help reveal the internal structures of the pyrite grains, as evidenced here. Note the idiomorphic shape of the pyrite, exposed by weathering.*

These enrichment processes are likely responsible for the presence of bornite, chalcocite and covellite in the samples from the trenches, though it should be noticed that the presence of these minerals is minute compared to the presence of chalcopyrite. In addition to explaining the presence of these Cu-enriched sulphide phases, weathering also accounts for the formation of skeletal grains in pyrite and the formation of goethite (see Fig. 44, 45 and 46).

Gossans and leached zones are also important indicators of sulphide mineralization, and as such represent an important tool for prospecting for surface-near sulphide deposits. The rust staining is distinctive, both on exposed rocks and in streams. The presence of sulphides and the acid conditions formed during the weathering of said sulphides will also potentially have

an effect on surface plants and plant life, though this depends on the thickness and nature of the overburden.

Figure 45: *Replacement of pyrite (white) by goethite (dark grey). Note the careous sphalerite (light grey) and chalcopyrite (yellow). TSK 13 – M4 – 2; width of field: 0.45 mm.*

The reactions indicated in the figure below are as follows:

- Breakdown of chalcopyrite in the leached zone (goethite formed from pyrite follows the same principle):

  $4CuFeS_2 + 17OH_2 + 10H_2O \rightarrow 4Fe(OH)_3 + 4Cu2^+ + 8SO_4^{2-} + 8H^+$
  (chalcopyrite)   (goethite)

- Formation of e.g. malachite in the oxidized zone:

  $2Cu^{2+} + CO_3^{2-} + 2OH^- \rightarrow Cu_2(OH)_2CO_3$
                              (malachite)

- Formation of chalcocite from chalcopyrite in the secondary zone of supergene enrichment:

  $CuFeS2 + 3Cu2+ \rightarrow 2Cu2S + Fe2+$
  (chalcopyrite)   (chalcocite)

The formulae above are from Robb (2005).
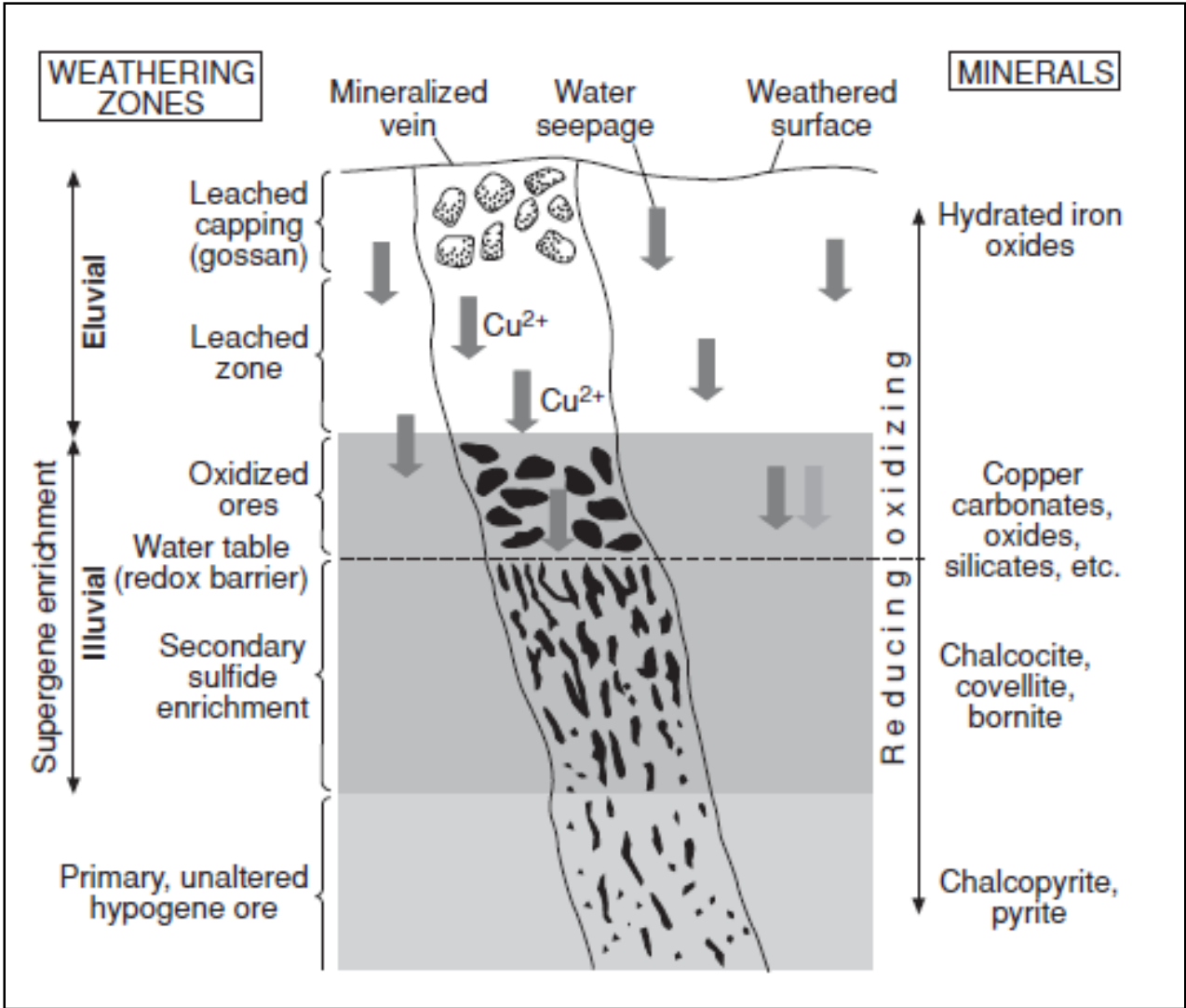
Figure 46: *Figure showing the zones of leaching and supergene enrichment in copper deposits from Robb (2005). This representation is typically used for Cu-porphyry deposits, but is also applicable in the case of weathered VMS-type deposits.*

4.4.2. Surface weathering and acid mine drainage (AMD)

Surface weathering is a naturally occurring process, as can be evidenced in the trenches at Skiftesmyr. Oxidation of sulphides, primarily pyrite, results in acidic conditions and production of sulphuric acid (see chapter 4.3.1, and Fig. 46). The environmental ramifications of the breakdown of sulphides are significant, even before any mining has taken place, as nearby lakes, streams and groundwater suffer from the influx of acid water, and potential

heavy metals contained in the sulphides (e.g. arsenic, cobalt, lead, nickel and zinc) are released (Murphy & Strongin, 2009). The problem is compounded once the material is excavated and deposited in tailing heaps around the mine site, and treatment and abatement of this acid run-off, referred to as acid mine drainage (AMD) represents a major expense in several different types of mines where the rocks have high sulphide contents (e.g. mining of coal, VMSDs and Cu-porphyries). Estimates presented by Murphy & Strongin (2009) show that the coal mining industry alone spends in excess of 1 million USD per day to prevent and limit the extent of AMD. So, while compounds leached from sulphides and entering adjacent waterways present an opportunity for the exploration industry with respect to hydrogeochemical analyses of water to localize deposits, it also represents a major environmental problem, both prior to and during mining.

Pyrite is generally the most abundant of the sulphides in an ore deposit, and as such also represents the main source of acid production in waste rocks, or tailings. While the pH of freshly exposed pyrite is relatively low (>4), the rate of acid production is low. At this stage, dissolved O_2 is the principle oxidant, but if acid production continues, a runaway reaction is initiated. This happens as the pH drops below four, and dissolved Fe (III) becomes the principal oxidant. This leads to a further reduction in pH, which releases more Fe (III) into solution as pyrite oxidizes faster. As a result, the acid needs to be neutralized as quickly as it is formed to be able to counteract this effect (Huminicki & Rimstidt, 2009).

Another important factor in the oxidation of sulphides at surface levels as well as deeper into the mineralization is microbial activity, which regenerates Fe(III) from the Fe(II) released by pyrite, thus ensuring that sufficient Fe(III) is present to sustain the runaway AMD condition (Huminicki & Rimstidt, 2009). The bacteria responsible, e.g. *Acidithiobacillus ferrooxidans*, thrives at extremely low pH conditions (pH 1 – 2) (Valdés et al., 2008). While playing an important part in AMD, e.g. *Acidithiobacillus ferrooxidans* also solubilizes copper and other metals (Valdés et al., 2008) by converting the metals from sulphides to sulphates, thereby extracting the metal into water (Rawlings, 2002). This is referred to as bioleaching (the terms biooxidation and biomining are also used), and represents an increasingly common beneficiation method.

One method utilized in combating AMD is the addition of alkaline substances to neutralize the acid as it forms, but this in effect treats the symptom (i.e. the acid) rather than the cause, which is the oxidation of pyrite. Recent research by Huminicki and Rimstidt (2009) shows

that an effective alternative is to promote the growth of Fe oxyhydroxides and Fe hydroxides on the surface of the pyrite, which acts as a barrier to oxidant transport to the pyrite surface. This slows the rate of acid production over time as the layer of limonite (e.g. goethite) grows thicker, and is done by adding alkaline materials (e.g. bicarbonates) to the tailings. The method was developed by observing naturally occurring examples of sulphide deposits with limonite pseudomorphs after pyrite, and is most effective at higher pH (~8) (Huminicki & Rimstidt, 2009).

The fact that this process to some extent is already occurring naturally at Skiftesmyr (e.g. Fig. 45) bodes well for an effective treatment of AMD in the case of future production.

4.5. Deformation structures in sulphides

Pyrite is the most well-studied and widespread of the sulphide minerals, both from a global perspective and with respect to Skiftesmyr. It has high thermal stability (up to 742 °C), and is as such stable in all but the highest grades of metamorphism (Craig & Vokes, 1993). As follows, it is stable under greenschist/amphibolite facies, the former of which is what is found in the Skiftesmyr area. Pyrite is also highly competent with respect to deformation. As a result of these attributes brittle deformation of pyrite is by far the most prevalent. McClay & Ellis (1983) have also shown that pressure solution and cataclastic flow, followed by annealing/grain growth are the major mechanisms responsible for deformation of pyrite. Recrystallization and retrograde metamorphism are also likely to account for the lack of pyrrhotite and marcasite, as the former may form pyrite during retrograde metamorphism, and the latter has been shown to be replaced by pyrite during recrystallization (Craig & Vokes, 1993).

As mentioned, pyrite readily recrystallizes during metamorphism, a feature that can be observed from the formation of a 'foam structure', i.e. triple 120° junctions between grain boundaries, and can be seen in Fig. 20. This readiness to recrystallize does however pose a problem in that it removes any earlier fabrics. Increased grain growth can lead to the formation of a larger single grain, resulting in ore minerals previously located at the intersections of grains or at triple junctions being incorporated into the larger grain as an inclusion. This can be seen in e.g. Fig. 21.

As a result of brittle deformation, particularly visible at the contacts between two or more grains (see Fig. 47) or as a result of extension, cracks will form. In some cases these cracks will be filled with another sulphide less stable at the given temperature and pressure conditions, e.g. chalcopyrite (see Fig. 21) (Barrie et al., 2010; Craig & Vokes, 1993). This provides some idea of which sulphides are mobile during metamorphic activity.
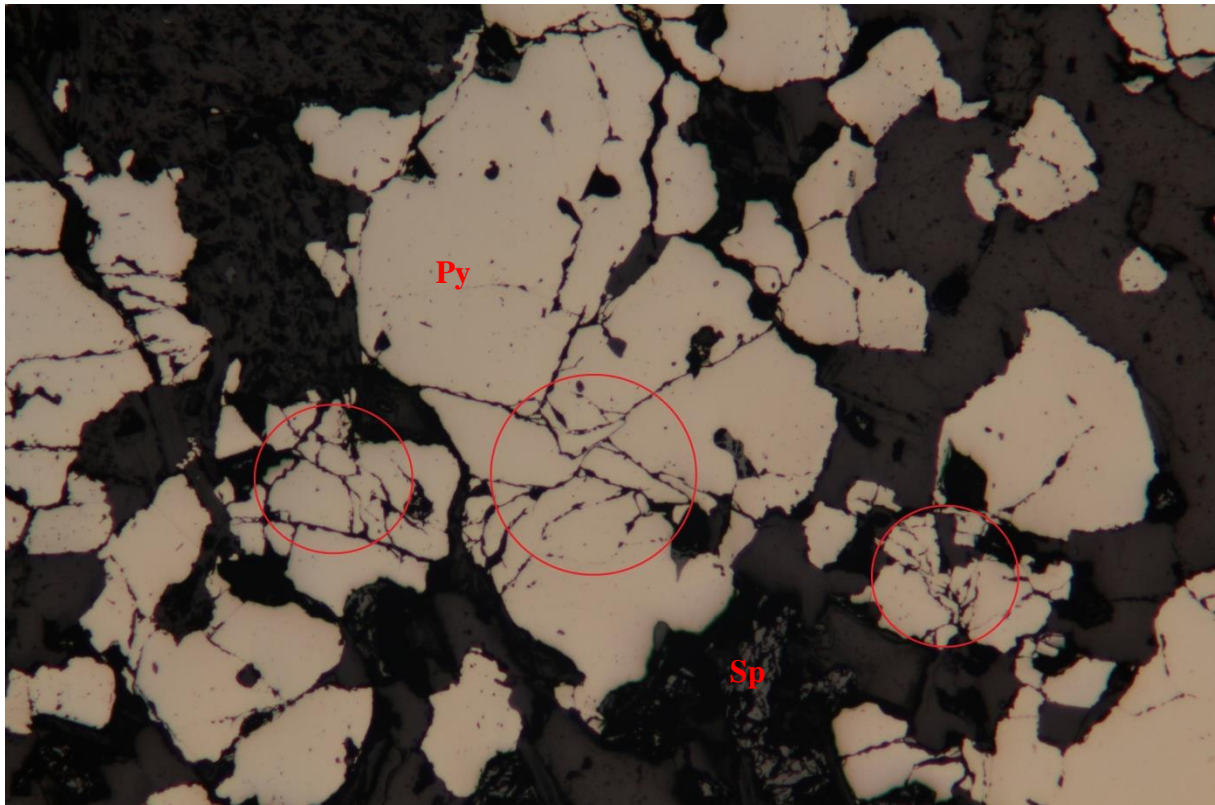
Figure 47: *Brittle deformation of pyrite (cream white). Red circles indicate areas where adjacent grains have been crushed at their contacts with each other. Sample TSK 1 – M14 – 2; width of field: 3.6 mm.*

5. Conclusion

The Skiftesmyr Cu-Zn VMS-type deposit was formed in a back-arc environment in relation to a mature (relative to e.g. the Skorovas deposit) island arc, likely in a position intermediate between the island arc and the adjacent back-arc basin. It is as such comparable to both the bimodal-mafic and mafic-dominated lithological associations proposed by Galley et al. (2007), and can as such be likened to e.g. Noranda, Quebec, and the deposits of the Troodos Massif in Cyprus.

The geology of the area in the immediate vicinity of the mineralization consists of a sequence of basalts and mafic tuffs, followed by keratophyres, which form the footwall of the deposit. Geochemical evidence suggests that the latter possibly represent silicified andesite/andesitic tuff rather than rhyodacitic tuffs as literature suggests, but other interpretations for the cause of this discrepancy between geochemical data and literature, including contamination from mafic pyroclastic materials, are also possible. The hanging wall of the deposit is composed of laminated mafic/intermediate tuffs. These rocks have undergone greenschist facies regional metamorphism during tectonic emplacement, and are also likely to have been subjected to similar conditions on the sea floor as a result of e.g. spilitization.

The primary ore minerals associated with the deposit are chalcopyrite and sphalerite, with minor amounts of Cu-enriched sulphides associated with supergene enrichment processes found in some samples. Precious metals seem to be associated with the copper-rich parts of the mineralization, but due to leaching as a result of surface weathering and ore remobilization during complex polyphase folding, such an association can only be indicated. The relatively large grain size and simple textures observed in the ore, as well as the limited amount of ore minerals displaying exsolution features or occurring as inclusions in e.g. pyrite, indicate that the ore is favorable with respect to beneficiation and that liberation of ore minerals should be fairly easy.

The natural occurrence of partial replacement of pyrite by limonite pseudomorphs as a result of surface weathering processes observed in the trench samples showcases the increased viability and effectiveness of modern long term acid mine drainage control for the Skiftesmyr deposit, from both a financial and environmental perspective.

References:

ALS GLOBAL, 2009: Geochemical Procedure: ME-ICP61: Trace level methods using conventional ICP-AES analysis. Available: http://www.alsglobal.com/en/Our-Services/Minerals/Geochemistry/Downloads [accessed on Nov. 11th, 2013]

ALS GLOBAL, 2005: Fire Assay Procedure: Au-AA23 & Au-AA24: Fire assay fusion, AAS finish. Available: http://www.alsglobal.com/en/Our-Services/Minerals/Geochemistry/Downloads [accessed on Nov. 11th, 2013]

BARRIE, C. R., BOYLE, A. P., COOK, N. J. & PRIOR, D. J., 2010, Pyrite deformation textures in massive sulfide ore deposits of the Norwegian Caledonides, *Tectonophysics 483*, pp. 269-286, Elsevier B. V.

BERNARD, L. M., 1997, Prefeasibility study of the Skiftesmyr and Godejord copper zinc projects, Grong, Central Norway, Braddick Resources Inc, Bergvesenet report number 4640.

BLATT, H, TRACY, R. J. & OWENS, B. E., 2006, *Petrology: Igneous, Sedimentary and Metamorphic*, Third Edition, W. H. Freeman and Company, New York

BUER, K. & HEIM, J. G., Rapport vedrørende malmletingssarbeide 1991, Skiftesmyr. Prospekteringsfondet 1991, Bergvesenet report number 1383.

COOK, N. J. & HOEFS, J., 1997, Sulphur isotope characteristics of metamorphosed Cu-(Zn) volcanogenic massive sulphide deposits in the Norwegian Caledonides, *Chemical Geology* 135 (1997), pp. 307-324.

CRAIG, J. R. & VAUGHAN, D. J, 1994, *Ore Microscopy & Ore Petrography*, Second Edition, John-Wiley & Sons Inc

CRAIG, J. R. & VOKES, F. M., 1993, The metamorphism of pyrite and pyritic ores: an overview, *Mineralogical Magazine 57,* pp. 3-18

FLOOD, B. & REINSBAKKEN, A., 1997, Exploration work within the Møklevatn property, Grong, Nord-Trøndelag 1996, Geologiske Tjenester AS; Braddick Resources Ltd; Norway Gold Exploration AS, Bergvesenet report number 4575.

FLOYD, P. A. & WINCHESTER, J. A., 1978, Identification and discrimination of altered and metamorphosed volcanic rocks using immobile elements, *Chemical Geology 21*, pp. 291-306, Elsevier Science Publishing Company, Amsterdam

GALLEY, A. G., 1993, Characteristics of semi-conformable alteration zones associated with volcanogenic massive sulphide districts, *Journal of Geochemical Exploration 48*, pp. 175-200, Elsevier Science Publishers B. V., Amsterdam

GALLEY, A. G., HANNINGTON, M. D. & JONASSON, I., 2007, Volcanogenic massive sulphide deposits, *Mineral Deposits of Canada: A Synthesis of Major Deposit Types, District Metallogeny, the Evolution of Geological Provinces, and Exploration Methods,* (ed.) W. D. GOODFELLOW, Geolocal Association of Canada, Mineral Deposits Division, Special Publication No. 5, pp. 141-161.

GIBSON, H. L., WATKINSON, D. H., COMBA, C. D. A., 1983, Silicification: Hydrothermal Alteration in an Archean Geothermal System within the Amulet Rhyolite Formation, Noranda, Quebec, *Economic Geology 78*, pp. 954-971.

HALLBERG, J. A., 1984, A Geochemical Aid to Igneous Rock Type Identification in Deeply Weathered Terrain, *Journal of Geochemical Exploration 20*, pp. 1-8, Elsevier Science Publishers B. V., Amsterdam

HALLS, C., REINSBAKKEN, A., FERRIDAY, I., HAUGEN, A. & RANKIN, A., 1977, Geological setting of the Skorovas orebody within the allochthonous volcanic stratigraphy of the Gjersvik Nappe, Central Norway, *Geological Society, London*, Special Publications 1977, v. 7, pp. 128-151

HAUGEN, A., 1982, Grong Gruber A/S: Exploration and Ore Potential in the Grongfield, Central Norway, Grong Gruber AS, Bergvesenet report number 6868.

HEIM, M., 1993, Berggrunnsgeologiske undersøkelser i det sørvestlige Grongfeltet (Rosset – Godejord – Skiftesmyr – Finnbu), Norsulfid AS, NGU report 92.311.

HEIM, M., 1993b, Berggrunnsgeologiske observasjoner i området Skiftesmyr-Bergsetran, Grong Gruber AS, Bergvesenet report number 5352.

HUMINICKI, D. M. C., RIMSTRIDT, D. J., 2009, Iron oxyhydroxide coating of pyrite for acid mine drainage control, *Applied Geochemistry 24,* pp. 1626-1634, Elsevier Science Publishers B. V., Amsterdam

HUSTON, D. L. & LARGE, R. R., 1989, A chemical model for the concentration of gold in volcanogenic massive sulphide deposits, *Ore Geology Reviews 4*, pp. 171-200, Elsevier Science Publishers B. V., Amsterdam

KITCO.COM: http://www.kitco.com/charts/popup/au3650nyb.html [accessed on Nov. 11th, 2013], http://www.kitcosilver.com/charts.html [accessed on Nov. 11th, 2013]

KOSKI, R. A. & MOSIER, D. L., 2012, Deposit types and associated commodities In: *Volcanogenic Massive Sulfide Occurrence Model*, (eds.) SHANKS III, P. W. C. & THURSTON, R, pp. 10-21, USGS Scientific Investigations Report 2010-5070-C

KRETZ, R. 1983. Symbols for rock-forming minerals. *American Mineralogist*, 68, pp. 277-279.

LANGLEY, K., 1973, Skiftesmyr Geological Report, Grong Gruber AS, Bergvesenet report number 5351.

LARGE, R. R., GEMMELL, J. B., PAULICK, H., HUSTON, D. L., 2001, The Alteration Box Plot: A Simple Approach to Understanding the Relationship between Alteration Mineralogy and Lithogeochemistry Associated with Volcanic-Hosted Massive Sulfide Deposits, *Economic Geology 96*, pp. 957-971.

LINDEMAN, E., 1992, Prelimenær prefeasibility study av Skiftesmyr forekomst, Norsulfid AS, Bergveneset report number 2400.

LINDEMAN, E., 1992b, Malmberegning av Skiftesmyr og Godejord, Norsulfid AS, Bergvesenet report number 2882.

LME.COM: http://www.lme.com/metals/non-ferrous/copper/ [accessed on Nov. 11th, 2013], http://www.lme.com/metals/non-ferrous/zinc/ [accessed on Nov. 11th, 2013]

MCCLAY, K. R., ELLIS, P. G., 1983, Deformation and recrystallization of pyrite, *Mineralogical Magazine 47*, pp. 527-538

METPROAS.NO: http://www.metproas.no [accessed on Nov. 11th, 2013]

MORTON, J. L., ZIERENBERG, R. A. & REISS, C. A., 1994: Geologic, Hydrothermal, and Biologic Studies at Escanaba Trough, Gorda Ridge, Offshore Northern California, *U.S. Geological Survey Bulletin 2022*

MOSIER, D. L., SINGER, D. A. & SALEM, B. B., 1983, Geologic and grade-tonnage information on volcanic-hosted copper-zinc-lead massive sulfide deposits, USGS Open-File Report 83-89

MURPHY, R., STRONGIN, D. R., 2009, Surface reactivity of pyrite and related sulfides, *Surface Science Reports 64,* pp. 1-45, Elsevier Science Publishers B. V., Amsterdam

MØRK, K., 1977, Skiftesmyr-forekomsten, Grong Nord-Trøndelag: En sammenstilling og vurdering av utførte arbeider, med forslag til videre undersøkelsesprogram, Grong Gruber AS, Bergvsenet report number 6842.

NESSE, W. D., 2000, *Introduction to Mineralogy*, Oxford University Press

NGU.NO: http://geo.ngu.no/kart/arealisNGU/ [accessed on Sept. 3rd, 2013]

NGU ORE DATABASE: Skiftesmyr:

http://aps.ngu.no/pls/oradb/!minres_dsp_deposit.link_object?p_sprakobjid=N0000000 202 [accessed Nov. 11th, 2013],

Tromselv:

http://aps.ngu.no/pls/oradb/!minres_dsp_deposit.link_object?p_sprakobjid=N0000000 248 [accessed Nov. 11th, 2013]

NISSEN, A. L., 1992, Mikroskopering av prøver av malm og sidebergart fra 6 norske gruver, NGU Bergvesenet, Bergvesenet report number 4257.

OHMOTO, H., 1996, Formation of volcanogenic massive sulfide deposits: The Kuroko perspective, *Ore Geology Reviews* 10 (1996), pp. 135-177, Elsevier

PEARCE, J. A. & CANN, J. R., 1973, Tectonic setting of basic volcanic rocks determined using trace element analyses, *Earth and Planetary Science Letters 19*, pp. 290-300, North Holland Publishing Company

REINSBAKKEN, A., 1993, Skiftesmyr. Diamantboring – tolkning 1992, Norsulfid AS, Bergvesenet report number 2402.

PIERCEY, S. J., 2009, Lithogeochemistry of volcanic rocks associated with volcanogenic sulphide deposits and applications to exploration, *Submarine Volcanism and Mineralization: Modern through Ancient*, (eds.) B. COUSENS & S. J. PIERCEY, Geological Association of Canada, Short Course 29-30 May 2008, Quebec City, Canada, pp. 15-40.

RAWLINGS, D. E., 2002, Heavy Metal Mining Using Microbes, *Annu. Rev. Microbiol. 56,* pp. 65-91.

ROBB, L., 2005, *Introduction to Ore-Forming Processes*, *Blackwell Publishing.*

SANDSTAD, J. S., DALSEGG, E., ELVEBAKK, H., GRENNE, T., HEIM, M., MEYER, G. B., 1996: Samtolkning av geodata i Grongfeltet – status pr. 15.12.95, NGU report number 95.147.

SAUNDERS, A. D. & TARNEY, J., 1984, Geochemical characteristics of basaltic volcanism within back-arc basins, *Geological Society, London, Special Publications 16¸* pp. 59-76.

SCHERMERHORN, L. J. G., 1973, What is keratophyre? *Lithos*, Volume 6, Issue 1, pp. 1-11.

SCHMID, R, 1981, Descriptive Nomenclature and Classification of Pyroclastic Deposits and Fragments, *Geologische Rundschau*, Volume 70, Issue 2, pp. 794-799.

SHANKS III, W. C. P. & KOSKI, R. A., 2012, Introduction. In: *Volcanogenic Massive*

Sulfide Occurrence Model, (eds.) SHANKS III, P. W. C. & THURSTON, R, pp. 4-8, USGS Scientific Investigations Report 2010-5070-C

STEPHENS, M. B., FURNES, H., ROBINS, B. & STURT, B. A., 1985, Igneous activity within the Scandinavian Caledonides. *In: GEE, D. G. & STURT, B. A. (eds), The Caledonide Orogen – Scandinavia and Related Areas*, pp. 623-656, John Wiley & Sons Ltd

STEPHENS, M. B. & GEE, D. G., 1985, A tectonic model for the evolution of the eugeoclinal terranes in the central Scandinavian Caledonides. *In: GEE, D. G. & STURT, B. A. (eds), The Caledonide Orogen – Scandinavia and Related Areas*, pp. 953-978, John Wiley & Sons Ltd

STEPHENS, M. B., GUSTAVSON, M., RAMBERG, I. B. & ZACHRISSON, E., 1985, The Caledonides of central-north Scandinavia – a tectonostratigraphic overview. *In: GEE, D. G. & STURT, B. A. (eds), The Caledonide Orogen – Scandinavia and Related Areas*, pp. 135-162, John Wiley & Sons Ltd

STEPHENS, M.B., 1988, The Scandinavian Caledonides: a complexity of collisions, *Geology Today*, v. 4, pp. 20–26

STEPHENS, M. B., KULLERUD, K. & CLAESSON, S., 1993, Early Caledonian tectonothermal evolution in outboard terranes, central Scandinavian Caledonides: new constraints from U-Pb zircon dates, *Journal of the Geological Society, London*, Vol. 150, pp. 51-56.

STRATEGI FOR MINERALNÆRINGEN, NÆRINGS- OG HANDELSDEPARTEMENTET, 2013: http://www.regjeringen.no/pages/38261985/mineralstategi_20130313.pdf [accessed on Nov. 11th, 2013]

SUNDBLAD, K., ANDERSEN, T., BECKHOLMEN, M. & NILSEN, O., 2006, Ordovician Escanaba type VMS deposits in the Scandinavian Caledonides, *Geological Society of Finland. Bulletin. Special Issue 1*, pp. 109-109

TAYLOR, B. & MARTINEZ, F., 2003, Back-arc basin basalt systematics, *Earth and Planetary Science Letters 210,* pp. 481-497, Elsevier Science B. V.

VALDÉS, J., PEDROSO, I., QUATRINI, R., DODSON, R. J., TETTELIN, H., BLAKE II, R., EISEN, J. A. & HOLMES, D. S., 2008, Acidithiobacillus ferrooxidans metabolism: from genome sequence to industrial applications, *BMC Genomics 9:597*.

VOKES, F. M., 1969, A review of the metamorphism of sulphide deposits, *Earth Science Reviews 5*, pp. 99-143, Elsevier, Amsterdam

ZVEZDOV, V. S., MIGACHEV, I. F., GIRFANOV, M. M., 1993, Porphyry copper deposits
of the CIS and the models of their formation, *Ore Geology Reviews, Vol. 7,*pp. 511-
549, Elsevier Science Publishers B. V., Amsterdam.

Appendices:

1. Abbreviated mineral names and other commonly used abbreviations

1.1.Abbreviated mineral names (from Kretz, 1983)

Table 1. Mineral Symbols

Acm	acmite	Elb	elbaite	Ntr	natrolite
Act	actinolite	En	enstatite (ortho)	Ne	nepheline
Agt	aegirine-augite	Ep	epidote	Nrb	norbergite
Ak	åkermanite	Fst	fassite	Nsn	nosean
Ab	albite	Fa	fayalite	Ol	olivine
Aln	allanite	Fac	ferroactinolite	Omp	omphacite
Alm	almandine	Fed	ferroedenite	Oam	orthoamphibole
Anl	analcite	Fs	ferrosilite (ortho)	Or	orthoclase
Ant	anatase	Fts	ferrotschermakite	Opx	orthopyroxene
And	andalusite	Fl	fluorite	Pg	paragonite
Adr	andradite	Fo	forsterite	Prg	pargasite
Anh	anhydrite	Gn	galena	Pct	pectolite
Ank	ankerite	Grt	garnet	Pn	pentlandite
Ann	annite	Ged	gedrite	Per	periclase
An	anorthite	Gh	gehlenite	Prv	perovskite
Atg	antigorite	Gbs	gibbsite	Phl	phlogopite
Ath	anthophyllite	Glt	glauconite	Pgt	pigeonite
Ap	apatite	Gln	glaucophane	Pl	plagioclase
Apo	apophyllite	Gt	geothite	Prh	prehnite
Arg	aragonite	Gr	graphite	Pen	protoenstatite
Arf	arfvedsonite	Grs	grossularite	Pmp	pumpellyite
Apy	arsenopyrite	Gru	grunerite	Py	pyrite
Aug	augite	Gp	gypsum	Prp	pyrope
Ax	axinite	Hl	halite	Prl	pyrophyllite
Brt	barite	Hs	hastingsite	Po	pyrrhotite
Brl	beryl	Hyn	haüyne	Qtz	quartz
Bt	biotite	Hd	hedenbergite	Rbk	riebeckite
Bhm	boehmite	Hem	hematite	Rds	rhodochrosite
Bn	bornite	Hc	hercynite	Rdn	rhodonite
Brk	brookite	Hul	heulandite	Rt	rutile
Brc	brucite	Hbl	hornblende	Sa	sanidine
Bst	bustamite	Hu	humite	Spr	sapphirine
Cam	Ca clinoamphibole	Ill	illite	Scp	scapolite
Cpx	Ca clinopyroxene	Ilm	ilmenite	Srl	schorl
Cal	calcite	Jd	jadeite	Srp	serpentine
Ccn	cancrinite	Jh	johannsenite	Sd	siderite
Crn	carnegieite	Krs	kaersutite	Sil	sillimanite
Cst	cassiterite	Kls	kalsilite	Sdl	sodalite
Cls	celestite	Kln	kaolinite	Sps	spessartine
Cbz	chabazite	Ktp	kataphorite	Sp	sphalerite
Cc	chalcocite	Kfs	K feldspar	Spn	sphene
Ccp	chalcopyrite	Krn	kornerupine	Spl	spinel
Chl	chlorite	Ky	kyanite	Spd	spodumene
Cld	chloritoid	Lmt	laumontite	St	staurolite
Chn	chondrodite	Lws	lawsonite	Stb	stilbite
Chr	chromite	Lpd	lepidolite	Stp	stilpnomelane
Ccl	chrysocolla	Lct	leucite	Str	strontianite
Ctl	chrysotile	Lm	limonite	Tlc	talc
Cen	clinoenstatite	Lz	lizardite	Tmp	thompsonite
Cfs	clinoferrosilite	Lo	loellingite	Ttn	titanite
Chu	clinohumite	Mgh	maghemite	Toz	topaz
Czo	clinozoisite	Mkt	magnesiokatophorite	Tur	tourmaline
Crd	cordierite	Mrb	magnesioriebeckite	Tr	tremolite
Crn	corundum	Mgs	magnesite	Trd	tridymite
Cv	covellite	Mag	magnetite	Tro	troilite
Crs	cristoballite	Mrg	margarite	Ts	tschermakite
Cum	cummingtonite	Mel	melilite	Usp	ulvöspinel
Dsp	diaspore	Mc	microcline	Vrm	vermiculite
Dg	diginite	Mo	molybdenite	Ves	vesuvianite
Di	diopside	Mnz	monazite	Wth	witherite
Dol	dolomite	Mtc	monticellite	Wo	wollastonite
Drv	dravite	Mnt	montmorillonite	Wus	wüstite
Eck	eckermannite	Mul	mullite	Zrn	zircon
Ed	edenite	Ms	muscovite	Zo	zoisite

1.2 Commonly used abbreviations and terms

This section aims to give a short summary of commonly used abbreviations (see section 1.1 for abbreviated mineral names):

VMS – volcangenic massive sulphide (alternative spellings include VHMS – volcanic hosted massive sulphide)

VMSD – volcanogenic massive sulphide deposit

NGU – Norwegian Geological Survey (Norges geologiske undersøkelse)

GOC – Grong-Olden culmination (basement rocks exposed south of the Skiftesmyr deposit)

AMD – Acid mine drainage

UiT – University of Tromsø (UiT – The Arctic University of Norway)

2. Trench collar locations
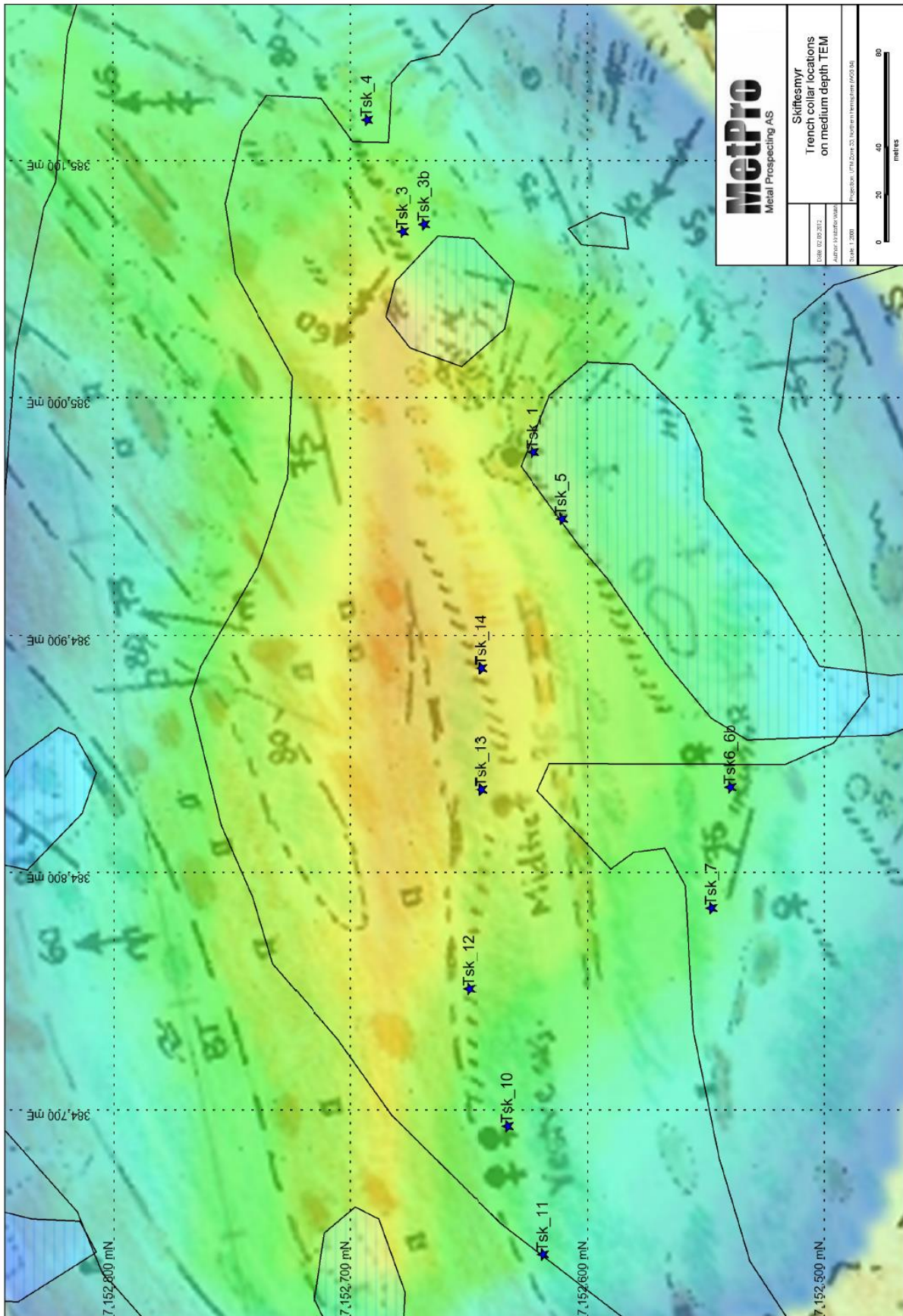
3. Geochemical data

3.1. ALS geochemical data (ME-ICP61 & AuAA23

Sample number:	Lithology:	Mineralization type:	Notes:
TSK 1 – M4	Massive sulphides	Massive	
TSK 1 – M14-1	Massive sulphides	Semi-massive	
TSK 1 – M14-2	Massive sulphides	Massive	Duplicate
TSK 1 – M15	Felsic dike	Disseminated	
TSK 3 – M4	Quartz keratophyre		
TSK 3 – M10	Mafic tuff		
TSK 5 – M1	Chlorite schist	Minor disseminations	Not analysed, no thin section prepared.
TSK 5 – M5	Quartz keratophyre	Minor disseminations	
TSK 5 – M23	Mafic tuff	Disseminated	
TSK 5 – M24	Metabasalt	Minor disseminations	
TSK 6 – M2	Quartz keratophyre	Disseminated	Quartz-sericite alteration zone
TSK 7 – M1	Metabasalt	Minor disseminations	
TSK 7 – M5	Massive sulphides	Semi-massive	
TSK 7 – M12	Quartz keratophyre	Minor disseminations	
TSK 10 – M8	Metabasalt	Minor disseminations	
TSK 10 – M10	Quartzite	Disseminated magnetite	
TSK 10 – M11	Quartz keratophyre		
TSK 10 – M13	Chlorite schist	Minor disseminations	Possible mafic flow, or altered metabasalt
TSK 11 – M2	Metabasalt	Minor disseminations	Basaltic metaandesite
TSK 13 – M2	Intermediate/mafic tuff	Disseminated	Tuff, or clay rich sediment+tuff.
TSK 13 – M4-1	Banded iron-pyrite-quartz	Banded, semi-massive	Fe-rich exhalative
TSK 13 – M4-2	Banded iron-pyrite-quartz	Banded, semi-massive	Duplicate
TSK 14 – M3	Quartz keratophyre	Minor disseminations	
TSK 14 – M3-2	Quartz keratophyre	Disseminated	Duplicate
TSK 14 – M5	Quartz keratophyre	Disseminated	
TSK 14 – M6	Metabasalt		

3.1. ALS geochemical data (ME-ICP61 & AuAA23

Sample number:	Analytical method:							
	ME-ICP61	ME-ICP61	ME-ICP61	ME-ICP61	ME-ICP61	ME-ICP61	ME-ICP61	ME-ICP61
	Ag	**Al**	**As**	**Ba**	**Be**	**Bi**	**Ca**	**Cd**
	ppm	%	ppm	ppm	ppm	ppm	%	ppm
TSK 1 – M4	0,8	6,69	10	480	0,90	<2	0,47	2,9
TSK 1 – M14-1	9,1	2,98	292	140	0,50	<2	0,77	23,3
TSK 1 – M14-2								
TSK 1 – M15	<0.5	8,01	9	370	0,90	<2	0,91	<0.5
TSK 3 – M4	<0.5	7,32	5	190	0,70	<2	1,41	<0.5
TSK 3 – M10	1,4	6,74	47	420	1,70	3	4,17	0,6
TSK 5 – M1								
TSK 5 – M5	<0.5	7,92	<5	300	1,30	<2	1,44	<0.5
TSK 5 – M23	<0.5	9,50	14	540	0,50	2	1,36	<0.5
TSK 5 – M24	<0.5	8,30	<5	150	1,20	2	4,57	<0.5
TSK 6 – M2	<0.5	5,47	38	910	<0.5	4	0,10	<0.5
TSK 7 – M1	<0.5	6,95	5	10	<0.5	<2	6,36	<0.5
TSK 7 – M5	37,7	6,71	17	210	<0.5	159	2,39	<0.5
TSK 7 – M12	<0.5	7,02	5	220	0,50	<2	1,30	<0.5
TSK 10 – M8	<0.5	7,36	<5	150	0,50	<2	6,89	<0.5
TSK 10 – M10	<0.5	4,73	6	150	0,50	<2	1,73	<0.5
TSK 10 – M11	<0.5	4,73	6	150	0,50	<2	1,73	<0.5
TSK 10 – M13	<0.5	7,15	<5	50	0,50	<2	2,59	0,6
TSK 11 – M2	<0.5	7,35	<5	70	<0.5	<2	4,22	<0.5
TSK 13 – M2	<0.5	8,19	<5	360	0,70	<2	3,99	<0.5
TSK 13 – M4-1	0,9	3,24	331	120	0,50	<2	0,32	3,8
TSK 13 – M4-2								
TSK 14 – M3	1,4	6,78	30	90	0,50	5	1,93	<0.5
TSK 14 – M3-2								
TSK 14 – M5	<0.5	8,28	16	340	0,50	4	2,94	<0.5
TSK 14 – M6	<0.5	7,49	10	130	<0.5	4	5,12	<0.5

Sample number:	Analytical method:							
	ME-ICP61	ME-ICP61	ME-ICP61	ME-ICP61	ME-ICP61	ME-ICP61	ME-ICP61	ME-ICP61
	Co	**Cr**	**Cu**	**Fe**	**Ga**	**K**	**La**	**Mg**
	ppm	ppm	ppm	%	ppm	%	ppm	%
TSK 1 – M4	12	234	2 980	10,5	20	1,38	10	1,76
TSK 1 – M14-1	16	194	4 680	27,4	30	0,64	<10	0,80
TSK 1 – M14-2								
TSK 1 – M15	10	133	51	3,0	20	1,20	<10	1,24
TSK 3 – M4	3	47	76	5,0	20	0,40	10	0,74
TSK 3 – M10	29	304	353	6,2	20	2,01	60	3,92
TSK 5 – M1								
TSK 5 – M5	6	65	23	2,9	20	0,83	20	1,07
TSK 5 – M23	44	165	277	6,2	20	2,73	<10	1,73
TSK 5 – M24	40	170	376	6,8	20	0,90	20	3,88
TSK 6 – M2	2	75	11	3,2	10	2,12	<10	0,19
TSK 7 – M1	47	423	28	7,2	10	0,07	<10	6,49
TSK 7 – M5	4	68	866	10,8	20	0,72	10	1,01
TSK 7 – M12	3	55	31	4,5	20	0,68	10	0,65
TSK 10 – M8	43	927	90	7,2	10	0,76	<10	4,17
TSK 10 – M10	14	319	117	6,1	10	0,96	<10	1,17
TSK 10 – M11	14	319	117	6,1	10	0,96	<10	1,17
TSK 10 – M13	45	32	114	7,4	20	0,53	<10	1,77
TSK 11 – M2	21	226	10	6,0	10	0,44	10	3,29
TSK 13 – M2	22	531	187	8,9	20	1,72	<10	3,66
TSK 13 – M4-1	75	200	988	27,4	20	1,06	<10	0,72
TSK 13 – M4-2								
TSK 14 – M3	28	735	414	8,2	10	0,47	<10	1,13
TSK 14 – M3-2								
TSK 14 – M5	44	1 440	205	7,2	10	2,52	<10	2,72
TSK 14 – M6	47	974	429	7,3	10	1,01	<10	4,66

Sample number:	Analytical method:								
	ME-ICP61	ME-ICP61	ME-ICP61	ME-ICP61	ME-ICP61	ME-ICP61	ME-ICP61	ME-ICP61	ME-ICP61
	Mn	**Mo**	**Na**	**Ni**	**P**	**Pb**	**S**	**Sb**	**Sc**
	ppm	ppm	%	ppm	ppm	ppm	%	ppm	ppm
TSK 1 – M4	488	13	1,71	54	740	22	7,18	5	21
TSK 1 – M14-1	163	48	0,08	39	300	348	>10.0	11	9
TSK 1 – M14-2									
TSK 1 – M15	271	2	3,80	9	180	27	0,51	<5	17
TSK 3 – M4	1 545	<1	3,89	<1	1 080	26	0,14	<5	21
TSK 3 – M10	681	2	2,35	101	2 030	127	1,75	5	23
TSK 5 – M1									
TSK 5 – M5	326	<1	4,52	11	710	10	0,43	<5	11
TSK 5 – M23	287	1	3,48	39	80	25	3,69	<5	50
TSK 5 – M24	990	3	3,09	93	1 320	24	1,03	5	32
TSK 6 – M2	35	12	0,38	1	70	35	1,51	<5	12
TSK 7 – M1	1 320	<1	1,33	179	160	22	<0.01	<5	29
TSK 7 – M5	1 190	8	2,92	3	820	205	7,87	<5	20
TSK 7 – M12	965	<1	4,21	<1	1 040	21	0,19	<5	18
TSK 10 – M8	2 020	<1	2,40	200	90	3	0,06	<5	60
TSK 10 – M10	883	3	1,97	74	290	9	0,17	5	20
TSK 10 – M11	883	3	1,97	74	290	9	0,17	5	20
TSK 10 – M13	884	<1	4,35	12	560	3	0,03	<5	35
TSK 11 – M2	1 080	1	2,62	60	710	6	0,06	<5	29
TSK 13 – M2	1 590	4	1,57	79	300	15	2,50	5	47
TSK 13 – M4-1	193	56	0,09	97	460	24	>10.0	<5	11
TSK 13 – M4-2									
TSK 14 – M3	1 050	11	3,62	66	360	23	1,18	<5	38
TSK 14 – M3-2									
TSK 14 – M5	813	<1	2,19	200	70	19	2,22	<5	66
TSK 14 – M6	918	2	2,31	172	90	13	1,85	<5	59

Sample number:	Analytical method:								
	ME-ICP61	ME-ICP61	ME-ICP61	ME-ICP61	ME-ICP61	ME-ICP61	ME-ICP61	ME-ICP61	Au-AA23
	Sr	Th	Ti	Tl	U	V	W	Zn	Au
	ppm	ppm	%	ppm	ppm	ppm	ppm	ppm	ppm
TSK 1 – M4	93	<20	0,27	<10	<10	195	<10	850	0,028
TSK 1 – M14-1	120	<20	0,05	<10	<10	133	<10	8 160	0,216
TSK 1 – M14-2									
TSK 1 – M15	290	<20	0,22	<10	<10	44	<10	269	0,005
TSK 3 – M4	166	<20	0,50	<10	<10	20	<10	165	0,020
TSK 3 – M10	805	20	0,54	<10	<10	161	<10	273	0,115
TSK 5 – M1									
TSK 5 – M5	471	<20	0,29	<10	<10	71	<10	132	<0.005
TSK 5 – M23	194	<20	0,23	<10	10	352	<10	181	0,005
TSK 5 – M24	805	<20	0,43	<10	<10	255	<10	290	<0.005
TSK 6 – M2	49	<20	0,09	<10	<10	38	<10	22	0,027
TSK 7 – M1	177	<20	0,27	<10	<10	274	<10	243	0,005
TSK 7 – M5	182	<20	0,40	<10	<10	71	<10	245	4,500
TSK 7 – M12	116	<20	0,47	<10	<10	14	<10	60	<0.005
TSK 10 – M8	279	<20	0,18	<10	<10	259	<10	221	<0.005
TSK 10 – M10	122	<20	0,18	<10	<10	97	10	100	<0.005
TSK 10 – M11	122	<20	0,18	<10	<10	97	10	100	<0.005
TSK 10 – M13	132	<20	0,54	<10	<10	409	<10	141	<0.005
TSK 11 – M2	137	<20	0,53	<10	10	234	<10	140	<0.005
TSK 13 – M2	198	<20	0,24	<10	<10	335	<10	251	<0.005
TSK 13 – M4-1	26	<20	0,11	<10	<10	131	<10	1 355	0,016
TSK 13 – M4-2									
TSK 14 – M3	108	<20	0,25	<10	<10	185	<10	255	0,066
TSK 14 – M3-2									
TSK 14 – M5	207	<20	0,23	<10	10	349	<10	212	<0.005
TSK 14 – M6	187	<20	0,19	<10	10	309	<10	190	0,005

3.2. XRF geochemical data

3.2.1. XRF trace elements

Sample:	CaO (%)	Sc (ppm)	TiO$_2$ (%)	V (ppm)	Cr (ppm)	MnO (%)	Fe$_2$O$_3$ (%)	Co (ppm)	Ni (ppm)	Cu (ppm)	Zn (ppm)
TSK 1 – M15	0,93	14,6	0,404	14	111,6	0,023	3,75	3,5	6,5	28,9	152,3
TSK 10 – M11	0,9	12,4	0,65	39,7	180	0,158	4,48	2,9	3,7	12	74,8
TSK 10 – M8	11,16	64,1	0,321	281,9	1430,4	0,306	10,11	44,7	235,4	340	235,5
TSK 11 – M2	6,72	29,4	1,683	218,2	87,1	0,194	9,62	16,1	29,6	9,5	146,3
TSK 14 – M6	13,53	48,6	0,249	236,2	776,1	0,17	8,38	50,4	166,2	11,7	144,7
TSK 7 – M1	8,1	40,2	0,497	288,1	700,4	0,199	10,34	58,7	204,8	66,5	223,8
TSK 7 – M12	1,54	16,1	0,888	8,6	176,8	0,125	5,61	2,8	2,6	26,3	64,9

Sample:	Ga (ppm)	Rb (ppm)	Sr (ppm)	Y (ppm)	Zr (ppm)	Nb (ppm)	Cs (ppm)	Ba (ppm)	La (ppm)	Ce (ppm)	Pb (ppm)	Th (ppm)
TSK 1 – M15	16,7	39,7	159,6	25,5	76,8	2,9	4,4	532,2	5,7	15,8	34,1	0
TSK 10 – M11	15,7	22,8	65,4	34,2	118,7	3,2	3,7	130,1	15,7	42,8	9,0	9
TSK 10 – M8	10,3	26,8	269,7	6,1	11,1	1,4	3,4	230,6	1,6	2,4	15,6	0
TSK 11 – M2	16,6	8,9	184,9	33,3	219,6	9,6	3,4	47,7	19,3	52,6	10,2	8,8
TSK 14 – M6	8,9	6,3	110,7	7,1	8,3	1,4	3,4	8,7	1,7	5,3	12,5	2,2
TSK 7 – M1	13,1	7,0	144,8	12,7	20,1	1,4	3,4	19,9	1,5	6,5	33,5	0
TSK 7 – M12	15,0	21,6	97,8	32,8	93,9	2,9	3,7	321,9	12,1	30,2	31,6	4,3

3.2.2. XRF ore elements

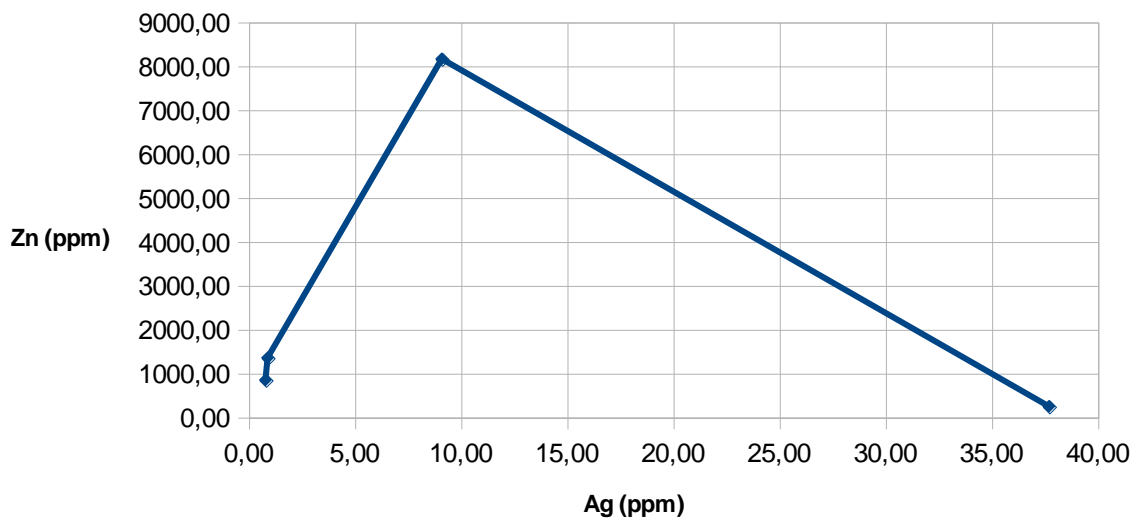| Sample	Ag (ppm)	Cu (%)	As (ppm)	Bi (ppm)	Sb (ppm)	Se (ppm)	S (%)	Zn (%)	Pb (%)	Sn (ppm)
TSK 1 – M4	7,6	0,251	63	3	1,3	9	32,3	0,024	0,001	5,7

4. Ore element correlation plots
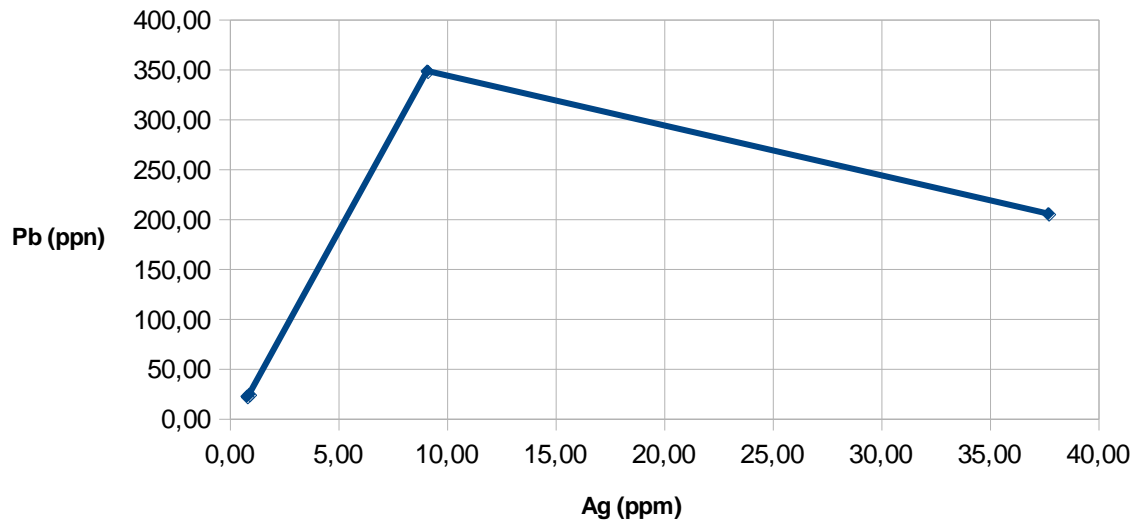
Au vs Ag
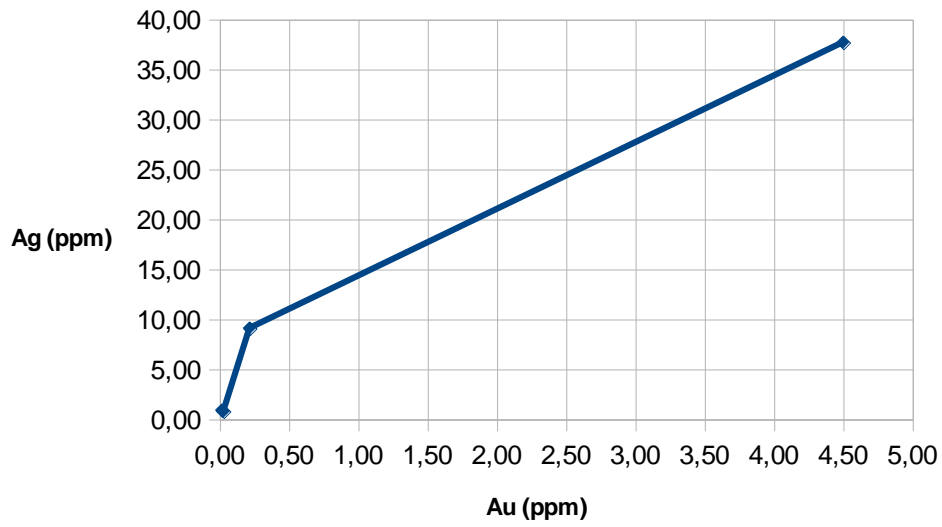
Au vs Cu
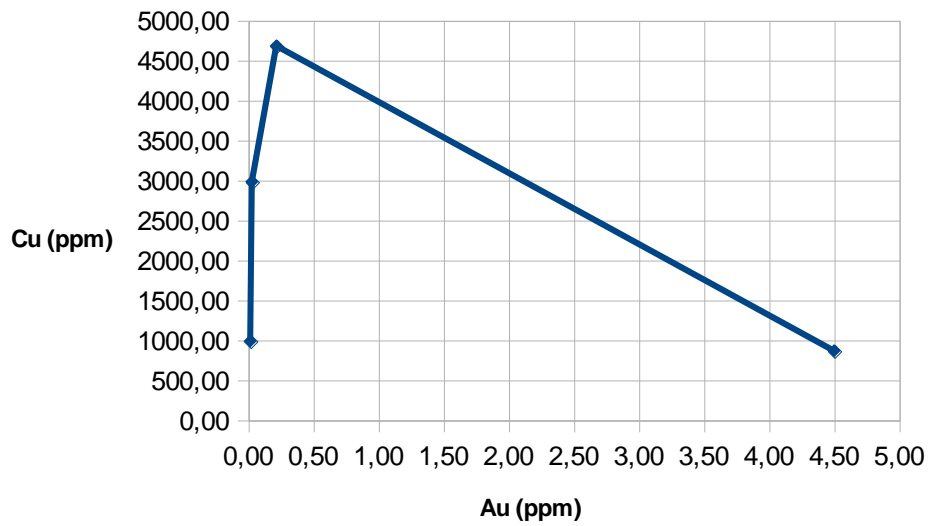
Au vs Zn
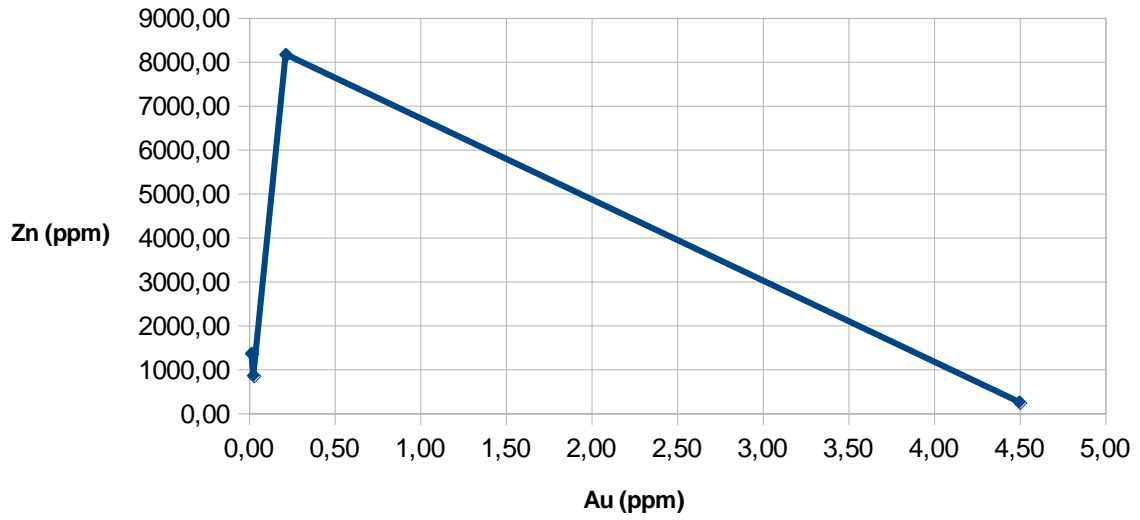
Au vs Pb
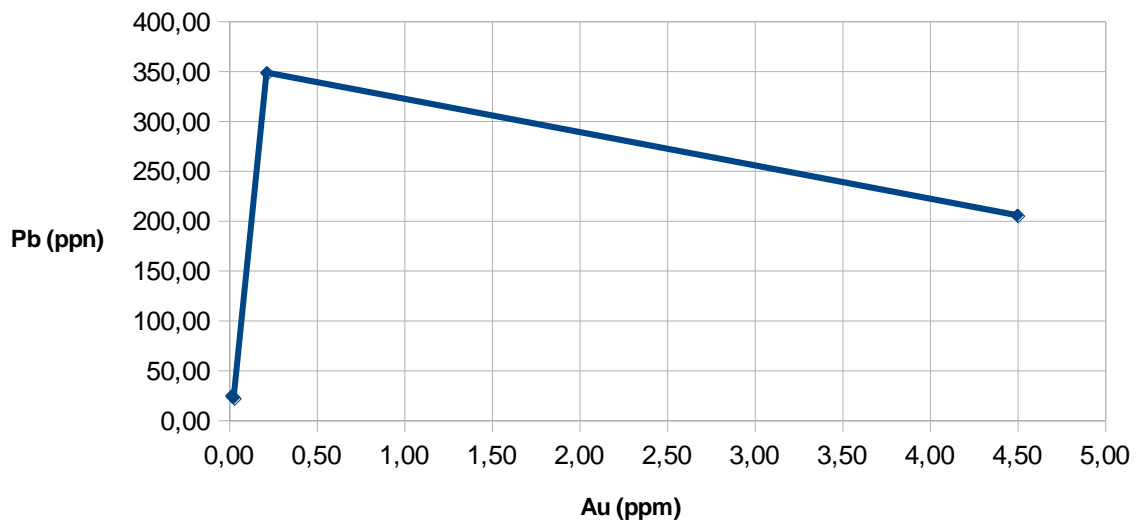
Ag vs Cu
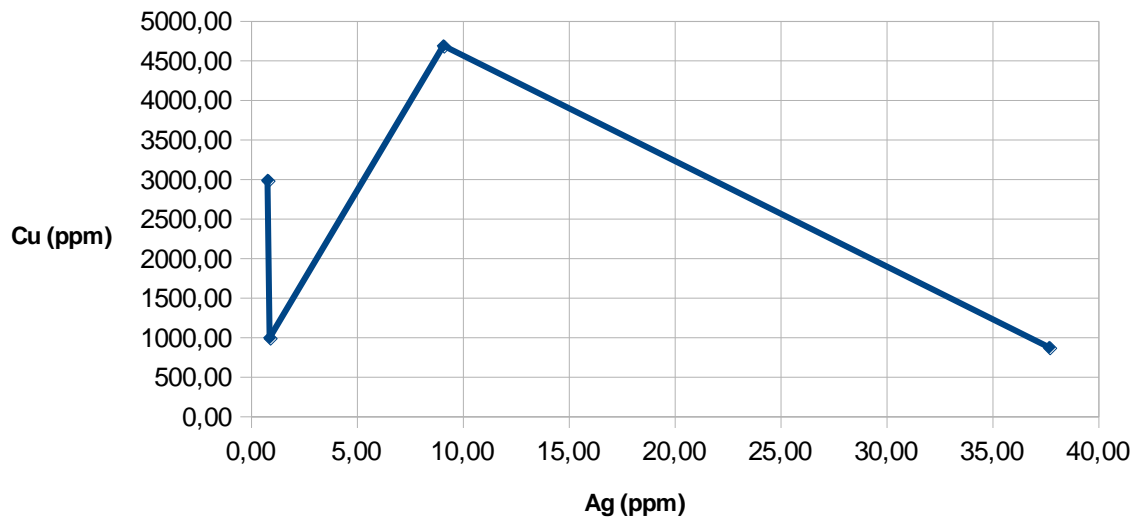
Ag vs Zn
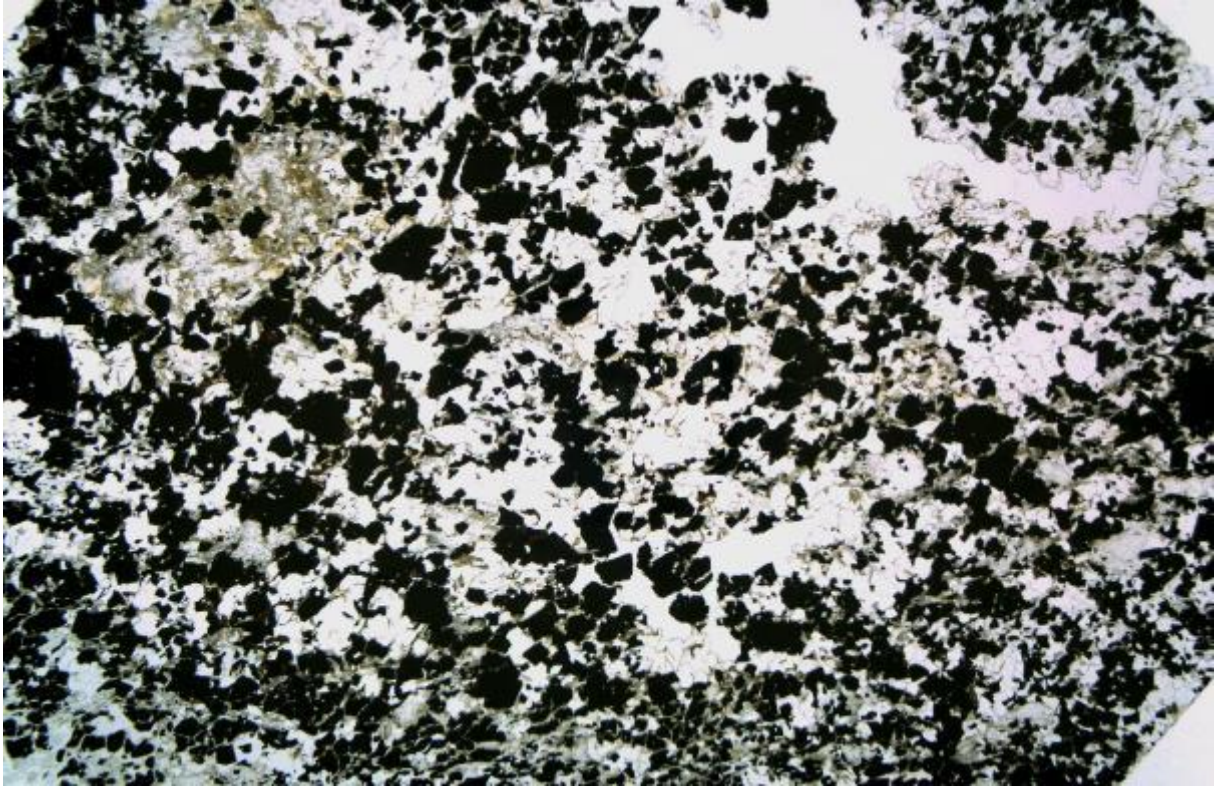
Ag vs Pb

5. Scanned thin sections
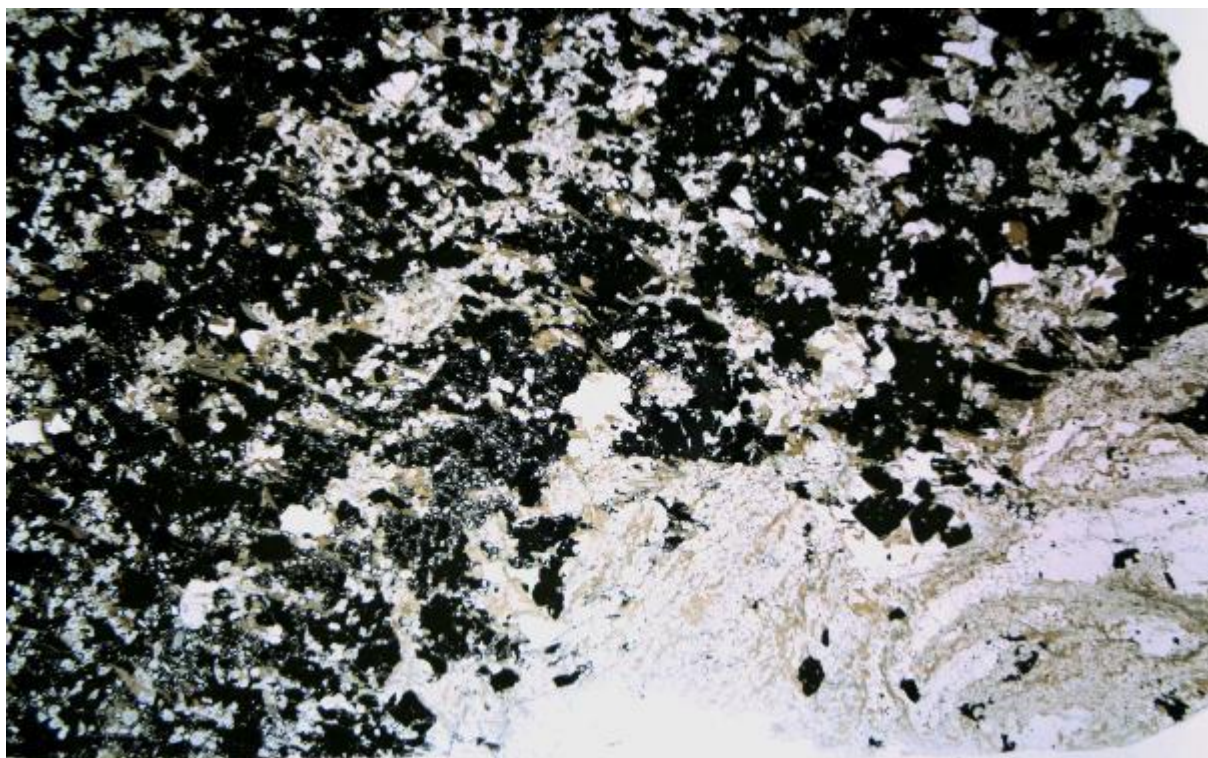
TSK 1 – M4
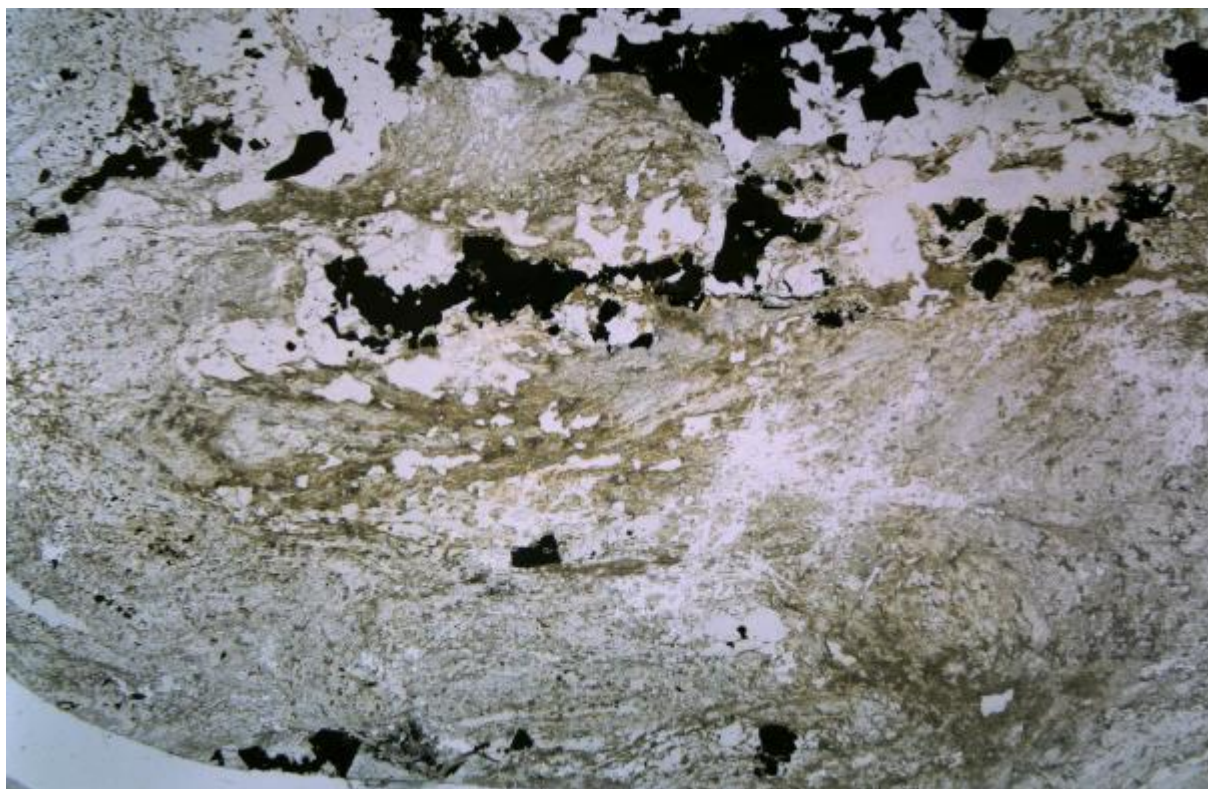
TSK 1 – M14 – 1

TSK 1 – M14 – 2

TSK 1 – M15

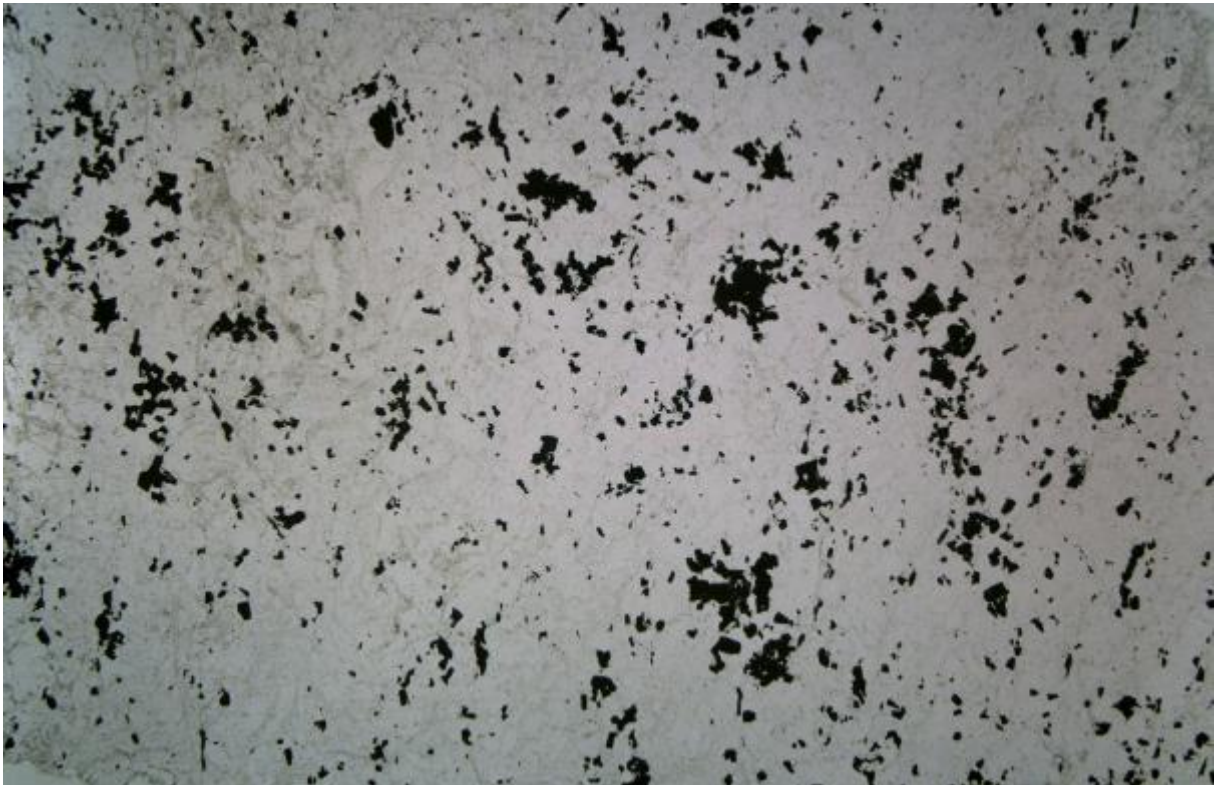*TSK 3 – M4*

TSK 3 – M10
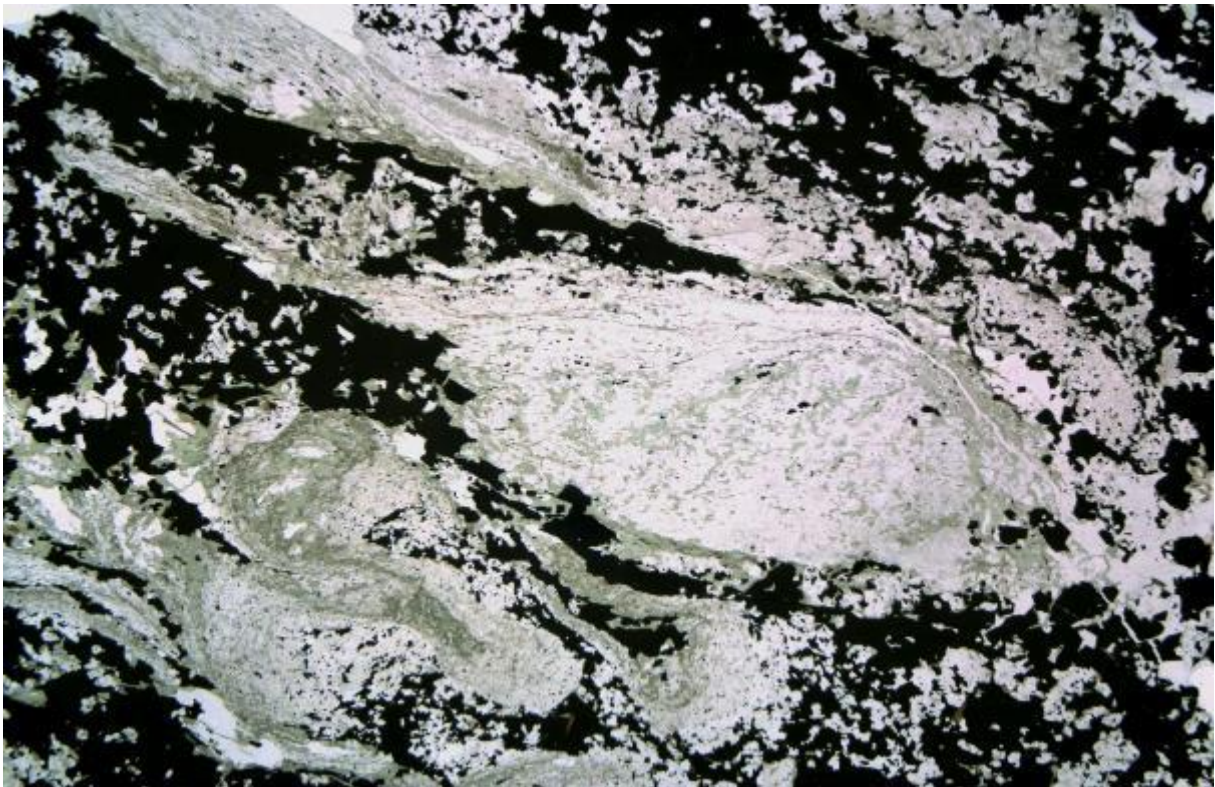
TSK 5 – M5
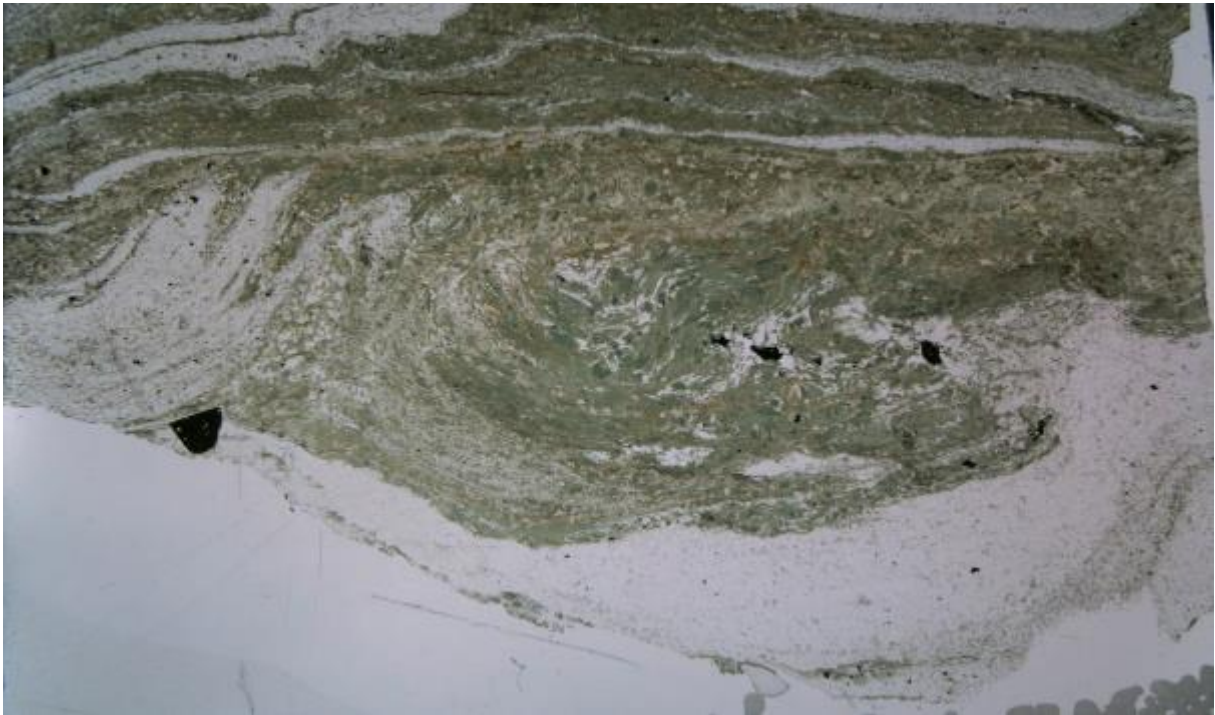

TSK 5 – M23

TSK 5 – M24

TSK 6 – M2

TSK 7 – M1

TSK 7 – M5

TSK 7 – M12

TSK 10 – M8

TSK 10 – M10

TSK 10 – M11

TSK 10 – M13
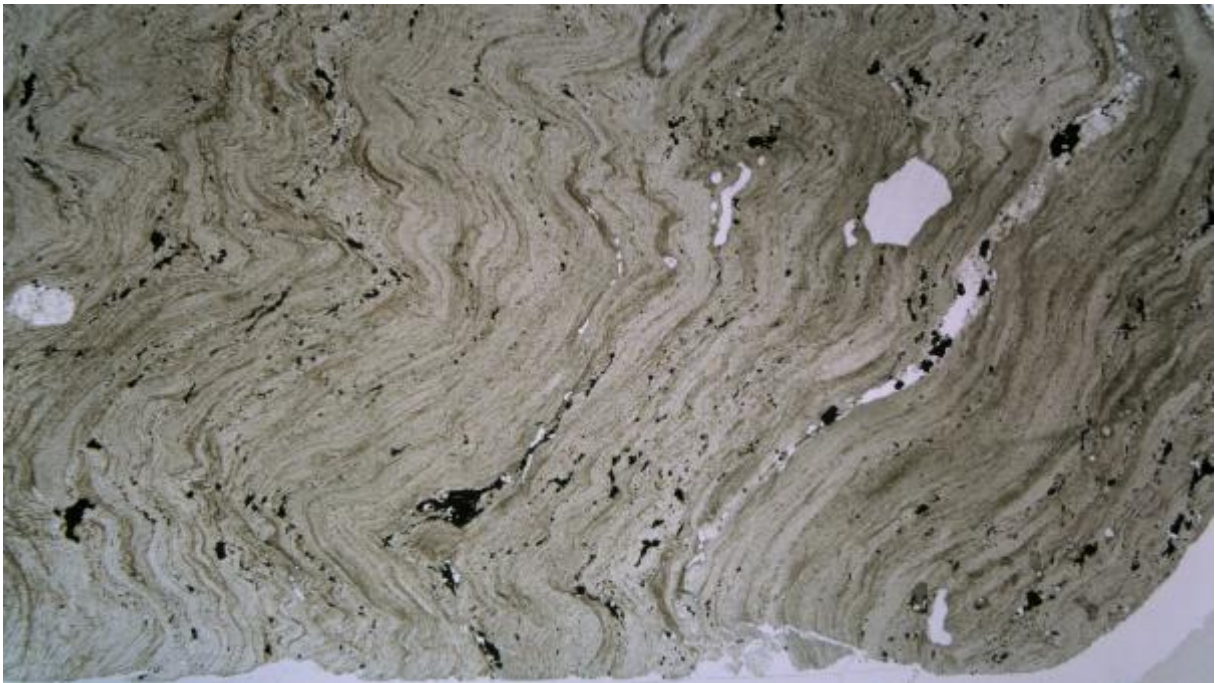

TSK 11 – M2

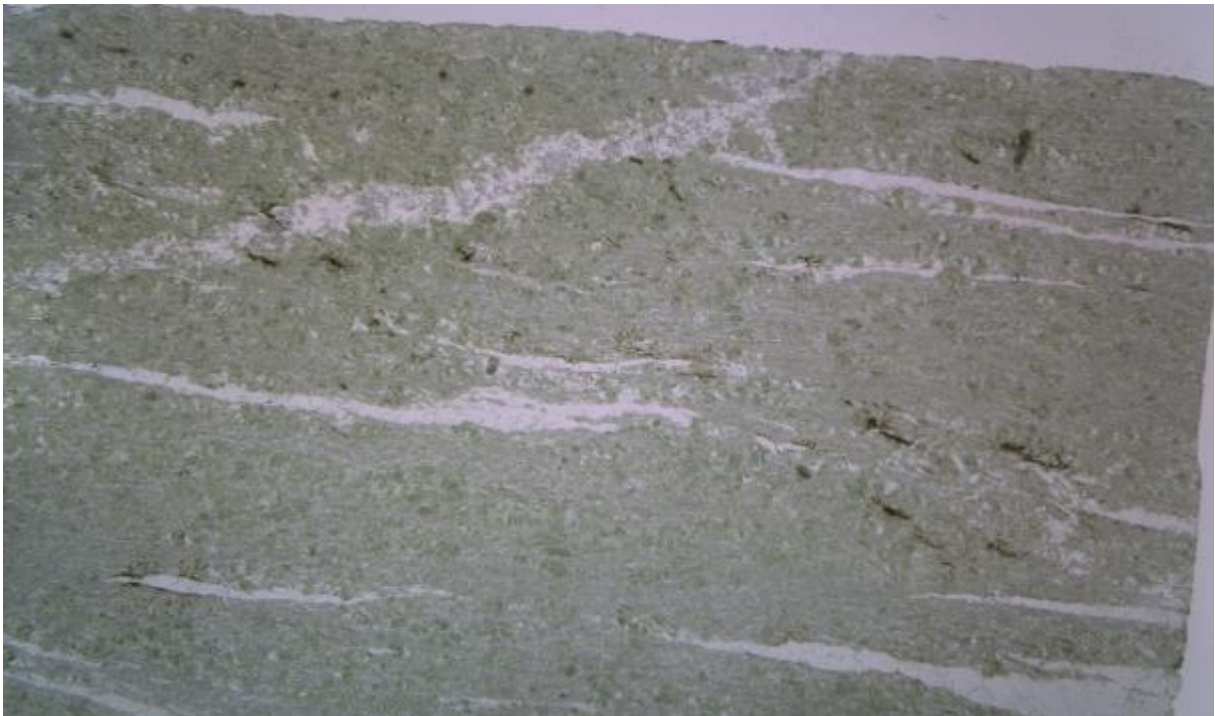*TSK 13 – M2*

TSK 13 – M4 – 1

TSK 13 – M4 – 2

TSK 14 – M3

TSK 14 – M5

TSK 14 – M6

6. Rough estimates of mineral assemblages

Thin section	Quartz (%)	Feldspar (%)	Biotite (%)	Chlorite (%)	White mica (%)	Amphibole (%)	Sulphides (%)	Epidote (%)	Garnet (%)	Calcite (%)
TSK 1 – M4	30		10				60			
TSK 1 – M14 – 1	40		10		30		20			
TSK 1 – M14 – 2	30				10		60			
TSK 1 – M15	60		5	35			5			
TSK 3 – M4	60	10		10	15				5	
TSK 3 – M10	15	5	50	10						20
TSK 5 – M5	50	15		25	5	Accessory	Accessory	Accessory		5
TSK 5 – M23	30		20	30	10		10	Accessory		
TSK 5 – M24	15			50	30					
TSK 6 – M2	60				30		10			
TSK 7 – M1	5	10		40		30	Accessory			
TSK 7 – M5	40			20			40	Accessory		
TSK 7 – M12	40	30	20	Accessory		Accessory	Accessory	10	Accessory	
TSK 10 – M8	25		15	15		30		10		Accessory
TSK 10 – M10	90			Accessory			10			
TSK 10 – M11	60	25	15				Accessory		Accessory	
TSK 10 – M13	30		Accessory	70			Accessory			
TSK 11 – M2		50		30			5	5		5
TSK 13 – M2	20	Accessory	10	35		20	5	10		

Thin section	Quartz (%)	Feldspar (%)	Biotite (%)	Chlorite (%)	White mica (%)	Amphibole (%)	Sulphides (%)	Epidote (%)	Garnet (%)	Calcite (%)
TSK 13 – M4 – 2	35			Accessory	10		50	5		
TSK 14 – M3	35	5		10			50			
TSK 14 – M5	50	5	20	5			5	15		
TSK 14 – M6	40	Accessory	40			5	5	10		
	5	Accessory		50	30					15